Sol-gel-derived optical oxygen, pH and dissolved carbon dioxide sensors

by

Dorota Wencel

A thesis presented to Dublin City University
for the Degree of Doctor of Philosophy

Research supervisor:
Prof. Colette McDonagh
School of Physical Sciences
National Centre for Sensor Research
Dublin City University

DCU

July 2008

Declaration

I hereby certify that this material, which I now submit for assessment on the programme of study leading to the award of Doctor of Philosophy is entirely my own work, that I have exercised reasonable care to ensure that the work is original, and does not to the best of my knowledge breach any law of copyright, and has not been taken from the work of others save and to the extent that such work has been cited and acknowledged within the text of my work.

Signed: . . . . (Candidate)   ID No.: . . . .

Date: . . . .

Acknowledgments

Over the past few years it has been my good fortune to encounter so many people who have given me so much of their time, professional help and companionship.

I would first of all like to thank my research supervisor, Prof. Colette McDonagh for her constant guidance, encouragement, good company and lots of good ideas. I would also like to thank Prof. Brian MacCraith for this fantastic opportunity to work here in OSL.

A big thank you is due to all OSL members, past and present, for their constant help with everything. Thanks in particular to Clare for calming influence and enjoyable working atmosphere, Anna for detailed introduction to the sol-gel chemistry and, what is more important, for friendship and great company, Ondra for putting up with my constant questions about mystery of all kinds of spectroscopy, Daniele for helping with dCO_2 instrumentation and valuable advice about Italian food, Mohamed for all appreciated suggestions concerning the sol-gel, in particular GPTMS, Aimeric for help with IR measurements, Conor for patience and understanding of struggle with my written English. My neverending questions about optical sensing must have been a real pain in the neck. Helen thank you for your cheerfulness and contagious enthusiasm. Rob C. thanks for exchanging information, Ph.D. related worries and discoveries, Christy for proofreading my thesis, John for assistance with electronics and Aisling for help and support with all the research project issues. Juncal for your input in the O_2 sensing project and unforgettable lunches, Deidre for chemical synthesis and great conversations and Ute for helping with last minute Raman spectra.

Thank you to Dr. Mary Pryce from the Chemistry Department in DCU for as-

sisting with lifetime measurements and to Dr. Mariusz Barczak and Prof. Andrzej Dąbrowski from Marie-Curie Sklodowska University in Lublin for the invitation, making it possible to use Raman and AFM microscopy, and very special treatment during my stay there.

I also wish to thank all other members of School of Physical Sciences and NCSR for creating enjoyable working atmosphere.

Very special thanks for Dr. Robert Koncki and Prof. Stanisław Głąb, (who first brought me into the world of research), for excellent guidance and input in my intellectual development during my Masters at Warsaw University. I especially want to thank my friends, Dagmara and Łukasz for their great support. Łukasz, if not for your loyal help with everything, I wouldn't achieve all that.

To my parents and my sister Olga for their mental support, faith in me and for constant motivation to get it done.

And finally, to Rafał for looking after me, for understanding, friendship, for everything.

In remembrance of Mr. and Mrs. O'Reagain who I couldn't thank enough for all their kindheartedness, love and precious knowledge and inspiration, which was always there when I needed it.

This thesis is dedicated to my parents and to Mr. and Mrs. O'Reagain.

"In the initial phase of the process (...), the scientist works through the imagination, as does the artist. Only afterwards, when critical testing and experimentation come into play, does science diverge from art..."

F. Jacob, 1997

Table of Contents

Abstract

The development and applications of optical chemical sensors have shown a significant growth over the past 20 years. Current sensor trends, such as multianalyte capability, miniaturisation and printability are important drivers for materials requirements in optical chemical sensors. The use of sol-gel materials in optical sensors is attractive due to the ease of fabrication, design flexibility of the process and compatibility with a range of deposition techniques. This work describes the development and characterisation of a range of sol-gel-derived sensor films for luminescence-based oxygen (O_2), pH and dissolved carbon dioxide (dCO_2) sensing.

O_2 sensing was based on the luminescence quenching of the ruthenium complex [Ru(II)-tris(4,7-diphenyl-1,10-phenanthroline)] dichloride, $[Ru(dpp)_3]^{2+}$, which was entrapped in the sol-gel matrix. Sensor films were fabricated using a wide range of organosilicon precursors including methyltriethoxysilane (MTEOS), ethyltriethoxysilane (ETEOS), n-propyltriethoxysilane (PTEOS), phenyltriethoxysilane (PhTEOS) and 3,3,3-trifluoropropyltrimethoxysilane (TFP-TMOS). The O_2-dependent luminescence was detected using the principle of phase fluorometry, which facilitates indirect monitoring of the luminescence lifetime. In addition to optimising O_2 sensor performance, issues such as the influence of humidity on O_2 sensing were addressed.

The pH sensor exploited the technique of excitation ratiometric detection of the fluorescence from the pH sensitive dye, 1-hydroxypyrene-3,6,8-trisulfonic acid, ion-paired with cetyltrimethylammonium bromide (HPTS-IP). Novel pH materials were developed based on 3-glycidoxypropyltrimethoxysilane (GPTMS) and ETEOS hybrid xerogel films which were optimised for fast and reversible pH determination in the physiological pH range. The use of a lipophilic dye, which minimised leaching from the host matrix, resulted in stable pH sensor films with excellent sensor resolution.

The dCO_2 optical sensor was also based on the use of a fluorescence detection technique employing the pH indicator, HPTS-IP, which was entrapped in PTEOS-derived xerogel films. This study was focused on optimisation of the sensitivity and dynamic range of the sensor through tailoring of the sol-gel matrix.

This work highlights the versatility and tailorability of sol-gel-derived materials for use in a wide range of optical sensor applications.

Abbreviations and Symbols

λ .... wavelength

λ_{exc} .... excitation wavelength

µm .... micrometer

µs .... microsecond

ϕ .... phase angle

ϕ_0 .... phase angle in 100% N_2

ϕ_{100} .... phase angle in 100% O_2

τ .... excited state lifetime of the luminophore

τ_0 .... excited state lifetime in the absence of quencher (oxygen)

° .... degree

3D .... three-dimensional

$[O_2]$ .... oxygen concentration

$[Ru(dpp)_3]^{2+}$ .... [Ru(II)-tris(4,7-diphenyl-1,10-phenanthroline)

A .... absorption

a .... activity

A^- .... basic (deprotonated) form of the pH indicator

AFM .... Atomic Force Microscope

APTMS 3-aminopropyltrimethoxysilane

c .... molar concentration

CCD .... charge coupled device

CO_2 .... carbon dioxide

CTAB .... hexadecyltrimethylammonium bromide

D .... diffusion coefficient

dCO_2 .... dissolved carbon dioxide

DI water .... deionised water

DLR .... Dual Lifetime Referencing

ETEOS .... ethyltriethoxysilane

EtOH .... ethanol

F .... fluorescence intensity

f_i .... fractional contribution to the total emission from site i

g/L .... gram/liter

GPTMS 3-glycidoxypropyltrimethoxysilane

h .... hour

HA .... acidic (protonated) form of the pH indicator

HCl .... hydrochloric acid

HPTS .... 1-hydroxypyrene-3,6,8-trisulfonic acid

HPTS-IP .... HPTS ion-paired with cetyltrimethylammonium bromide

I .... luminescence intensity in the presence of quencher (oxygen)

I_0 .... luminescence intensity in the absence of quencher (oxygen)

IC .... internal conversion

IS .... ionic strength

ISC .... intersystem crossing

K_i .... equilibrium constant

k_q .... bimolecular quenching constant

k_r .... rate of radiative decay

k_{nr} .... rate of non-radiative decay

K_{SV} .... Stern-Volmer constant

K_{SVi} .... discrete Stern-Volmer constant associated with site i

kHz .... kilohertz

LED .... Light Emitting Diode

LOD .... limit of detection

MI 1-methylimidazole

MLCT .... Metal-to-Ligand Charge Tranfer

mM .... millimolar

mms^{-1} .... milimeter/second

mol/L .... mol/liter

MTEOS .... methyltriethoxysilane

N_2 .... nitrogen

nm .... nanometer

NO_2 .... nitrogen dioxide

ns .... nanosecond

O_2 .... oxygen

ORMOSIL .... ORganically MOdified SILicate

P .... phosphorescence intensity

PC .... polycarbonate

PhTEOS .... phenyltriethoxysilane

pKa .... negative logarithm of an acid dissociation constant

pKa' .... apparent pKa

pO_2 .... partial pressure of oxygen

PTEOS .... n-propyltriethoxysilane

Q .... quencher

r^2 .... regression

RH .... relative humidity

RSD .... relative standard deviation

S_0 .... ground state

S_1 .... first singlet excited state

S_2 .... second singlet excited state

SEM .... Scanning Electron Microscope

SNAFL .... carboxyseminaphthofluorescein

SNARF .... seminaphtharhodafluor

SO$_2$ .... sulphur dioxide

T$_1$ .... first triplet excited state

t$_{90}$ .... response time, time taken to achieve 90% of signal change

TEOS .... tetraethoxysilane

TFP-TMOS 3,3,3-trifluoropropyltrimethoxysilane

UV-Vis .... ultraviolet-visible

V$_R$ .... vibrational relaxation

Chapter 1

Introduction

1.1 Introduction

This thesis describes the development of sol-gel-derived materials for optical luminescence-based sensing of oxygen (O_2), pH and dissolved carbon dioxide (dCO_2). This introductory chapter will give a short summary, including some theoretical background of the main elements of the work namely, optical chemical sensors, luminescence, the sol-gel process and the key analytes. An outline of the thesis is presented and the objectives of the work are stated. A more detailed description of the background of the work is given in chapter 2.

1.2 Optical chemical sensors

A chemical sensor can be defined as a *'miniaturised analytical device which can deliver real-time on-line information on the presence of specific compounds or ions in complex samples'* [1]. These devices are regarded as *'senses of electronics'*, eyes and ears capable of seeing and hearing beyond the human perception [2]. In ancient Greece a papyrus test was known that was used to detect contamination of copper coins by iron [3]. Coins were dissolved in acid and the presence of ferric ions was determined with a test strip impregnated with an extract of certain apples.

An ideal sensor should possess adequate selectivity, sensitivity and limit of detection for its application. It should also be robust, easy to calibrate, show long term

stability and allow non-destructive testing [3–5]. A schematic representation of the basic components of a sensor is shown in Figure 1.1.

Chemical sensors can be categorised according to the transducer type: electrochemical (measurement of electrical parameters), optical (measurement of changes in optical properties), mass- (measurement of mass changes) and heat-sensitive (measurement of the change of reaction heat) [5, 6]. Electrochemical sensors are the oldest group of sensors and are widely used. Techniques such as potentiometry, voltammetry and amperometry have all grown out of the field of electrochemistry. A wide range of potentiometric ion-selective electrodes are available for example for analysis of blood electrolytes such

Figure 1.1: Schematic representation of the basic components of the chemical sensor.

as sodium, potassium, calcium and chloride ions. Ion-selective pH electrodes have been employed for pH, CO_2 and ammonia determination for decades.

Optical chemical sensors referred to as opt(r)odes are also well established [3]. Optodes employ optical transduction techniques to yield analyte concentration. The most widely used optical signals that can be measured are absorbance, luminescence and reflectance, but optical sensors based on refractive index measurements have also been reported [7].

1.2.1 Luminescence-based optical chemical sensors

This study centers on luminescence-based optical chemical sensors. Luminescence is the emission of light (ultraviolet, visible or infrared) from an electronically excited species [8]. The word luminescence comes from Latin (lumen means light) and was

introduced by physicist Eilhardt Wiedemann in 1888 [9]. Our ancestors were already fascinated by natural luminescent phenomena such as the Northern Lights and glow-worms (Figure 1.2).
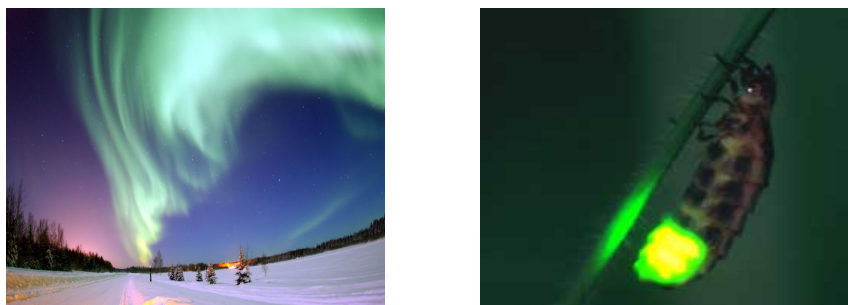
Figure 1.2: Natural phenomena of luminescence: Northern Lights (left) [10] and glow-worm (right) [11].

Luminescence-based optical sensing has many advantages over sensors using electrical or other transduction methods, for example immunity to electrical interference, no analyte consumption, wide choice of sensor platforms and detection systems and highly sensitive detection. The high sensitivity of detection associated with luminescence was used as long ago as 1877 to demonstrate that two rivers, the Danube and the Rhine were connected by underground streams [8]. The fluorescent molecule called fluorescein was placed in one river and its characteristic green fluorescence appeared in a small river some time later that led to the Rhine.

In the past, luminescence-based techniques may not have been widely used due to lack of suitable light sources, detectors and cost-effective instrumentation. Currently, luminescence spectroscopy is regarded as a very powerful research tool in many areas and there is a significant growth in the use of luminescence-based detection in a broad range of disciplines, including biochemistry, biophysics, environmental monitoring, genetic analysis, clinical and analytical chemistry [12]. Nowadays, the development of optical chemical sensors is a rapidly expanding area of research, as huge progress has been made in the development of low-cost, miniature opto-electronic sources and detectors. Optodes allow for non-destructive and long distance monitoring. In addition,

ease of miniaturisation, possibility of mass production and emerging novel optosensing schemes have helped them to become commercially available.

It is worth noting that sensing based on luminescence properties offer higher detection sensitivity than alternative optical methods based on absorbance measurements. Higher sensitivity arises from the fact that light absorbance is measured as the difference in intensity between light passing through the reference and the sample. In contrast, luminescence is measured directly, without any comparison and single photons are easily measured with most photomultiplier tubes.

In this work luminescence-based detection schemes were used namely, the phase fluorometry technique which is based on luminescence lifetime monitoring for O_2 sensing, excitation ratiometric detection for pH sensing and direct luminescence intensity measurements for dCO_2 optical sensing. All methods allow for practical, low-cost and rapid analyte determination.

1.3 Sol-gel-derived materials

Sol-gel processing provides a versatile route for the fabrication of gels, glasses, ceramics and hybrid inorganic-organic materials at low temperatures [13, 14]. Sol-gel-based materials were used historically as decorative and construction materials long before scientific understanding had been developed. The earliest use can be seen in the cave paintings in France, dating back 17 000 years [15]. The idea of using chemically-linked particles as a matrix led to the development of concrete in 700 BC. In 790 AD, Mayan artists prepared a pigment known as Maya Blue (Figure 1.3). This blue pigment survived twelve centuries in a jungle environment because it is not an ordinary dye but a sol-gel hybrid inorganic-organic material in which the organic dye molecules were entrapped and protected [16, 17].

The first sol-gel synthesis of silica was described by Ebelmen about 150 years ago [19]. The present sol-gel technology started around 1970. In 1971 Dislich prepared transparent borosilicate glass using a sol-gel process [20, 21]. In 1981 the

Figure 1.3: Mural painting of Mayan warriors at Bonampak, Mexico. Image copyrighted by Microsoft Corporation [18].

First International Workshop on Glasses and Ceramics was held. During the last few decades, sol-gel-derived materials have received considerable attention and sol-gel science has become better understood. These materials are of interest because they are easy to prepare, modify and process and result in components that have high optical quality, chemical and mechanical stability. They can be prepared in a variety of sizes and shapes and their physical and chemical properties can be easily tailored via manipulations of the processing conditions. Sol-gel-derived glasses can be made at room temperature, which is a benefit when compared with those required for traditional glass melts (higher than 1100 °C). Lower temperatures save energy, reduce volatility problems, and eliminate the need for specialised equipment. In addition, ambient processing conditions allow the incorporation of organic and biological molecules within the sol-gel matrix without chemical modification.

The sol-gel approach has been used extensively in the development of novel materials for applications in optics, solid state electrochemical devices, catalysis, chromatography, and chemical sensors [22–25]. The diversity associated with sol-gel materials processing and preparation is leading to the development of novel materials and new approaches for advanced applications.

In this study, the main focus was on the development of sol-gel-derived materials as matrices for optical chemical sensing. The approach involves the entrapment of an analyte-sensitive reagent into a suitable sol-gel-derived matrix. As hosts, these

matrices provide very good optical transparency, stability, permeability, flexibility and low chemical reactivity [26–30]. The matrix is adequately porous to allow the target analyte to diffuse into the matrix and react with the entrapped chemical agent, while ideally it should be sufficiently dense to prevent the dye from leaching out into the analyte solution.

Sol-gel-based materials show tremendous potential for the development of advanced sensors. Sol-gel technology, coupled with today's light sources and detection schemes, is a promising tool for the production of portable, robust and low-cost sensing systems.

1.4   The importance of O_2, pH and CO_2 sensing

O_2, pH and CO_2 are common target analytes due to their importance in a broad range of research fields such as environmental, clinical and industrial analysis. Measurement of O_2, pH and CO_2 provides information on water quality in both freshwater and marine environments [31–37]. In addition, they are key physiological parameters in clinical analysis, as monitoring of their levels in blood and body fluids provides information about a patient's state of health [38–44]. In the food industry, they are important quality parameters used to determine freshness of food and integrity of the package seal [45–47]. There is also a growing interest in their detection during the fermentation process in bioprocess management for quality control purposes [48–51]. In addition, pH sensors are used in measuring acidity of rain and O_2 and CO_2 sensors are required to monitor of automobile exhaust emissions [52–54]. Surface O_2 pressure measurements have been developed for aerodynamic tests in wind tunnels and in-flight environments as they can provide pressure data with high spatial resolution [55, 56].

This work is centered on the development, characterisation and optimisation of optical sol-gel-derived sensors for O_2, pH and dCO_2 detection. The target application of O_2 and pH sensors is in bioprocessing applications, whereas the dCO_2 sensor has been developed for freshwater quality monitoring.

1.4.1 O_2 and pH monitoring during bioprocesses

The biotechnology sector has experienced significant growth that has been generated by advances in microbiology and genetic engineering. Bioprocesses are extremely important in a variety of industries such as biopharmaceutical, food and environment. The spectrum of biotechnology applications ranges from the production of fermented food and chemicals such as antibiotics, ethanol and vitamins to cell cultivation and waste water treatment [57].

  Bioreactors are systems where microorganisms can be cultivated under controllable conditions. Bioprocess monitoring is performed by measuring critical parameters such as temperature, pH, O_2 (in gas and dissolved phase), and dCO_2 among others [58]. Control of these parameters result in increased efficiency, reproducibility, product-oriented productivity and reduced costs. Even a small change in pH or temperature can alter cell metabolism and influence efficiency and productivity leading to an un-profitable process. Control of bioprocesses aims to adjust the environment in which the cells are cultivated in order to achieve optimal growth conditions. Optical sensors are very convenient and effective tools for such control, as they provide non-invasive, continuous and simultaneous multianalyte monitoring [59,60]. Bioprocess monitoring is a demanding application area for sensors used for on-line monitoring. The sensor should not contaminate the bioprocess for example, leaching of substances from the sensor into the culture media is undesirable and needs to be sterilisable. In addition, bioprocesses might run for long periods and during this time the sensor must perform without recalibration.

  The most commonly monitored parameter is pH, as it significantly influences cell growth, recombinant protein production and cell metabolism [61]. Currently, the electrochemical glass electrode is usually used in bioreactors. O_2 is also an important parameter to control and can be measured in the exhaust gas to monitor the O_2 uptake or in dissolved phase. O_2 uptake rate of cells is an indicator of metabolic activity and can be used to predict the state of growth [61]. The current state of the

art in O_2 measurement is the widely used Clark electrode.

Optical sensors possess several advantages over electrochemical pH and O_2 sensors used in bioprocess monitoring applications which are discussed in detail in chapter 2.

1.4.2 The role of dCO_2 in environmental monitoring

The impact of human activities on environmental systems is becoming an increasingly important issue. Sensor development plays a vital role in establishing the state of our environment and monitoring changes due to our activities. Efficient evaluation of ecosystems such as lakes, oceans or ground water require the acquisition of large data sets in order to take into account spatial and temporal variations. This requires the use of in-situ or field-deployable sensors for continuous, real-time monitoring.

dCO_2 monitoring in fresh waters provide important information in relation to [62, 63]:

- Determining inorganic carbon equilibria as CO_2 plays a major role as a component of the carbon cycle in which carbon is exchanged between the atmosphere, the terrestrial biosphere (which includes freshwater systems and soil), the oceans and sediments
- Assessing carbon fluxes in the open ocean
- Assessing the balance between uptake of CO_2 by aquatic organisms (for photosynthesis), release of CO_2 (by respiration) and CO_2 transfer at the air-water interface
- Assessing the biological influences of CO_2 fluctuations in rivers, for example formation of calcium carbonate (limestone) in the water.

Gaseous CO_2 has a strong tendency to dissolve in water and forms carbonic acid, which in turn affects surface water pH [64]. There is considerable concern that, as a result of increased CO_2 in the atmosphere, the acidity of water will increase and may affect aquatic organisms. Aquatic plant life (microscopic as well as large-rooted

plants) depend on adequate CO_2 levels for growth. They utilise CO_2 in photosynthesis and the carbon in these plant materials comes from CO_2 in the water. Recent reports indicate that elevation of atmospheric CO_2 may induce drastic changes in the species dominance in freshwaters systems [65]. The rise in CO_2 levels is also dangerous for fish, as it can impair the transport of O_2 in fish blood [66]. It was also reported that chronic exposure to high CO_2 concentration (higher that 35 ppm) can reduce rainbow trout and salmon growth [67].

1.5   Thesis structure

This thesis describes the development, optimisation and characterisation of luminescence-based, sol-gel-derived O_2, pH and dCO_2 sensor films.

Chapter 1 provides a short introduction to this work. Optical chemical sensors, the phenomenon of luminescence, sol-gel-derived materials and the importance of O_2, pH and CO_2 sensing are introduced. An outline of the thesis is presented and the objectives of the work are stated.

Chapter 2 details the theory of luminescence and the theoretical background of O_2, pH and CO_2 sensing. It also provides an overview of the state of the art in this area along with a range of detection techniques and the application of the sol-gel process to optical chemical sensing are described.

Chapter 3 contains experimental results on the development, characterisation and optimisation of sol-gel-derived O_2 sensor films where the O_2 concentration is measured via phase fluorometric detection. It reports on the experiment that led to development of humidity-insensitive sol-gel-based O_2 sensors with enhanced sensitivity for use in bio-pharma industry. The last part of this chapter characterises highly sensitive O_2 sensors that are based on sol-gel materials containing a fluorinated precursor. Such sensors are required for applications where continuous O_2 measurements are maintained at a low O_2 level.

Chapter 4 describes the development of a sol-gel-derived matrix suitable for pH

sensing using the technique of dual excitation detection. A wide range of sol-gel precursors were used in order to design and optimise a matrix suitable for fast and reversible pH determination in the near neutral pH range. In addition to the full characterisation of the optimised pH sensor performance, the influence of temperature and ionic strength on sensor response is described. Raman measurements were also performed in order to correlate the chemical structure of the sol-gel-derived matrix with optimum pH sensor performance.

Chapter 5 presents the development and characterisation of fluorescence-based sol-gel-derived dCO_2 sensor films. The influence of the organic base on sensor response is discussed and the sensor performance is analysed in terms of pH and flow interference. Interrogation of the sensor film with a robust, low-cost optical probe is investigated with a view to producing a sensor that may be used outside a laboratory environment.

Chapter 6 draws conclusions and discusses future work.

1.6   Research objectives

The main research objectives were:

1. To develop novel humidity-insensitive, optical sol-gel-derived O_2 sensor films with enhanced sensitivity based on dynamic quenching of luminescence for application in bioprocess monitoring.

2. To develop a novel optical sol-gel-derived pH sensor that uses dual excitation ratiometric detection for application in bioprocess monitoring.

3. To develop a fluorescence-based sol-gel-derived sensor for dCO_2 measurements for use in environmental applications.

All sensors should demonstrate improved performance over previously reported optical O_2, pH and dCO_2 sensors.

References

[1] K. Cammann, E. Hall, R. Kellner, H. L. Schmidt, and O. S. Wolfbeis, *The Cambridge Definition of Chemical Sensors, Cambridge Workshop on Chemical Sensors and Biosensors*. Cambridge University Press, New York, 1996.

[2] F. Baldini, A. N. Chester, J. Homola, and S. Martellucci, eds., *Optical chemical sensors. Proceedings of the NATO Advanced Study Institute on Optical Chemical Sensors, Chapter 6*. Springer, The Netherlands, 2006.

[3] O. S. Wolfbeis and R. Narayanaswamy, eds., *Optical Sensors: Industrial, Environmental and Diagnostic Applications*. Springer-Verlag, Berlin, 2004.

[4] D. Diamond, ed., *Principles of Chemical and Biological Sensors*. Wiley-Interscience, New York, 1998.

[5] J. Janata, *Principles of Chemical Sensors*. Plenum Press, New York, 1989.

[6] J. Janata, "Chemical sensors," *Analytical Chemistry*, vol. 64, no. 12, pp. R196–R219, 1992.

[7] C. McDonagh, C. S. Burke, and B. D. MacCraith, "Optical chemical sensors," *Chemical Reviews*, vol. 108, no. 2, pp. 400–422, 2008.

[8] J. R. Lakowicz, *Principles of Fluorescence Spectroscopy*. Springer-Verlag, New York, 3rd edition, 2006.

[9] B. Valeur, *Molecular Fluorescence. Principles and Applications*. Wiley-VCH, Weinheim, 2001.

[10] *"The Aurora Borealis, or Northern Lights, shines above Bear Lake, Eielson Air Force Base, Alaska"*. http://commons.wikimedia.org/wiki/Image:Polarlicht_2.jpg.

[11] *"Female glow-worm"*. http://nationalinsectweek.co.uk/images/gbbu/Bful_Lampyris-noctiluca.jpg.

[12] J. R. Lakowicz, ed., *Topics in Fluorescence Spectroscopy: Probe Design and Chemical Sensing, Vol. 4, Chapter 1*. Kluwer Academic Publishers Group, 1994.

[13] C. J. Brinker and G. W. Scherer, *Sol-Gel Science: The Physics and Chemistry of Sol-Gel Processing*. Academic Press, Boston, 1990.

[14] L. C. Klein and C. Sanchez, "Organic inorganic hybrid materials by the sol-gel process - introduction," *Journal of Sol-Gel Science and Technology*, vol. 5, no. 2, pp. U4–U4, 1995.

[15] J. D. Wright and N. Sommerdijk, *Sol-Gel Materials: Chemistry and Applications, Chapter 1*. CRC Press, Boca Raton, 2000.

[16] N. Ugarte, L. Polette, M. Ortega, A. Metha, C. Wing, and R. R. Chianelli, "In-situ identification of palygorskite in Maya Blue samples using X-Ray powder diffraction," *SSRL Activity Report*, p. 7307308, 1998.

[17] P. Gomez-Romero and C. Sanchez, "Hybrid materials. Functional properties. From Maya Blue to 21st century materials," *New Journal of Chemistry*, vol. 29, no. 1, pp. 57–58, 2005.

[18] *"Maya warriors standing guard over prisoners of war"*. http://encarta.msn.com/media_701610277/maya_warriors_in_bonampak_murals.html, Microsoft® Encarta® Online Encyclopedia, 2008.

[19] M. Ebelmen, "Untersuchungen über die Verbindung der Borsaüre und Kieselsaüre mit Aether," *Annales de Chimie et de Physique*, vol. 15, pp. 319–355, 1845.

[20] H. Dislich, "Preparation of multicomponent oxide glasses by polycondensation," *Angewandte Chemie-International Edition*, vol. 10, no. 11, p. 825, 1971.

[21] H. Dislich, "New routes to multicomponent oxide glasses," *Angewandte Chemie-International Edition*, vol. 10, no. 6, p. 363, 1971.

[22] J. D. Wright and N. Sommerdijk, *Sol-Gel Materials. Chemistry and Applications, Chapter 6 and 7*. CRC Press, Boca Raton, 2001.

[23] C. Sanchez, B. Julian, P. Belleville, and M. Popall, "Applications of hybrid organic-inorganic nanocomposites," *Journal of Materials Chemistry*, vol. 15, no. 35-36, pp. 3559–3592, 2005.

[24] M. M. Collinson, "Analytical applications of organically modified silicates," *Mikrochimica Acta*, vol. 129, no. 3-4, pp. 149–165, 1998.

[25] J. D. Mackenzie and E. P. Bescher, "Structures, properties and potential applications of Ormosils," *Journal of Sol-Gel Science and Technology*, vol. 13, no. 1-3, pp. 371–377, 1998.

[26] O. Lev, M. Tsionsky, L. Rabinovich, V. Glezer, S. Sampath, I. Pankratov, and J. Gun, "Organically modified sol-gel sensors," *Analytical Chemistry*, vol. 67, no. 1, pp. A22–A30, 1995.

[27] G. E. Badini, K. T. V. Grattan, A. C. C. Tseung, and A. W. Palmer, "Sol-gel properties for fiber optic sensor applications," *Optical Fibre Technology*, vol. 2, pp. 378–386, 1996.

[28] B. D. MacCraith, C. McDonagh, A. K. Mcevoy, T. Butler, G. O'Keeffe, and V. Murphy, "Optical chemical sensors based on sol-gel materials: Recent advances and critical issues," *Journal of Sol-Gel Science and Technology*, vol. 8, no. 1-3, pp. 1053–1061, 1997.

[29] C. M. Ingersoll and F. V. Bright, "Using sol gel-based platforms for chemical sensors," *CHEMTECH*, vol. 27, no. 1, pp. 26–31, 1997.

[30] M. M. Collinson, "Recent trends in analytical applications of organically modified silicate materials," *Trac-Trends in Analytical Chemistry*, vol. 21, no. 1, pp. 30–38, 2002.

[31] C. M. McDonagh, A. M. Shields, A. K. McEvoy, B. D. MacCraith, and J. F. Gouin, "Optical sol-gel-based dissolved oxygen sensor: Progress towards a commercial instrument," *Journal of Sol-Gel Science and Technology*, vol. 13, no. 1-3, pp. 207–211, 1998.

[32] C. R. French, J. J. Carr, E. M. Dougherty, L. A. K. Eidson, J. C. Reynolds, and M. D. DeGrandpre, "Spectrophotometric pH measurements of freshwater," *Analytica Chimica Acta*, vol. 453, no. 1, pp. 13–20, 2002.

[33] H. Stahl, A. Glud, C. R. Schröder, I. Klimant, A. Tengberg, and R. N. Glud, "Time-resolved pH imaging in marine sediments with a luminescent planar optode," *Limnology and Oceanography-Methods*, vol. 4, pp. 336–345, 2006.

[34] B. Hales, D. Chipman, and T. Takahashi, "High-frequency measurement of partial pressure and total concentration of carbon dioxide in seawater using microporous hydrophobic membrane contactors," *Limnology and Oceanography-Methods*, vol. 2, pp. 356–364, 2004.

[35] T. Ishiji, D. W. Chipman, T. Takahashi, and K. Takahashi, "Amperometric sensor for monitoring of dissolved carbon dioxide in seawater," *Sensors and Actuators B-Chemical*, vol. 76, no. 1-3, pp. 265–269, 2001.

[36] C. Gueguen and P. D. Tortell, "High-resolution measurement of Southern Ocean CO_2 and O_2," *Marine Chemistry*, vol. 108, no. 3-4, pp. 184–194, 2008.

[37] Y. Nakano, H. Kimoto, S. Watanabe, K. Harada, and Y. W. Watanabe, "Simultaneous vertical measurements of in situ pH and CO_2 in the sea using spectrophotometric profilers," *Journal of Oceanography*, vol. 62, no. 1, pp. 71–81, 2006.

[38] C. Higgins, D. Wencel, C. S. Burke, B. D. MacCraith, and C. McDonagh, "Novel hybrid optical sensor materials for in-breath O_2 analysis," *Analyst*, vol. 133, no. 2, pp. 241–247, 2008.

[39] B. M. Hoelper, B. Alessandri, A. Heimann, R. Behr, and O. Kempski, "Brain oxygen monitoring: in-vitro accuracy, long-term drift and response-time of Licox- and Neurotrend sensors," *Acta Neurochirurgica*, vol. 147, no. 7, pp. 767–774, 2005.

[40] F. Baldini, A. Falai, A. R. D. Gaudio, D. Landi, A. Lueger, A. Mencaglia, D. Scherr, and W. Trettnak, "Continuous monitoring of gastric carbon dioxide with optical fibres," *Sensors and Actuators B-Chemical*, vol. 90, no. 1-3, pp. 132–138, 2003.

[41] M. Cajlakovic, A. Bizzarri, and V. Ribitsch, "Luminescence lifetime-based carbon dioxide optical sensor for clinical applications," *Analytica Chimica Acta*, vol. 573, pp. 57–64, 2006.

[42] S. A. Grant, K. Bettencourt, P. Krulevitch, J. Hamilton, and R. Glass, "Development of fiber optic and electrochemical pH sensors to monitor brain tissue," *Critical Reviews in Biomedical Engineering*, vol. 28, no. 1-2, pp. 159–163, 2000.

[43] O. S. Wolfbeis, I. Klimant, T. Werner, C. Huber, U. Kosch, C. Krause, G. Neurauter, and A. Dürkop, "Set of luminescence decay time based chemical sensors for clinical applications," *Sensors and Actuators B-Chemical*, vol. 51, no. 1-3, pp. 17–24, 1998.

[44] A. G. Mignani and F. Baldini, "Fibre-optic sensors in health care," *Physics in Medicine and Biology*, vol. 42, no. 5, pp. 967–979, 1997.

[45] A. Mills, "Oxygen indicators and intelligent inks for packaging food," *Chemical Society Reviews*, vol. 34, no. 12, pp. 1003–1011, 2005.

[46] C. Bohnke, H. Duroy, and J. L. Fourquet, "pH sensors with lithium lanthanum titanate sensitive material: applications in food industry," *Sensors and Actuators B-Chemical*, vol. 89, no. 3, pp. 240–247, 2003.

[47] C. von Bültzingslöwen, A. K. McEvoy, C. McDonagh, B. D. MacCraith, I. Klimant, C. Krause, and O. S. Wolfbeis, "Sol-gel-based optical carbon dioxide sensor employing dual luminophore referencing for application in food packaging technology," *Analyst*, vol. 127, no. 11, pp. 1478–1483, 2002.

[48] H. R. Kermis, Y. Kostov, P. Harms, and G. Rao, "Dual excitation ratiometric fluorescent pH sensor for noninvasive bioprocess monitoring: Development and application," *Biotechnology Progress*, vol. 18, no. 5, pp. 1047–1053, 2002.

[49] X. D. Ge, Y. Kostov, and G. Rao, "Low-cost noninvasive optical CO_2 sensing system for fermentation and cell culture," *Biotechnology and Bioengineering*, vol. 89, no. 3, pp. 329–334, 2005.

[50] S. Lee, B. L. They, G. L. Cote, and M. V. Pishko, "Measurement of pH and dissolved oxygen within cell culture media using a hydrogel microarray sensor," *Sensors and Actuators B-Chemical*, vol. 128, no. 2, pp. 388–398, 2008.

[51] X. D. Ge, M. Hanson, H. Shen, Y. Kostov, K. A. Brorson, D. D. Frey, A. R. Moreira, and G. Rao, "Validation of an optical sensor-based high-throughput bioreactor system for mammalian cell culture," *Journal of Biotechnology*, vol. 122, no. 3, pp. 293–306, 2006.

[52] S. I. Wakida, M. Yamane, S. Takeda, Z. Siroma, Y. Tsujimura, and J. H. Liu, "Studies on pH and nitrate checkers made of semiconductor devices for acid rain monitoring," *Water Air and Soil Pollution*, vol. 130, no. 1-4, pp. 625–630, 2001.

[53] S. J. Litzelman, A. Rothschild, and H. L. Tuller, "The electrical properties and stability of $SrTi_{0.65}Fe_{0.35}O_{3-\delta}$ thin films for automotive oxygen sensor applications," *Sensors and Actuators B-Chemical*, vol. 108, no. 1-2, pp. 231–237, 2005.

[54] J. Mulrooney, J. Clifford, C. Fitzpatrick, and E. Lewis, "Detection of carbon dioxide emissions from a diesel engine using a mid-infrared optical fibre based sensor," *Sensors and Actuators A-Physical*, vol. 136, no. 1, pp. 104–110, 2007.

[55] J. Hradil, C. Davis, K. Mongey, C. McDonagh, and B. D. MacCraith, "Temperature-corrected pressure-sensitive paint measurements using a single camera and a dual-

lifetime approach," *Measurement Science Technology*, vol. 13, no. 10, pp. 1552–1557, 2002.

[56] A. Castaldo, E. Massera, L. Quercia, and G. D. Francia, "Development of pressure sensitive paints based on silicon nanostructured powders," *Sensors and Actuators B-Chemical*, vol. 118, no. 1-2, pp. 328–332, 2006.

[57] J. R. Smith, *Biotechnology*. Cambridge University Press, 1996.

[58] J. R. Lakowicz, ed., *Topics in Fluorescence Spectroscopy: Probe Design and Chemical Sensing, Vol. 4, Chapter 13*. Kluwer Academic Publishers Group, 1994.

[59] R. Ulber, J. G. Frerichs, and S. Beutel, "Optical sensor systems for bioprocess monitoring," *Analytical and Bioanalytical Chemistry*, vol. 376, no. 3, pp. 342–348, 2003.

[60] V. Vojinovic, J. M. S. Cabral, and L. P. Fonseca, "Real-time bioprocess monitoring. Part I: In situ sensors," *Sensors and Actuators B-Chemical*, vol. 114, no. 2, pp. 1083–1091, 2006.

[61] E. Trummer, K. Fauland, S. Seidinger, K. Schriebl, C. Lattenmayer, R. Kunert, K. Vorauer-Uhl, R. Weik, N. Borth, H. Katinger, and D. Muller, "Process parameter shifting: Part I. Effect of DOT, pH, and temperature on the performance of Epo-Fc expressing CHO cells cultivated in controlled batch bioreactors," *Biotechnology and Bioengineering*, vol. 94, no. 6, pp. 1033–1044, 2006.

[62] C. Neal, C. Watts, R. J. Williams, M. Neal, L. Hill, and H. Wickham, "Diurnal and longer term patterns in carbon dioxide and calcite saturation for the River Kennet, south-eastern England," *Science of the Total Environment*, vol. 282, pp. 205–231, 2002.

[63] H. P. Jarvie, C. Neal, D. V. Leach, G. P. Ryland, W. A. House, and A. J. Robson, "Major ion concentrations and the inorganic carbon chemistry of the Humber rivers," *Science of the Total Environment*, vol. 194, pp. 285–302, 1997.

[64] V. L. Snoeyink and D. Jenkins, *Water Chemistry, Chapter 4*. John Wiley Sons, New York, 1990.

[65] P. Schippers, J. E. Vermaat, J. de Klein, and W. M. Mooij, "The effect of atmospheric carbon dioxide elevation on plant growth in freshwater ecosystems," *Ecosystems*, vol. 7, no. 1, pp. 63–74, 2004.

[66] J. Colt, "Water quality requirements for reuse systems," *Aquacultural Engineering*, vol. 34, no. 3, pp. 143–156, 2006.

[67] J. Clingerman, J. Bebak, P. M. Mazik, and S. T. Summerfelt, "Use of avoidance response by rainbow trout to carbon dioxide for fish self-transfer between tanks," *Aquacultural Engineering*, vol. 37, no. 3, pp. 234–251, 2007.

Chapter 2

Background

2.1 Introduction

This chapter describes the background to all elements of the sensor development which is the subject of this thesis. Optical chemical sensors and, in particular, luminescence-based sensing is described and current state of the art is reviewed for luminescence-based O_2, pH and CO_2 sensors. A description is given of the sol-gel process, in particular, the elements which are relevant to sensor films development.

2.2 Luminescence

2.2.1 Mechanism of luminescence

Luminescence is the emission of light from electronically excited states of an atom or molecule [1]. It is characterised depending on the excitation method. If luminescence occurs after irradiation by light, it is called photoluminescence, which can be subdivided into fluorescence and phosphorescence, depending upon the electronic configuration of the excited state and the emission pathway.

At room temperature, the valence electrons are in the lowest vibrational level of the ground electronic state. A transition of these electrons from the ground state (S_0) to a higher energy level (S_1, S_2...) takes place upon absorption of light (A). Electronic and vibrational level transitions involved in luminescence phenomena are shown in Figure 2.1 on a so-called Jablonski diagram.
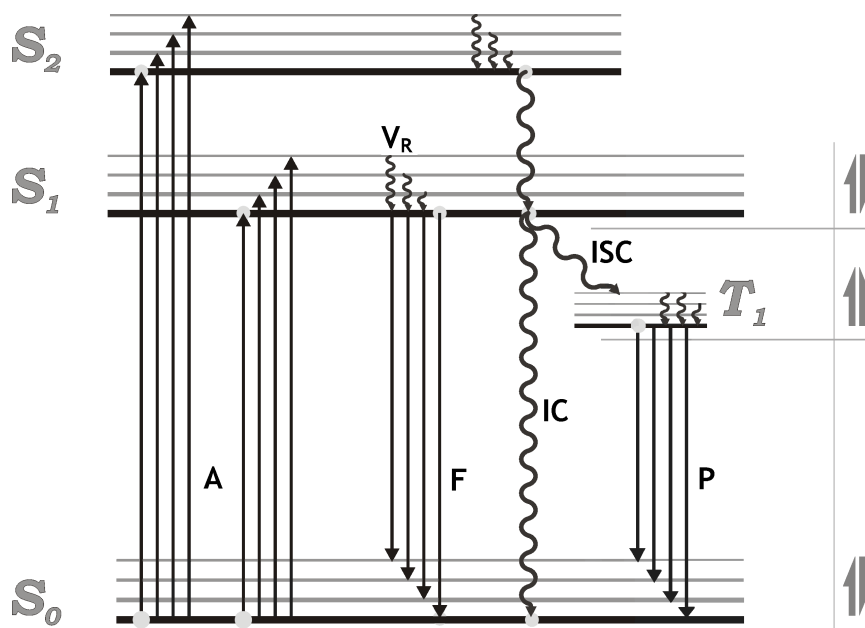
Figure 2.1: Jablonski energy level diagram. Symbols explained in text.

Following the absorption of a photon there are different pathways for de-excitation of a molecule:

1. **Radiative:**

   - **Fluorescence (F)** - transition when a molecule in the first excited singlet state (S_1) returns to the ground state (S_0) (molecules excited to higher vibrational levels of the first excited singlet state rapidly relax (V_R) to the lowest vibrational level of this state).

   - **Phosphorescence (P)** - transition from first excited triplet state (T_1) to the ground state. Radiative transitions between states of different multiplicity are, in principle, forbidden but sometimes they do take place.

2. **Non-radiative:**

   - **Internal conversion (IC)** - transition between two electronic states of the same spin multiplicity.

   - **Intersystem crossing (ISC)** - transition between two vibrational levels belonging to electronic states of different multiplicities ($S_1 \rightarrow T_1$).

The low probability of the intersystem crossing arises from the fact that molecules must first undergo spin conversion to produce unpaired electrons, an unfavorable process.

Usually luminophores can be excited and emit light many hundred to thousands of times before the highly reactive excited state molecule is photobleached and a molecule loses the ability to luminesce due to chemical damage or chemical modification.

The luminescence processes occur on timescales that are separated by several orders of magnitude. Excitation happens in femtoseconds, while vibrational relaxation can be measured in picoseconds. The emission of a longer wavelength photon and return of a molecule to the ground state occurs in the relatively long time period of nanoseconds [1]. Two features of the luminescence to note are that the same luminescence emission spectrum is observed irrespective of the excitation wavelength (Kasha's rule) and that the energy of the emission is less than that of absorption as the resulting emitted photons have less energy. Therefore luminescence occurs at longer wavelengths (lower energy). The energy gap between the maximum of the absorption band and the maximum of the emission band is called the Stokes shift. The size of the shift varies with molecular structure and can range from just a few nanometers to over several hundred nanometers. In optical sensing the large Stokes shift enables the use of precision bandwidth optical filters to effectively block excitation light from reaching the detector or in some cases filters are not required.

Three fundamental parameters are used in describing and comparing luminescent molecules [2]:

- **Extinction coefficient (ε)**
- **Quantum yield (Φ)**
- **Luminescence lifetime (τ)**

Extinction coefficients are a direct measure of the ability of a luminophore to absorb light. Quantum yield is expressed as the ratio of photons emitted to the number of

photons absorbed and is given by:

$$\Phi = \frac{\Gamma}{\Gamma + k_{nr}} \qquad (2.1)$$

where Γ is the emissive rate of the luminophore and k_{nr} is the rate of non-radiative decay to the ground state. Quantum yields typically range between a value of zero and one. Species with large Φ, approaching unity display the brightest emission.

Luminescence lifetime is the average time a molecule remains in the excited state. In the case of a single-exponential decay, the lifetime τ is defined as the time after which the fraction $1/e$ of the excited molecules still exists in the excited state. It determines the time available for the luminophore to interact or diffuse in its environment. Fluorescence lifetimes are typically around 10^{-8}-10^{-9} seconds, while phosphorescence lifetimes usually occur between milliseconds and seconds.

It is known, that the distinction between the fluorescence and phosphorescence is not always clear. Transition metal-ligand complexes such as $[Ru(dpp)_3]^{2+}$, which was used in this study for optical O_2 sensing, display mixed singlet-triplet states. These complexes also display intermediate lifetimes in the range of hundreds of nanoseconds to several microseconds. In this work, the term luminescence is used with regard to O_2 sensing. Fluorescence, which is characterised by much shorter lifetime is used for pH and dCO_2 sensors.

2.2.2 Luminescence quenching

The term luminescence quenching refers to any process that decreases the emission intensity of a given substance [1]. A variety of competing processes that induce non-radiative relaxation of the excited state electrons to the ground state can result in quenching. These mechanisms include static quenching, dynamic (collisional) quenching, energy transfer or electron transfer. The mechanism of quenching depends on the luminophore-quencher pair. Both static and dynamic quenching require molecular contact between the quencher and luminophore. In the case of static quenching,

the analyte interacts with the luminophore in its ground state and a non-luminescent complex, comprising the analyte and luminophore, is formed. In a dynamic quenching situation, the excited indicator returns to the ground state by collision with the analyte and this process does not chemically alter the molecules. A number of molecules are known that can act as collisional quenchers, for example, molecular oxygen, aromatic and aliphatic amines or halogens. Static quenching does not influence the lifetime of the luminophore, but decreases its emission intensity. Dynamic quenching, in contrast, reduces both the lifetime and luminescence intensity. Figure 2.2 illustrates the dynamic quenching process.
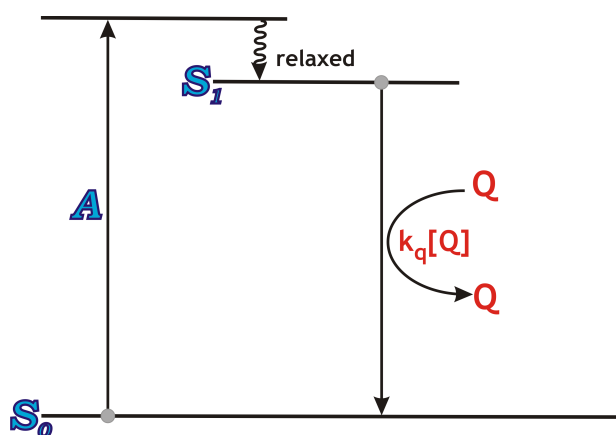

Figure 2.2: Simplified Jablonski diagram illustrating dynamic quenching. A - absorption of light, S_0 - singlet ground state, S_1 - first singlet excited state, k_q - bimolecular quenching constant, Q - quencher, [Q] - quencher concentration.

In this work O_2 sensing is based on the collisional quenching of luminescence of the ruthenium complex. The theory of collisional quenching is described in detail in section 2.3.2.

2.3 Optical chemical sensors

Optical sensors are based on substances that change their optical properties on interaction with the analyte [3–6]. The most commonly measured optical properties are absorbance, luminescence intensity and decay time, but in addition, reflectance, refractive index, light scattering, and light polarisation have also been used as ana-

lytical parameters [5, 7, 8]. One of the most attractive features of an optode is that it does not require a separate reference sensor and it does not suffer from electrical and electromagnetic interferences, unlike electrochemical sensors. Optical fibers allow transmission of optical signals over large distances and, therefore, optodes are ideal for remote sensing applications. Optodes are also attractive for other reasons: their ease of handling, capability of real-time measurements, their low energy consumption, low production cost, ease of miniaturisation and possibility of mass production. Their small size allows for the measurements of analyte concentration without significantly perturbing the sample. There are also disadvantages namely, the limited long-term stability caused by photobleaching or leaching of the dye. The sensor has to be optically isolated from the sample to avoid interference of ambient light. Turbid samples can also cause problems for absorbance and luminescence measurements.

Optodes, despite a few limitations, do have the potential to become very attractive tools, providing solutions for environmental and bio-pharmaceutical applications and, for these reasons, luminescence-based sensors have formed the focus of this work.

2.3.1 O_2, pH and CO_2 sensors - State of the Art

2.3.1.1 O_2 sensors

Several methods for O_2 determination have been reported [9]. Winkler titration is considered to be the standard method for the determination of dissolved O_2 [10]. However, this method is time consuming and cannot be used in process monitoring due to its cumbersome nature. The second method is the conventional electrochemical method, which uses the so-called Clark electrode [11]. O_2 determination in both gas and dissolved phase is based on the reduction of O_2 on the platinum cathode surface into hydroxide ions resulting in a current that is proportional to the O_2 concentration. Clark electrodes are available for the detection of O_2 in a broad range of applications. Unfortunately, like any other analytical technique, Clark electrodes have their disadvantages. They consume O_2, are prone to electrical interferences, are sensitive to flow, difficult to miniaturise and have limited operational lifetime because

the electrolyte has to be periodically replaced and the anode needs to be cleaned in order to prevent accumulation of a layer of silver chloride. Clark-type microelectrodes have been developed but they are expensive to fabricate, fragile and therefore their usefulness is limited. [12, 13]. For applications where these considerations are important, luminescence-based O_2 sensors have been developed as an alternative. They are attractive due to their high sensitivity, high selectivity and low-cost. O_2 optodes do not consume O_2, operate independently of sample flow rates and are easy to miniaturise.

Optical O_2 sensors based on luminescence quenching by O_2 of the emission intensity or excited state lifetime of the O_2-sensitive luminophore are the most widely used methods in the development of such optical sensors. For most optical O_2 sensors, hydrophobic O_2-permeable polymers have been used as a solid matrix for immobilising an O_2-sensitive indicator. The hydrophobic nature of such polymers reduces problems associated with dye leaching and quenching by interferents therefore improving selectivity. They also provide very good mechanical and chemical stability.

Optical sensing of O_2 started in 1930's [14]. Kautsky and Hirsch reported that O_2 quenched the phosphorescence of certain dyes which were adsorbed on silica gel. The first optical O_2 sensor system was developed by Bergman in 1968 [15]. He used fluoranthene as an O_2-sensitive indicator which was adsorbed on a porous glass. Nowadays, a wide variety of polymeric matrices have been explored including polystyrene [16], polysulfone and polyetherimide [17], poly(methyl methacrylate) [18], poly(vinyl chloride) [19], ion-exchange polymers [20] and cellulose acetate butyrate [21]. In addition, fluoropolymers are frequently used as they are photostable and exhibit high permeability towards O_2 [22]. Silicone rubber has been widely used as a matrix to entrap dyes as it displays much higher O_2 permeability than other organic polymers [23]. Sol-gel-derived matrices have also been very popular in optical O_2 sensing [24]. In particular, organically modified silicates, so called ORMOSILs, exhibit excellent physical and chemical properties for use in optical O_2 sensing (see section 2.5) [25–28].

2.3.1.2   pH sensors

The pH electrode is the most widely used device for pH determination as it is reliable, easy to operate, low cost and facilitates rapid measurement. It allows for a two-point calibration strategy and shows a wide working range. However, the size, rigid design and susceptibility to electrical interference and aggressive analytes such as alkaline solutions or fluoride ions limit its usefulness. It is also not suitable for long-term measurements due to electrode signal drift and measuring in small sample volumes can be difficult. Miniature ISFETs (Ion-Sensitive Field-Effect Transistors) have also been developed but the use of a reference electrode, which is difficult to miniaturise, limits their field of applications [29]. Optical pH sensors are an alternative solution. Nowadays, optical pH sensors can be miniaturised down to sub-micrometer dimensions, and combined with fiber-optic technology, can provide remote measurements. Optical pH sensors exhibit a sigmoidal response towards changes in pH and the dynamic range is usually limited to ca. pKa $\pm$ 1.5 (pKa - negative logarithm of an acid dissociation constant). The narrow dynamic range results in a high signal change with pH and a high sensor resolution and therefore is suitable for many applications. pH measurements depend on the pKa of the dye and the development of sensors for an extended pH range is also well established. This has been accomplished by using indicators with two pKa values [30] or by using a group of similar dyes with different pKa values [31].

The sensing principle of most pH sensors is related to excited state proton transfer photochemistry. Most of the pH optodes consist of a pH sensitive indicator, immobilised in a proton-permeable solid matrix, which reversibly interacts with the protons. Such a matrix dictates the characteristics of the sensor. The indicator changes its spectral properties, such as absorbance, fluorescence or reflectance with varying pH.

There are three widely used methods for the immobilisation of pH indicators in a solid matrix: adsorption, entrapment and covalent binding. Adsorption is not very reliable, as the dye may easily leach out. Covalent binding is usually complicated,

time consuming and needs an appropriate sensing reagent with a functional group suitable for the immobilisation. This method is reliable, as the dye is not likely to leach out. In contrast, entrapment is a relatively straightforward and rapid method to implement and was used in this work. One disadvantage of this technique is the possibility of slow indicator leaching.

The first colorimetric pH strips suitable for continuous pH measurements were developed in the 1970's [32]. In 1980 Peterson et al. reported on the first fiber optic absorption-based pH sensor which utilised phenol red as an indicator dye immobilised in polystyrene microspheres [33] and in 1982 Seitz et al. reported on the first fluorescence-based pH sensor using covalently immobilised fluoresceinamine in a cellulose matrix [34]. Polymer matrices used in optical pH sensing reported to date include: cellulose acetate [35], poly(vinyl alcohol) [36], poly(hydroxyethyl methacrylate) [37], Nafion [38], ethyl cellulose [39] and hydrogels such as polyurethane [40]. In addition sol-gel-derived matrices have been used as they allow fine tuning of their physical and chemical properties and therefore application-tuned sol-gel formulations can be developed [41, 42]. In particular, ORMOSILs are a very promising class of sol-gel materials as they have many advantages over their organic polymer counterparts (see section 2.5).

2.3.1.3 CO_2 sensors

Conventional CO_2 analysis is usually carried out using infra-red spectroscopy (IR) or electrochemical (Severinghaus electrode) measurements [43, 44]. The IR method uses the fact that CO_2 absorbs strongly at 4.26 μm. Unfortunately, it suffers from significant drawbacks such as: the bulky, expensive nature of the equipment used, its susceptibility to humidity and pressure interferences and difficulties in adapting the technique to dCO_2 analysis.

The Severinghaus type dCO_2 electrode makes use of the acidic nature of CO_2 and consists of a pH electrode in contact with a bicarbonate buffer solution, trapped behind a gas permeable but ion-impermeable layer. However, it has a long response

time (5 to 15 min), suffers from electrical and chemical interferences, is expensive, difficult to miniaturise and depends on the effects of osmotic pressure. Other devices for CO_2 analysis include gas chromatographs and mass spectrometers, both of which are very expensive and, in the case of chromatography, cannot be used for real time measurements. The search for optical CO_2 measurement methods to replace electrochemical and infrared absorption methods is a major issue in current research. Nowadays, optical systems are more attractive due to the availability of low-cost optoelectronic components, higher sensitivity, short response time and the fact that such sensors do not consume the analyte of interest.

Optical CO_2 sensors use pH sensitive dyes to determine pH variations. The pH sensitive dye can be based on absorbance or fluorescence measurements. In the first optical CO_2 sensors, so called 'wet sensors', a pH-sensitive dye was dissolved in a sodium bicarbonate solution. A gas-permeable, ion-impermeable membrane such as silicone or teflon was used to prevent leaching of the indicator dye and to avoid hydrogen ions interference. CO_2 diffuses through the membrane and changes the pH of the bicarbonate buffer solution resulting in a shift in the acid-base equilibrium of the pH indicator. One of the first such optical CO_2 sensors were reported in 1975 by Lübbers and Opitz [45]. Such CO_2 sensors have also been reported by other authors [46–48]. Single membrane sensors have also been developed and they rely on the formation of water droplets emulsified in hydrophobic polymers [49,50]. CO_2 sensing has been reported which is based on fluorescence quenching of a ruthenium complex by CO_2 [51]. The first solid-state CO_2 sensor which does not require the presence of the carbonate buffer was described by Kawabata et al. [52] and in 1991 Raemer and his co-workers published a patent where they reported on the use of an ion-pair and the addition of a liphophilic base, both entrapped in a hydrophobic matrix [53] which was later developed by Mills et al. [54–57]. They replaced aqueous buffer system with a quaternary ammonium hydroxide, such as tetraoctylammonium hydroxide. This approach minimises the effects of osmotic pressure as there is no aqueous buffer. The hydrophobic support acts as a barrier to ions so no additional ion-impermeable layer is required.

Reports employing this scheme were described using different polymers such as: ethyl cellulose [58, 59], silicone [60–62], polystyrene [63], poly(dimethylsiloxane) [64] and sol-gel-derived matrices [65–67]. The dynamic range of these CO_2 sensors depends on the type of buffer system used and on the pKa value of the pH-indicator [58, 68]. However, a limited shelf life of these sensors has been reported due to the presence of other acidic gases such as SO_2 or NO_2 in the atmosphere that irreversibly protonate the indicator.

2.3.2 Principles of optical O_2, pH and CO_2 sensing

Principles of optical O_2 sensing

Molecular oxygen is a very well known collisional quencher and as a triplet molecule is able to quench efficiently the luminescence of many luminophores. Advantages associated with using O_2 as a quencher include high collisional efficiency and high diffusion coefficient which results from its uncharged nature and very small molecular dimensions [1, 69]. The degree of quenching is dependent on O_2 concentration. This sensing mechanism has been widely used in conjunction with ruthenium(II) complexes, as they are effective, very well understood luminescent indicators for optical O_2 sensing [70–75]. In O_2 sensing, luminescence quenching results from collisions between the luminophore such as the ruthenium complex in its excited state and the quencher in its ground state - molecular oxygen. The ruthenium complex returns to the ground state without emission of a photon. O_2 is transformed from its ground state to its excited state. A schematic representation of the dynamic quenching process is shown in Figure 2.3.

The mechanism of quenching when using transition metal complexes as O_2-sensitive probes, is thought to be by intersystem crossing [1]. It appears that an encounter with the triplet O_2 molecule causes the excited singlet state to become an excited triplet. A schematic representation of this process using a Jablonski diagram is shown in Figure 2.4. Long-lived triplet states are also quenched by O_2 and there
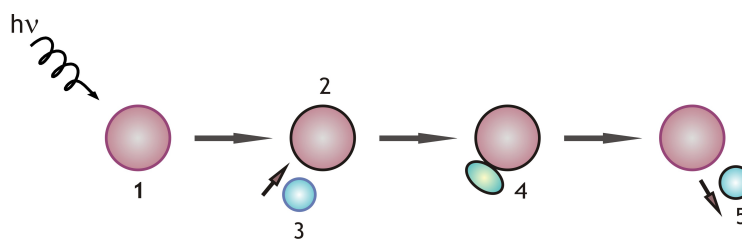
Figure 2.3: Schematic representation of the dynamic quenching phenomenon. 1 - luminophore in its ground state, 2 - luminophore in its excited state, 3 - quencher in its ground state, 4 - collision, 5 - quencher in its excited state.
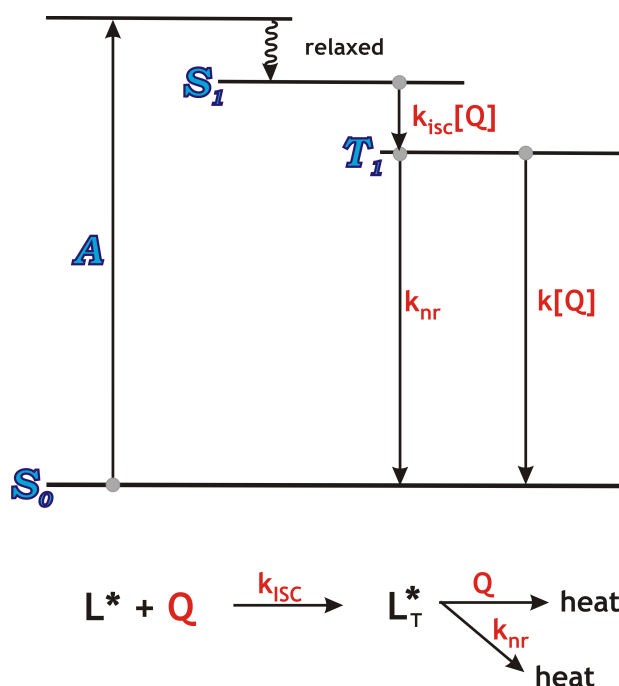

Figure 2.4: Simplified Jablonski diagram illustrating the mechanism of quenching by intersystem crossing. A - absorption of light, S_0 - singlet ground state, S_1 - first singlet excited state, T_1 - first triplet excited state, Q - quencher, k_{ISC} - rate of singlet to triplet intersystem crossing, k_{nr} - non-radiative decay rate, L^* - luminophore in the excited singlet state, L^*_T - luminophore in the excited triplet state.

is a probability that they can be quenched to the ground state by the same quencher or return to the ground state by non-radiative decay. Mixed mechanisms that include intersystem crossing, charge and electron transfer have also been reported [76–78]. If luminescence quenching is purely collisional, the emission intensity and excited state lifetime are related to the partial pressure of O_2 by the Stern-Volmer equation

(Equation 2.2) [79]:

$$\frac{I_0}{I} = \frac{\tau_0}{\tau} = 1 + K_{SV} \cdot pO_2 = 1 + k_q\tau_0 \cdot pO_2 \tag{2.2}$$

$$K_{SV} = k_q\tau_0 = k_q(k_r + k_{nr})^{-1} \tag{2.3}$$

where I_0, I, τ_0 and τ are the luminescence intensities and decay times of the luminophore in the absence and presence of O_2, respectively. K_{SV} is the Stern-Volmer constant, pO_2 is the partial pressure of O_2 and k_q is the bimolecular quenching constant. The excited state lifetime is dependent on the radiative (k_r) and non-radiative (k_{nr}) decay rates as shown by Equation 2.3. K_{SV} is related to τ_0 (Equation 2.2) and the diffusion coefficient, D, by Equation 2.4 hence the dynamic quenching mechanism is a diffusion-dependent process and is therefore affected by temperature. Higher temperatures result in faster diffusion and therefore larger amounts of collisional quenching.

$$k_q = 4\pi g R^* ND \tag{2.4}$$

In Equation 2.4, g is the spin statistical factor, R^* is the collision radius, and N is Avogadro's number.

The graphical representation of I_0/I or τ_0/τ versus pO_2 is called Stern-Volmer plot. For an ideal, homogeneous environment this plot yields a straight line with an intercept at 1 and a slope of K_{SV}, which represents sensor sensitivity. If the luminophore is distributed in the solid matrix, where the embedded luminescent species encounters different environmental influences, the host microheterogeneity will cause different sites to be quenched differently with a resultant downward curve in the Stern-Volmer plot [19, 80–85]. Different models were developed and have been used to describe such processes [80, 81, 83, 86–89]. In this study, the two-site model of Demas et al. described by Equation 2.5 was used in addition to the Stern-Volmer model to analyse the O_2 quenching data:

$$\frac{I_0}{I} = \frac{\tau_0}{\tau} = \left[\frac{f_1}{1 + K_{SV1} \cdot pO_2} + \frac{f_2}{1 + K_{SV2} \cdot pO_2}\right]^{-1} \tag{2.5}$$

where f_1 and f_2 (f_2 = 1 - f_1) denote the fractional distribution of the total emission from the luminophore located at different sites 1 and 2, respectively. K_{SV1} and K_{SV2} are the Stern-Volmer quenching constants for these sites. This model is based on the assumption that the luminophore is distributed in the solid matrix at two different sites and that each fraction shows a different quenching constant. Demas et al. found from their work that a two-site model well describes all their quenching data [83, 90]. However, they say that it is easy to over-interpret the parameters derived from the model. In addition, one has to be aware that a broad Gaussian distribution of sites can also be well-represented by two exponentials [82].

Principles of optical pH sensing

pH indicators are typically weak organic acids or bases with distinct optical properties associated with their protonated and deprotonated forms. In most cases, pH sensitivity is based on a colour or fluorescence intensity change with a change in the concentration of hydrogen ions. A schematic representation of fluorescence-based pH sensing is shown in Figure 2.5.
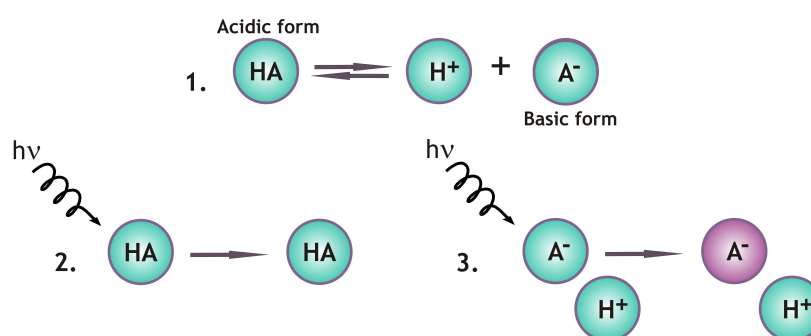

Figure 2.5: Schematic representation of fluorescence-based pH sensing. 1 - pH indicator at equilibrium e.g., weak acid HA at equilibrium with its conjugate base A^-, 2 - protonated (acidic) form HA when excited does not change its fluorescence properties, 3 - deprotonated (basic) form A^- changes its fluorescence properties upon excitation.

pH indicators may be characterised on the basis of their pKa's. For a particular application, the pKa of an indicator should be close to the pH range that the appli-

cation requires. An approximate definition is that the working range of the pH dye in solution is $\pm$ 1.5 pH unit of the pKa.

pH is defined in terms of hydrogen ion activity a_{H+} [3]:

$$pH = -\log a_{H+} \tag{2.6}$$

where a_{H+} is the activity of the hydrogen ions (sometimes called protons, H^+ or more correctly hydronium ions, H_3O^+). Activity and concentration are linked by the activity coefficient f_{H+}:

$$a_{H+} = f_{H+} \cdot [H^+] \tag{2.7}$$

Optical pH measurement uses the well known Henderson-Hasselbalch equation:

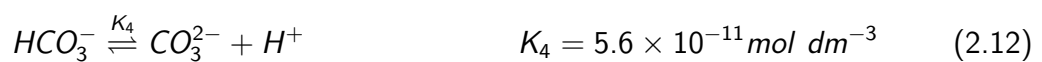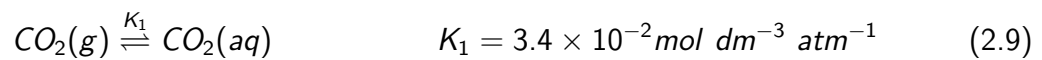$$pH = pKa + \log \frac{a_{A^-}}{a_{HA}} = pKa + \log \frac{c_{A^-} \cdot f_{A^-}}{c_{HA} \cdot f_{HA}} \tag{2.8}$$

where Ka is the thermodynamic constant, $pKa = -\log Ka$, (a stronger acid will have a lower pKa, while a weaker acid will have a higher pKa), a_{A^-} and a_{HA} are the activities and f_{A^-} and f_{HA} are the activity coefficients of the basic and acidic form of the pH indicator, respectively. The activity coefficient, f, is close to unity only in dilute solutions.

It is important to notice the fundamental difference between electrochemical and optical determination of pH. The pH electrode yields a response which is directly linked to the activity of protons in aqueous solutions whereas the optical technique measures the concentration of the acidic and basic forms of the pH indicator and the pH value is defined in terms of activities [91]. Therefore, optical pH sensors are cross-sensitive towards ionic strength, which is related to activity coefficient. Ionic strength influences activity coefficients resulting in the shift in a calibration plot and pKa is only valid for a given ionic strength and temperature of the buffer solutions. Ionic strength cross-sensitivity can cause pH errors of up to 1.5 pH units and depends on the pH indicator charge and its environment or the electrolyte concentration of

the sample [92]. It is important to use buffer solutions of constant ionic strength when calibrating an optical pH sensor. In order to keep ionic strength constant a background electrolyte such as potassium chloride has to be introduced into the calibrating buffer solutions. Recently, Wolfbeis et al. published a paper where an optical pH sensor has been presented with negligible sensitivity to ionic strength [40].

Principles of optical CO_2 sensing

The principle behind most of the optical CO_2 sensors centers on the acidic nature of dissolved CO_2. They utilise pH indicator dyes that change their absorption or fluorescence properties when the pH changes upon its exposure to different levels of CO_2. The CO_2 affects the pH of a buffered aqueous medium via the carbonic acid formation and its subsequent deprotonation reactions. The following reversible reactions occur:

$$CO_2(g) \overset{K_1}{\rightleftharpoons} CO_2(aq) \qquad\qquad K_1 = 3.4 \times 10^{-2} mol\ dm^{-3}\ atm^{-1} \qquad (2.9)$$

$$CO_2(aq) + H_2O \overset{K_2}{\rightleftharpoons} H_2CO_3 \qquad\qquad K_2 = 2.6 \times 10^{-3} \qquad (2.10)$$

$$H_2CO_3 \overset{K_3}{\rightleftharpoons} HCO_3^- + H^+ \qquad\qquad K_3 = 1.7 \times 10^{-4} mol\ dm^{-3} \qquad (2.11)$$

$$HCO_3^- \overset{K_4}{\rightleftharpoons} CO_3^{2-} + H^+ \qquad\qquad K_4 = 5.6 \times 10^{-11} mol\ dm^{-3} \qquad (2.12)$$

where K_i is the equilibrium constant.

The concentration of protons generated in this process can be measured optically employing a pH sensitive dye with pKa values between 7.5 and 9, which changes its optical properties with pH as a result of the following process:

$$HA \rightleftharpoons H^+ + A^- \qquad\qquad\qquad (2.13)$$

where HA and A^- are the protonated and deprotonated forms of the dye, respectively. Besides the pH sensitive dye present in the CO_2 sensing element, a base must also be

added so that the dye is initially in its deprotonated form, A^-. The overall reaction is given by:

$$A^- + H_2O + CO_2 \rightleftharpoons HA + HCO_3^- \tag{2.14}$$

where the deprotonated A^- and protonated HA forms of the indicator exhibit different absorption or emission spectral properties.

In solid state CO_2 sensors, carbonate buffer is replaced with the liphophilic organic base such as a quaternary ammonium hydroxide (Q^+OH^-) that act as the buffer system. In this method, the base is used to:

- Help dissolve the indicator dye within the hydrophobic matrix by the formation of the ion-pair between the quaternary ammonium cation and the pH dye anion, along with water which is required for the production of H_2CO_3 and deprotonation of the pH indicator. It is possible because the ion-pair is associated with a few molecules of water and is given by formula $Q^+A^- \cdot xH_2O$ (Q^+ = quaternary ammonium cation and A^- = pH dye anion)

- Provide the basic environment within the matrix that is essential for the sensor to work.

The overall process can be described by the following equilibrium process:

$$Q^+A^- \cdot xH_2O + CO_2 \overset{K}{\rightleftharpoons} +Q^+HCO_3^- \cdot (x-1)H_2O \cdot HA \tag{2.15}$$
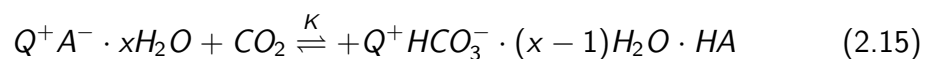
where K is the equilibrium constant of this process. A schematic of the principle of the solid fluorescent CO_2 sensor is shown in Figure 2.6.

Solid optical CO_2 sensors can be employed both in gas and dissolved phase sensing. In gas phase, the response time is usually of the order of seconds. Such sensors used for dCO_2 measurements exhibit negligible sensitivity to changes in osmotic pressure in contrast to the Severinghaus electrode which suffers from these effects.
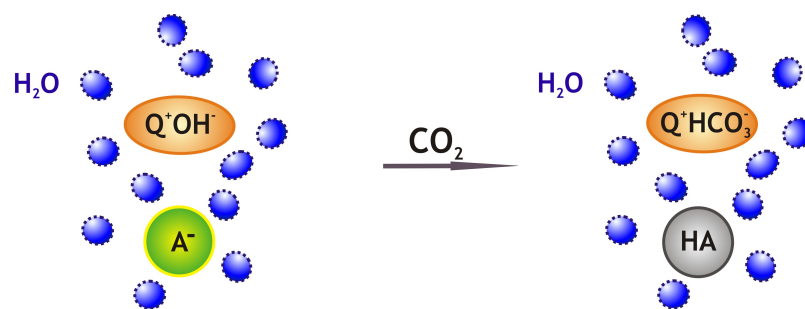
Figure 2.6: Schematic representation of fluorescence-based CO_2 sensing. HA - pH dye in its acidic form, A^- - pH dye in its basic form, Q^+OH^- - organic base, $Q^+HCO_3^-$ - base and HCO_3^- ion pair.

2.3.3 Dyes and complexes for optical sensing of O_2, pH and CO_2

O_2 indicators

Ideal sensor-probe characteristics for luminescence-based O_2 sensing should include high luminescence efficiencies and long excited state τ values, specific environmental sensitivity and binding properties and chemical and photochemical robustness. At the earliest stage of optical O_2 sensor development, polycyclic aromatic hydrocarbons (PAHs) such as diphenylantracene [93], decacyclene [94] and pyrene [95] were used. However, they exhibited poor photostability, short decay times and non-linear response.

Nowadays, the field of optical O_2 sensors is dominated by luminescent platinum group metal complexes with α-diimine ligands [96]. The most useful are luminescent ruthenium(II) diimine complexes with the excited state lifetimes in the microseconds range. In addition, phosphorescent platinum(II) and palladium(II) porphyrins are widely used because of their long lifetimes (in the range of hundred to thousand µs) and their consequent high O_2 sensitivity [97, 98]. Desirable features of all these materials for use in O_2 sensing applications include: long excited state lifetimes, which make lifetime measurements relatively simple and low-cost in comparison to short lifetimes (low nanosecond range) of the organic fluorophores, large Stokes shifts and high quantum efficiency. In addition, they possess intense visible absorptions that

simplifies sensor design and are chemically, thermally and photochemically stable. They exhibit chemical flexibility, that allows for the design of systems with desired absorption-emission properties that are compatible with available excitation sources and detectors and for ionic or covalent attachment to the desired solid support. In particular, the most widely used O_2 probes are: ruthenium(II) tris(2,2'-bipyridyl), $[Ru(bpy)_3]^{2+}$ [47, 90], ruthenium(II) tris(1,10-phenanthroline), $[Ru(phen)_3]^{2+}$, [99] and ruthenium(II) tris(4,7-diphenyl-1,10-phenantroline), $[Ru(dpp)_3]^{2+}$ [80, 100], platinum(II) octaethylporphyrin, (PtOEP) [101], very photostable platinum(II) tetrakis-(pentafluorophenyl)porphyrin, (PtTFPP) [102] and palladium(II) octaethylporphyrin, (PdOEP) [103]. Recently Klimant et al. reported on novel ultrabright cyclometalated iridium(III) coumarin complexes as new probes for optical O_2 sensing [104].

In this study, the ruthenium complex [Ru(II)-tris(4,7-diphenyl-1,10-phenanthroline)] dichloride ($[Ru(dpp)_3]^{2+}$) (Figure 2.7), was used as the O_2-sensitive luminescent indicator. This is due to its high stability, long excited state lifetime ($\tau_0 \sim 5$ μs), high quantum yield (0.4) and large Stokes shift as its absorption maximum occurs at 450 nm, which is compatible with low-cost blue light emitting diodes (LEDs), and its emission at 610 nm [105].

The strong absorption band at 450 nm has been assigned to a spin-allowed d-π^* Metal-to-Ligand Charge Transfer (MLCT) transition [106]. Upon absorption of light one of the ligands is reduced and ruthenium is oxidised. The resulting orange-red luminescence arises from a radiative π^*-dπ electronic transition and is formally phosphorescence as the lowest excited state responsible for

Figure 2.7: Chemical structure of $[Ru(dpp)_3]^{2+}$.

the emission is regarded as a triplet (^{3}MLCT) level generated by intersystem crossing. The luminescence of MLCTs is shorter-lived than phosphorescent states due to spin-orbit coupling with the ruthenium atom, which increases the probability of the normally forbidden transition to the ground state [105].
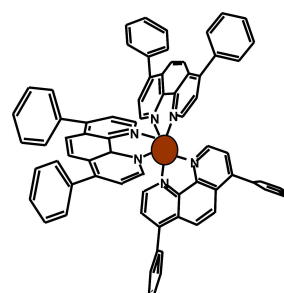
As well as luminescent O_2 indicators, colorimetric dyes have also been reported including hemoglobin [107], myoglobin [108] and redox dye-based indicators [109]. However, the first two indicators are not stable and all of them require special storage conditions.

pH and CO_2 indicators

Classical optical pH sensors are based on changes in absorbance and use indicators such as phenol red [110], bromocresol green [111], bromothymol blue and cresol purple [112], congo red [113] and phenolphthalein [114]. As discussed earlier, fluorescent pH indicators offer better selectivity and sensitivity than absorption-based pH indicators. The most widely used fluorescent pH indicators are: 1-hydroxypyrene-3,6,8-trisulfonic acid (HPTS) [115], fluorescein and derivatives thereof [116, 117], seminaphthofluorescein (SNAFL) [118] and seminaphthorhodafluor (SNARF) [119]. Recently novel pH-sensitive dyes have been reported based on iminocoumarin and liphophilic fluorescein derivatives [120, 121]. UV-excitable pH probes with multiple pKa values from 1.7 to 9.0 [30], pH-sensitive ruthenium metal-ligand complex and a pH-dependent lanthanide have been also reported [122, 123].

HPTS is the most widely used pH-sensitive dye and its acid-base equilibrium is shown in Figure 2.8. The sulfonate groups impart solubility in water and the hy-
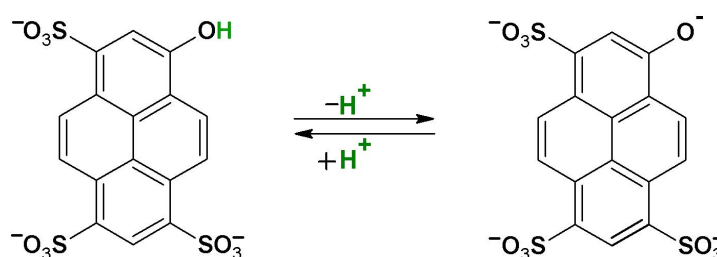

Figure 2.8: Acid-base equilibrium of HPTS.

droxyl group provides pH sensitivity. The pH-dependent fluorescence properties are described in detail in ref. [124, 125]. HPTS is an inexpensive, O_2-insensitive and non-toxic pH indicator with pKa of ~ 7.3 which makes it suitable for pH determination in

the physiological pH range. In addition, large Stokes shift and compatibility with the blue LED excitation make it a very attractive pH indicator for practical applications. Depending on the pH, HPTS exhibits two different absorption maxima, one at 404 nm for the acidic form, the other at 455 nm for the basic form and it exhibits one emission maximum at 515 nm. These spectroscopic properties make it suitable for wavelength-ratiometric measurements (see section 2.4.3). The pH-dependent absorption and emission spectra of HPTS are illustrated in Figure 2.9.
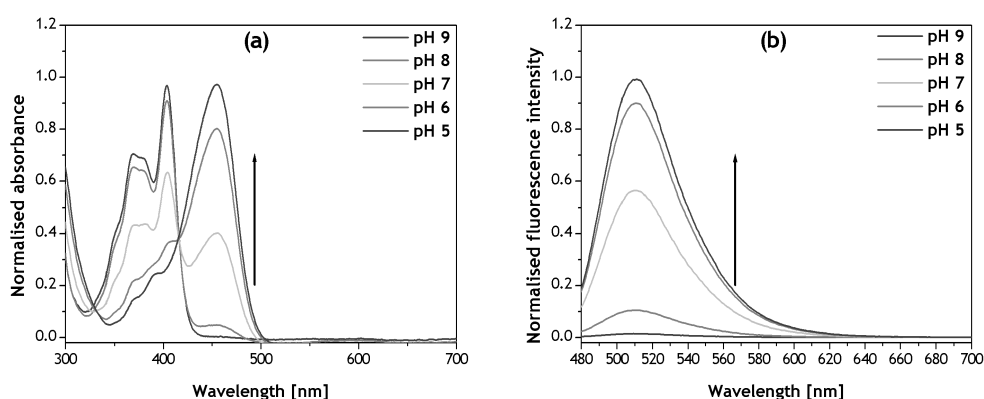

Figure 2.9: Normalised (a) absorption spectra and (b) fluorescence emission spectra (λ_{exc} = 460 nm) of HPTS in 0.15 M phosphate buffers at different pH values. Concentration of HPTS = 1.64×10^{-5} mol/L.

CO_2 is usually sensed via the acid-base chemistry occurring inside a sensor layer. Therefore, pH-sensitive probes (with pKa between 7.5 and 9.0) are used for optical CO_2 sensing. The number of these probes is limited as only some pH indicators satisfy this pKa requirement and exhibit good photostability. Most optical CO_2 sensors utilise HPTS due to the above mentioned properties [56, 126, 127]. Other dyes used include: SNAFL-1 [128], a europium(III) complex combined with three colorimetric pH indicators [129] and a ruthenium complex combined with Sudan(III) employing fluorescence energy transfer [65]. Colorimetric indicators were also applied such as: thymol blue [130], phenol red [131] and cresol red [54] but such dyes exhibit lower sensitivity toward CO_2 when compared to fluorescent indicators.

In this study, a liphophilic HPTS derivative has been used as an indicator for

pH and dCO_2 sensing. It exhibits the same pH-dependent optical properties as the unmodified HPTS indicator and is described in section 4.3.1.

2.4   Measurement techniques for optical O_2, pH and CO_2 sensors

2.4.1   Introduction

Luminescence-based chemical sensors have been extensively researched in recent years due to their importance in industrial, environmental and biomedical applications. These sensors combine the high intrinsic sensitivity of the luminescence process with the wide availability of optoelectronic components, thereby enabling the design of a broad range of sensor configurations. However, direct luminescence measurements are prone to many interferences such as: external quenchers, inner filter effects and effects of temperature. Fluctuations in the optoelectronic system can cause a signal drift and also turbid samples can cause problems. Furthermore, leaching and photobleaching also have an effect on the intensity reading. The measurement of the luminescence lifetime rather than luminescence intensity enables the elimination of many of these issues and therefore offers certain advantages with respect to the performance of the sensors. Ratiometric measurement methods are recommended whenever possible, as they also have a number of advantages over unreferenced intensity measurements.

In this work phase fluorometry, which facilitates indirect monitoring of the luminescence lifetime and allows the use of low-cost optoelectronic components is used for O_2 sensing and a referenced dual excitation scheme is used for pH sensing. The dCO_2 optical sensor was based on the use of a fluorescence intensity detection technique. However, the extension of the dCO_2 work will involve the development of a ratiometric dual excitation probe.

2.4.2 Luminescence lifetime measurement techniques

Time-resolved measurements are advantageous over steady-state measurements. As the luminescence lifetime of a luminophore is an intrinsic property it is virtually independent of fluctuations in light intensity, detector sensitivity, leaching, photobleaching, concentration of the luminophore and changes in optical alignment. In addition, it is less susceptible to inhomogeneous indicator distribution, turbidity or coloration of the sample and varying thickness of the sensor film. Therefore, the long-term stability of such sensors is much improved compared with that of luminescence intensity-based sensors.

There are two widely used methods for the measurement of luminescence excited-state lifetime: the pulse (or time-domain) method and the phase modulation (or frequency-domain) method. This section highlights the principle underlaying the determination of the excited state lifetime in each domain.

2.4.2.1 Time-domain measurements

In the time-domain method, the luminophore is excited with a short pulse of light and the time-dependent decay of the luminescence intensity is measured [132]. For a single exponential decay this process is described by Equation 2.16:

$$I(t) = I_0 \exp(-t/\tau) \tag{2.16}$$

where I_0 is the luminescence intensity at time zero and τ is the luminescence excited state lifetime. Therefore, the luminescence lifetime can be calculated from the slope of a plot of $\log I(t)$ versus time or by fitting the data to assumed decay models. Figure 2.10 displays the time-domain lifetime measurement principle.

Often, the intensity decay is not well described by a single exponential decay law. This is the case, for example, when the luminophore is in an inhomogeneous environment where each luminophore molecule experiences a slightly different microenvironment. In this case, the observed intensity is described by a sum of exponentials with
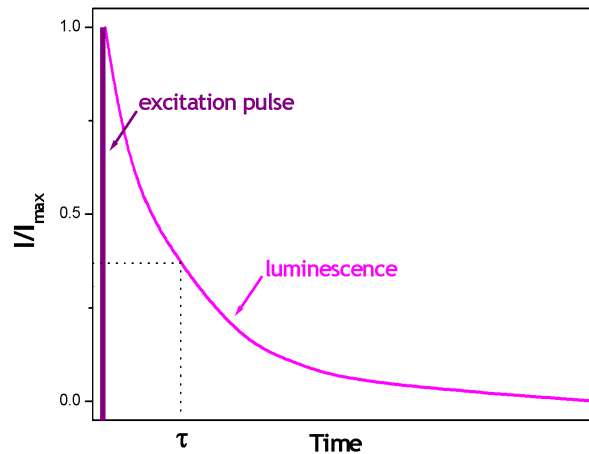
Figure 2.10: Principle of luminescence lifetime measurement of a single exponential decay.

n components and is given by Equation 2.17:

$$I(t) = \sum_{i=1}^{n} \alpha_i \exp(-t/\tau_i) \tag{2.17}$$

where α_i is the pre-exponential factor which denotes the contribution to the total time-resolved decay of the component with lifetime τ_i. It is generally difficult to resolve the sums of exponentials because the parameters describing the decay are highly correlated.

2.4.2.2 Frequency-domain measurements

In frequency-domain measurements, which were used in this work for O_2 sensing, the sample is excited by a sinusoidally modulated light at frequency f [1]. The principle of this technique is illustrated in Figure 2.11. The luminescent molecules are excited with light having a time-dependent intensity I(t):

$$I(t) = A\sin(\omega t) \tag{2.18}$$

where A is the amplitude of the excitation signal, ω is the angular frequency.

Excitation with sinusoidally modulated light results in a luminescence signal which
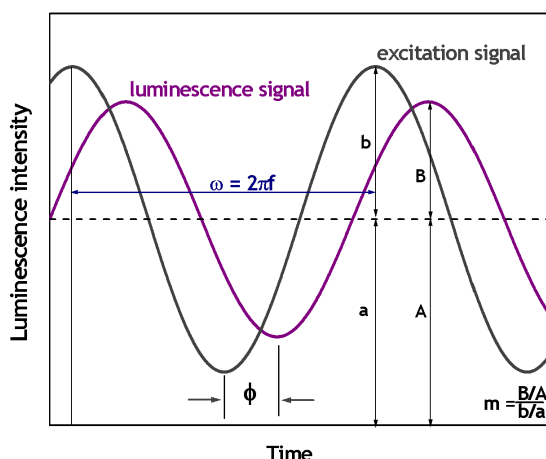
Figure 2.11: Principle of the phase fluorometric technique. The sinusoidally modulated light is phase shifted (φ) and demodulated (m), a is the average intensity of the incident light, b is the modulated amplitude of the incident light, A is the average intensity of the emission and B is the modulated amplitude of the emission.

is also sinusoidally modulated with the same frequency but is phase shifted by an angle φ relative to the excitation signal. The finite lifetime of the sample also results in demodulation of the emission which does not precisely follow the excitation. This results in a decrease in the amplitude of the modulated emission relative to the incident light and is called demodulation, m. The amplitude (B/A) of the emission is smaller than the amplitude of the excitation (b/a). The phase shift and the modulation of the emission depend on the relative values of the lifetime and the light modulation frequency. The phase shift is related to the lifetime by:

$$\tau = \frac{\tan \phi}{2\pi f} \tag{2.19}$$

where f is the modulation frequency. The demodulation factor can also be used to calculate the lifetime of the luminophore using Equation 2.20:

$$\tau = \frac{1}{2\pi f} \left[\frac{1}{m^2} - 1 \right]^{1/2} \tag{2.20}$$

In practice, phase fluorometry, as indirect monitoring of the luminescence lifetime, is a very attractive measurement technique as it needs relatively simple low-cost instru-

mentation in contrast to instruments used for direct luminescence lifetime measurements which require expensive high-speed electronics. In phase fluorometry, LEDs can serve as the excitation light sources and photodiodes for the detection of the emitted light. In addition, suitable excitation and emission filters and a lock-in amplifier are used. Electronic cross talk and ambient light have little effect on the obtained signal. Phase fluorometry necessitates that the lifetime of the luminophores be in the μs or hundreds of ns region in order to avoid using very high frequency and hence minimise the cost of the instrumentation. O_2-sensitive indicators fulfill this requirement. Unfortunately, pH indicators usually exhibit shorter lifetime in the ns range and therefore ratiometric measurements are more suited and are discussed in the next section.

2.4.3 Referencing via ratiometric measurements

Ratiometric measurement methods are recommended whenever possible, as they have a number of advantages over unreferenced intensity measurements. They are independent of dye concentration, leaching, photobleaching and instrument fluctuations [2]. There are three different ratiometric methods and they require dyes with suitable spectral characteristics:

- Two excitation and one emission wavelength
- One excitation and two emission wavelengths
- Two excitation and two emission wavelengths.

In this study, the dual excitation technique with one emission wavelength was used and the principle of this method is shown in Figure 2.12. In dual excitation measurements, the pH indicator must exhibit two different absorption maxima. The ratio of the emission intensities at two excitation wavelengths can then be used to measure pH according to the modified Henderson-Hasselbalch Equation:

$$pH = pKa + \log \frac{R - R_{HA}}{R_{A^-} - R} + \log \frac{I_{HA}(\lambda_2)}{I_{A^-}(\lambda_2)} \qquad (2.21)$$

where R is the ratio $I(\lambda_1)/I(\lambda_2)$ of the fluorescence intensities at the two excitation wavelengths λ_1 and λ_2, R_{HA} and R_{A^-} are the values of R when only the acidic form or basic form is present, respectively. $I_{HA}(\lambda_2)/I_{A^-}(\lambda_2)$ is the ratio of the fluorescence intensity of the acidic form alone to the intensity of the basic form alone at the wavelength λ_2.
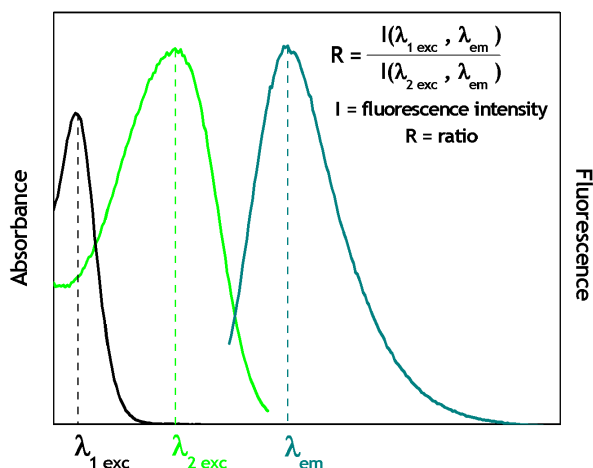

Figure 2.12: Principle of dual excitation measurements.

There are several fluorescent pH indicators that facilitate ratiometric measurements such as: fluorescein (excitation ratio 490 nm/435 nm), SNAFL dyes (excitation ratio 490 nm/540 nm or emission ratio 540 nm/630 nm), SNARF dyes (excitation ratio 600 nm/510 nm or emission ratio 550 nm/670 nm) and HPTS (excitation ratio 405 nm/455 nm). HPTS ion paired with cetyltrimethylammonium bromide, the pH-sensitive dye used in this work is suitable for dual excitation measurements relating the ratio of fluorescence intensities emitted at 510 nm when excited at 405 nm (acidic form) and 455 nm (basic form).

Another technique employed in this study for pH measurements was Dual Lifetime Referencing (DLR), a new frequency-domain dual lifetime scheme to reference fluorescence intensities via decay times [133]. The DLR scheme uses two luminophores with different decay times: an inert long-lived (decay time in the μs or ms range) luminescent standard and a fluorescent pH indicator (fast decay time of a few ns, most pH

indicators have short lifetimes, in the nanosecond ranges: for example approximately 5 nanoseconds for HPTS). Both luminophores must have overlapping excitation and emission spectra, allowing for simultaneous excitation with a single light source and detection with one photodetector. As in phase fluorometry, the excitation light is sinusoidally modulated and, therefore, the emission is modulated and phase shifted. The principle of DLR measurements is shown in Figure 2.13. There is a linear relation
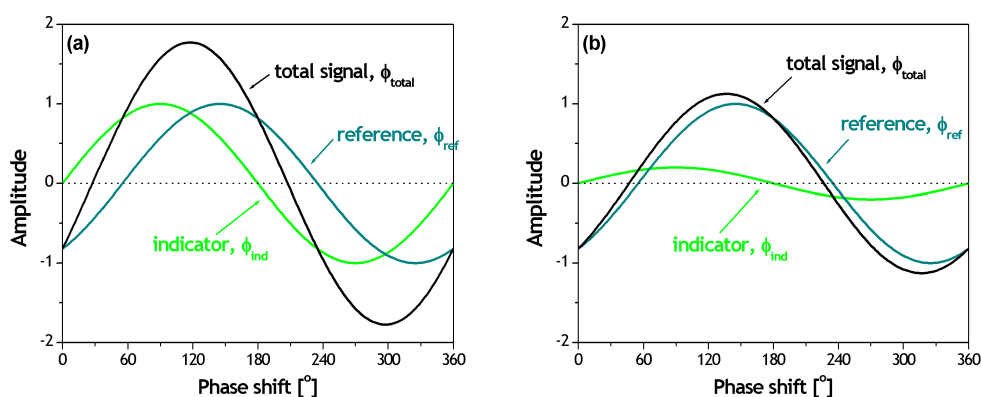

Figure 2.13: Principle of DLR measurements. Phase shift of the indicator (ϕ_{ind}), the reference (ϕ_{ref}) and the overall luminescence (ϕ_{total}) in (a) absence and (b) presence of the analyte.

between the cotangent of the phase shift angle and the fluorescence intensity of the pH indicator:

$$\cot \phi_{total} = \cot \phi_{ref} + \frac{1}{\sin \phi_{ref}} \cdot \frac{A_{pH}}{A_{ref}} \qquad (2.22)$$

where ϕ_{total} is the overall phase shift, A_{pH} and A_{ref} are the pH-dependent and reference luminescence intensities, respectively, expressed as their amplitudes.

The DLR scheme has been applied to optical sensors for different analytes including pH [121], CO_2 [126] and Cu^{2+} [134].

In this study, most of the pH measurements were taken using the dual excitation technique, but some measurements were made also using the DLR scheme. In this case, the fluorescent pH sensitive dye encapsulated in a sol-gel matrix was combined with the luminescent standard $[Ru(dpp)_3]^{2+}$.

2.5 The sol-gel process and sol-gel-derived sensors

2.5.1 Introduction

Sol-gel-derived materials play an important role in the design and fabrication of optical chemical sensors. They are used as host matrices for the immobilisation of the analyte-sensitive indicators allowing for free diffusion of the analyte to and from the indicator molecule. Compared with polymers, sol-gel-based matrices exhibit better optical transparency (down to 300 nm) and better thermal, mechanical and chemical stability [135]. These factors along with simplicity of the process, low fabrication temperature, ease of entrapment of the recognition element in the porous sol-gel cage-like microstructure and versatility of coating and deposition techniques on a variety of sensor platforms contribute to the suitability of sol-gel as host matrix for optical chemical sensing.

This section describes the sol-gel process along with the parameters that influence the resulting sol-gel microstructure. Finally, entrapment of the sensing molecules within the sol-gel matrix is described, which is the final step in the development of the luminescence-based sensor films used in this work.

2.5.2 The sol-gel process

The sol-gel process has been widely studied, as it is well suited to the preparation of materials and the design of devices with very specific, application-tuned properties [136–138]. It is a chemical synthesis technique for the preparation of inorganic or inorganic-organic materials with high purity through the hydrolysis and condensation of semi-metal or metal

Figure 2.14: TEOS chemical structure.

alkoxides at low temperature. Silicon alkoxides, $(Si(OR)_4)$ are the most widely used, in particular tetraethoxysilane (TEOS) shown in (Figure 2.14). Therefore, the funda-
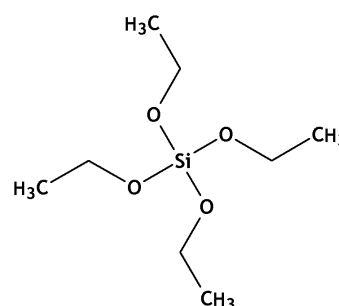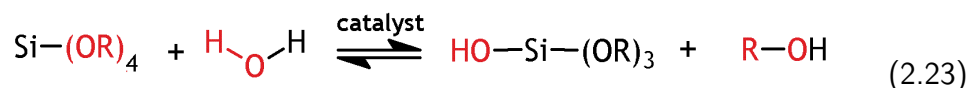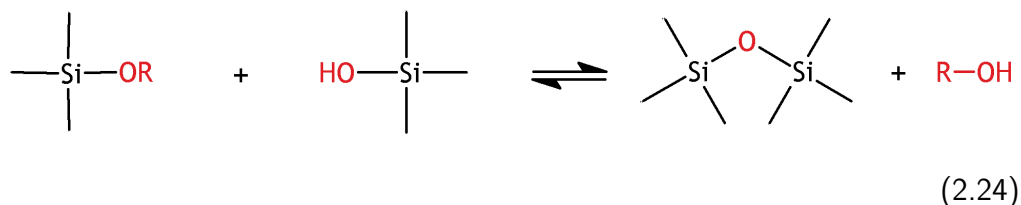
mental reaction principles are described here using silicon alkoxide as a model system. The basic sol-gel process is a simple three step reaction usually described as [139]:

1. The hydrolysis of the silicon alkoxide precursor to form the hydroxylated product (silanol groups) and the corresponding alcohol:

$$Si-(OR)_4 \;+\; H{\diagdown}_O{\diagup}H \;\overset{\text{catalyst}}{\rightleftharpoons}\; HO-Si-(OR)_3 \;+\; R-OH \tag{2.23}$$
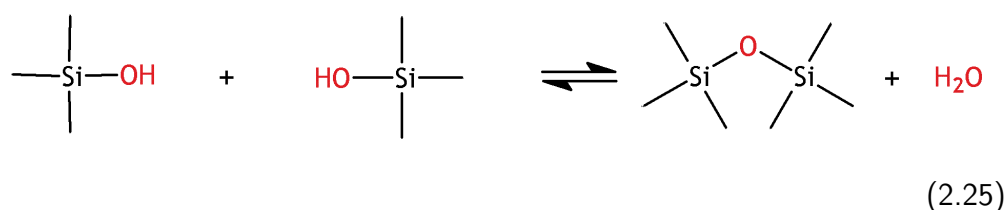
2. The condensation between an unhydroxylated alkoxide group and a hydroxyl group (Equation 2.24) or between two hydroxyl groups (Equation 2.25) eliminates the solvent, which leads to the formation of a colloidal mixture called the sol:

(a) alcohol condensation

$$-\overset{|}{\underset{|}{Si}}-OR \;+\; HO-\overset{|}{\underset{|}{Si}}- \;\rightleftharpoons\; {\diagdown}Si{\diagup}{\diagdown}O{\diagdown}Si{\diagup} \;+\; R-OH \tag{2.24}$$

(b) water condensation

$$-\overset{|}{\underset{|}{Si}}-OH \;+\; HO-\overset{|}{\underset{|}{Si}}- \;\rightleftharpoons\; {\diagdown}Si{\diagup}{\diagdown}O{\diagdown}Si{\diagup} \;+\; H_2O \tag{2.25}$$

3. Polycondensation between sols and additional networking that result in a porous, three-dimensional (3D) crosslinked network.

In a typical procedure, the semi-metal or metal alkoxide is combined with water in a mutual solvent along with a suitable catalyst (acid or base). During the sol-gel transformation, the viscosity of the solution gradually increases as the sol becomes

interconnected to form a rigid, porous network, the gel. Under most conditions, condensation begins before hydrolysis completes. The steps of the sol-gel process are shown in Figure 2.15.
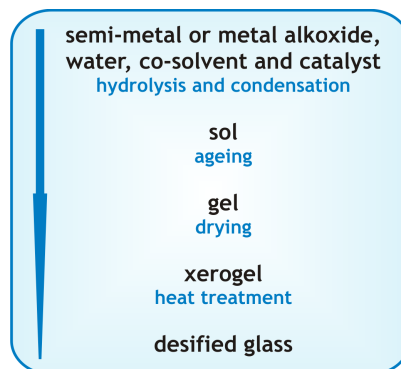

Figure 2.15: Steps of the sol-gel process.

The physical properties of the dried gel are strongly influenced by the sol-gel processing parameters, such as type of molecular precursor, concentration and nature of the catalyst, water to silane ratio, sol ageing time and temperature [140–145]. The structure of the precursors can influence the reaction kinetics as larger substituents decrease the reaction time due to steric hindrance. The process is dramatically promoted when catalysed by acids (HCl, HNO_3, H_2SO_4) or bases (NaOH, HOH, amines) resulting in different reaction mechanisms and different kinetics. Acid-catalysed conditions initially lead to chain elongation and to the formation of linear polymers (Figure 2.16a). Cross-linking occurs by accidental interlinking of chains and leads to homogeneous, relatively dense gels. In contrast, base-catalysed reactions lead to highly crosslinked sol particles as cross-linking already starts at the early stages in the process (Figure 2.16b). The water to silane ratio (r-value) plays an important role in the structural evolution of the sol-gel material. Both the size of sol-gel particles and the degree of material cross-linking are dependent on the r-value. Sol ageing, another relevant parameter, takes place after initial mixing of the sol's components. The sol is left at room or elevated temperatures in order to facilitate the hydrolysis and condensation process that leads to an increase in connectivity and therefore the viscosity of the sol, which is necessary when using dip-coating or spin-coating as a film
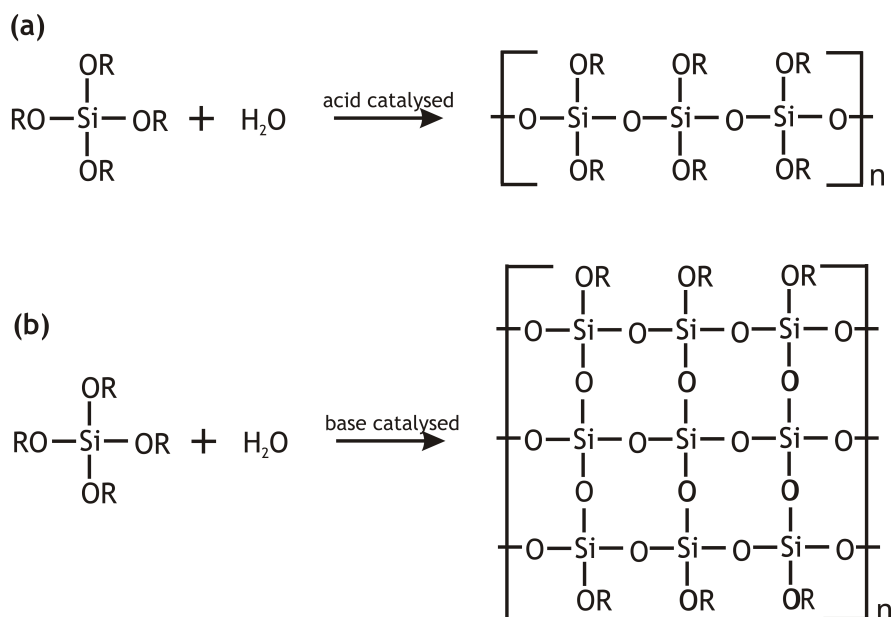
(a)

(b)

Figure 2.16: Structural variations of (a) acid and (b) base catalysis.

deposition method. The temperature programme is also a major process parameter as during drying the sol-gel-derived material shrinks and stiffens (due to associated crosslinking) and acquires a more compact structure. During drying, capillary forces of the evaporating liquids appear and can lead to cracking of the material. If a homogeneous material is required, the parameters described above must be optimised.

From a physical and chemical point of view, sol-gel-derived materials possess many advantages [140]:

- Chemical, thermal and photochemical stability particularly when compared with polymer matrices

- High optical transparency

- Compatibility with many inorganic and organic reagents - can be used for the entrapment of different sensing agents

- Low temperature and mild chemical reaction conditions - allowing for entrapment of biological molecules and other molecules with poor thermal and chemical stability

- Can be produced in various forms - monoliths, films, fibers and powders.

2.5.3   ORganically MOdified SILicates (ORMOSILs)

Materials prepared using sol-gel technology can range from simple inorganic glasses (e.g., when using TEOS) to more complex inorganic-organic materials called ORganically MOdified SILicates (ORMOSILs) developed by Schmidt and co-workers [146–151]. These materials are of the general form R'$_{4-x}$Si(OR), where R' represents an organic group, such as -CH$_3$, -C$_2$H$_5$, -C$_3$H$_7$, -C$_6$H$_5$, (-CH$_2$)$_n$NH$_2$, and they represent a very interesting area for the development of innovative materials (see Figure 2.17). R' is generally bound to the silicon via a Si-C bond which is not hy-
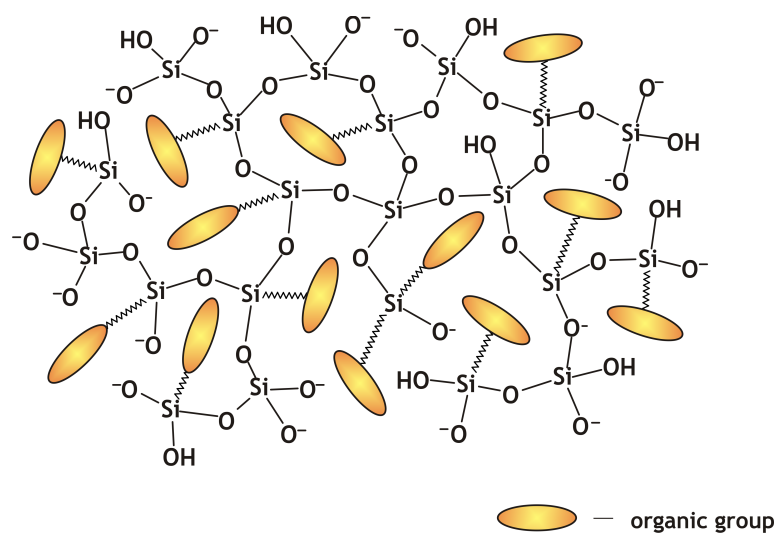

Figure 2.17: Schematic representation of an ORMOSIL network.

drolysable and these silanes are often used as network modifiers and network formers. They can favorably combine the advantages of the inorganic and organic constituents within the same matrix and the chemical properties can be tailored through judicious choice of R'. One can fabricate materials with the desired hydrophobicity, flexibility, toughness, porosity and stability. Specific functional groups can be covalently bound to the network, thereby minimising leaching. There is almost no limit to the combinations of inorganic and organic components in the design of hybrid materials and it is possible to include more than one function into a sol-gel material by incorporating a second component. The possibilities of combination of different properties in

one material has lead to new ideas and potential applications of ORMOSILs. Hybrid materials have been used as decorative and scratch-resistant coatings, as third order non-linear optics materials, in electronic and optoelectronic applications [152, 153]. They are also used as dental filling because their mechanical properties can be tuned in combination with their biocompatibility. Hybrids can be impregnated with drugs, cells or proteins and can provide various kinds of biomedical functions as they can be released in a controlled release design [154–156]. Chitosan-based hybrid materials have been reported and are promising for bone tissue engineering [157, 158]. These are only some applications and there is a plethora of systems under development for future applications.

2.5.4   Sol-gel-derived optical sensors

Sensor technology is an area in which the use of hybrid sol-gel-derived materials is becoming increasingly prevalent. Materials fabricated using the sol-gel method possess many advantages for use in the design of optical chemical sensors [135, 159–162]. In 1984, Avnir and co-workers showed that reagents can be entrapped in a porous sol-gel matrix via physical doping during the condensation reaction [163]. Reagents of various size and charge can be trapped into a stable, cage-like host. Figure 2.18 shows a schematic representation of the inorganic sol-gel-derived network with entrapped sensing molecules. The matrix is porous enough to allow external, low molecular weight analyte species to diffuse into the network and react with the entrapped chemical reagent. Variation of the processing parameters makes it possible to tailor the microstructure for different sensing applications.

For chemical sensor applications, thin films are mostly used as sensing platforms due to the short diffusion pathlength, which improves sensor response time. They also provide flexibility in terms of the surfaces and substrates that can be used. Sol-gel-derived films can be prepared using various deposition techniques such as dip-coating (substrate is dipped directly in the sol-gel solution, Figure 2.19a), spin-coating (substrate is rotated until a film is formed on the surface, Figure 2.19b) and spray
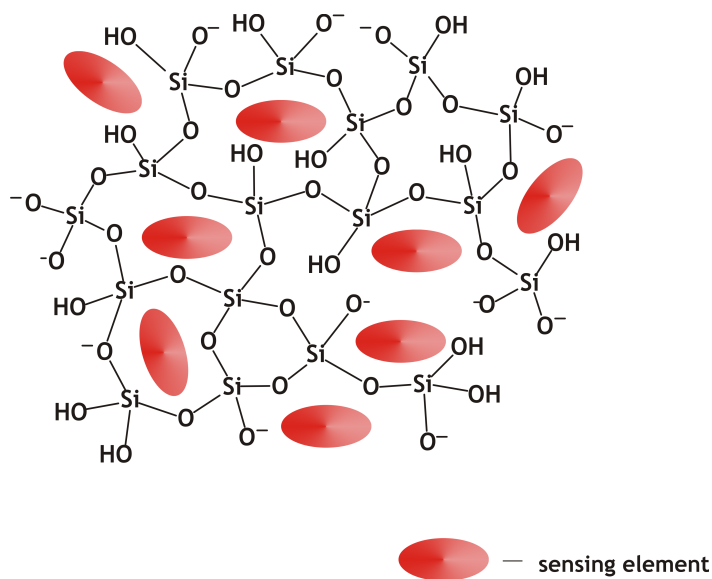
Figure 2.18: Schematic representation of inorganic sol-gel-derived network with an entrapped sensing element.

coating (deposition of an aerosol mist of sol-gel solution on the substrate). Ink-jet printing and pin-printing can also be used and are methods more feasible for mass production. A high degree of thickness uniformity is achievable and sol-gel-derived films such as silica coatings exhibit strong adhesion to the glass substrate.
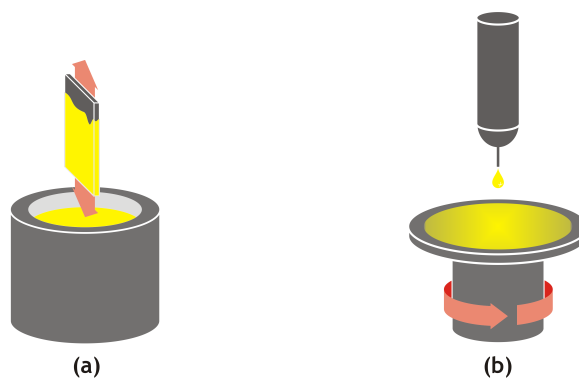

Figure 2.19: Schematic representation of (a) dip-coating and (b) spin-coating processes.

Many sol-gel-derived chemical sensors and biosensors have been developed for the determination of various analytes, for example oxygen, both in gas and dissolved phase [164, 165], carbon dioxide [126], glucose [166], pH [117], ammonia [167], gaseous iodine [168] and ethanol [169], to name but a few.

2.6   Conclusions

This chapter has described the background science which relates to the various elements of the sensors which are the subject of this thesis. A short description has been given of the principles of luminescence and of the sensing principles used for the sensors developed here. More importantly, the current state of the art has been detailed for optical O_2, pH and CO_2 sensing. Sol-gel-derived materials have been selected as the optimum support materials for all the sensors described in this thesis due to the many advantages of these materials which have been detailed above. Furthermore, the sensor performance achieved compares well with published work and, in some cases, demonstrates an improvement on the state of the art. Since the three different sensors developed here have in general different modes of operation and use different sol-gel-based matrices, it has been decided not to include a general chapter on experimental techniques, but to incorporate the specific materials and methods in the relevant results chapters.

References

[1] J. R. Lakowicz, *Principles of Fluorescence Spectroscopy*. Springer-Verlag, New York, 3rd edition, 2006.

[2] B. Valeur, *Molecular Fluorescence. Principles and Applications*. Wiley-VCH, Weinheim, 2001.

[3] O. S. Wolfbeis, ed., *Fiber Optic Chemical Sensors and Biosensors, Vol. 1*. CRC Press, Boca Raton, 1991.

[4] D. Diamond, ed., *Principles of Chemical and Biological Sensors*. Wiley-Interscience, New York, 1998.

[5] G. Gauglitz, "Direct optical sensors: principles and selected applications," *Analytical and Bioanalytical Chemistry*, vol. 381, no. 1, pp. 141–155, 2005.

[6] F. Baldini, A. N. Chester, J. Homola, and S. Martellucci, eds., *Optical chemical sensors. Proceedings of the NATO Advanced Study Institute on Optical Chemical Sensors*. Springer, The Netherlands, 2006.

[7] R. Narayanaswamy, "Optical chemical sensors - transduction and signal-processing," *Analyst*, vol. 118, no. 4, pp. 317–322, 1993.

[8] A. Brecht and G. Gauglitz, "Recent developments in optical transducers for chemical or biochemical applications," *Sensors and Actuators B-Chemical*, vol. 38, no. 1-3, pp. 1–7, 1997.

[9] R. Ramamoorthy, P. K. Dutta, and S. A. Akbar, "Oxygen sensors: Materials, methods, designs and applications," *Journal of Materials Science*, vol. 38, no. 21, pp. 4271–4282, 2003.

[10] T. Labasque, C. Chaumery, A. Aminot, and G. Kergoat, "Spectrophotometric Winkler determination of dissolved oxygen: re-examination of critical factors and reliability," *Marine Chemistry*, vol. 88, no. 1-2, pp. 53–60, 2004.

[11] L. C. Clark, "Monitor and control of blood and tissue oxygen tensions," *Transactions American Society for Artificial Internal Organs*, vol. 2, pp. 41–57, 1956.

[12] H. Suzuki, A. Sugama, and N. Kojima, "Miniature Clark-type oxygen electrode with a three-electrode configuration," *Sensors and Actuators B-Chemical*, vol. 2, no. 4, pp. 297–303, 1990.

[13] C. C. Wu, T. Yasukawa, H. Shiku, and T. Matsue, "Fabrication of miniature Clark oxygen sensor integrated with microstructure," *Sensors and Actuators B-Chemical*, vol. 110, no. 2, pp. 342–349, 2005.

[14] H. Kautsky, "Quenching of luminescence by oxygen," *Transactions Faraday Society*, vol. 35, pp. 216–219, 1939.

[15] I. Bergman, "Rapid-response atmospheric oxygen monitor based on fluorescence quenching," *Nature*, vol. 218, p. 396, 1968.

[16] R. Shinar, Z. Q. Zhou, B. Choudhury, and J. Shinar, "Structurally integrated organic light emitting device-based sensors for gas phase and dissolved oxygen," *Analytica Chimica Acta*, vol. 568, no. 1-2, pp. 190–199, 2006.

[17] H. S. Voraberger, H. Kreimaier, K. Biebernik, and W. Kern, "Novel oxygen optrode withstanding autoclavation: technical solutions and performance," *Sensors and Actuators B-Chemical*, vol. 74, no. 1-3, pp. 179–185, 2001.

[18] A. Mills and M. Thomas, "Fluorescence-based thin plastic film ion-pair sensors for oxygen," *Analyst*, vol. 122, no. 1, pp. 63–68, 1997.

[19] K. Eaton, B. Douglas, and P. Douglas, "Luminescent oxygen sensors: Time-resolved studies and modelling of heterogeneous oxygen quenching of luminescence emission from Pt and Pd octaethylporphyrins in thin polymer films," *Sensors and Actuators B-Chemical*, vol. 97, no. 1, pp. 2–12, 2004.

[20] V. V. Vasilev and S. M. Borisov, "Optical oxygen sensors based on phosphorescent water-soluble platinum metals porphyrins immobilized in perfluorinated ion-exchange membrane," *Sensors and Actuators B-Chemical*, vol. 82, no. 2-3, pp. 272–276, 2002.

[21] A. Mills and A. Lepre, "Controlling the response characteristics of luminescent porphyrin plastic film sensors for oxygen," *Analytical Chemistry*, vol. 69, no. 22, pp. 4653–4659, 1997.

[22] Y. Amao, Y. Ishikawa, and I. Okura, "Green luminescent iridium(III) complex immobilized in fluoropolymer film as optical oxygen-sensing material," *Analytica Chimica Acta*, vol. 445, no. 2, pp. 177–182, 2001.

[23] I. Klimant and O. S. Wolfbeis, "Oxygen-sensitive luminescent materials based on silicone-soluble ruthenium diimine complexes," *Analytical Chemistry*, vol. 67, no. 18, pp. 3160–3166, 1995.

[24] B. D. MacCraith, G. O'Keeffe, C. McDonagh, and A. K. McEvoy, "LED-based fiber optic oxygen sensor using sol-gel coating," *Electronics Letters*, vol. 30, no. 11, pp. 888–889, 1994.

[25] C. McDonagh, B. D. MacCraith, and A. K. McEvoy, "Tailoring of sol-gel films for optical sensing of oxygen in gas and aqueous phase," *Analytical Chemistry*, vol. 70, no. 1, pp. 45–50, 1998.

[26] C. Higgins, D. Wencel, C. S. Burke, B. D. MacCraith, and C. McDonagh, "Novel hybrid optical sensor materials for in-breath O_2 analysis," *Analyst*, vol. 133, no. 2, pp. 241–247, 2008.

[27] R. M. Bukowski, M. D. Davenport, A. H. Titus, and F. V. Bright, "O_2-responsive chemical sensors based on hybrid xerogels that contain fluorinated precursors," *Applied Spectroscopy*, vol. 60, no. 9, pp. 951–957, 2006.

[28] Y. Tang, E. C. Tehan, Z. Y. Tao, and F. V. Bright, "Sol-gel-derived sensor materials that yield linear calibration plots, high sensitivity, and long-term stability," *Analytical Chemistry*, vol. 75, no. 10, pp. 2407–2413, 2003.

[29] P. Bergveld, "Thirty years of ISFETOLOGY - what happened in the past 30 years and what may happen in the next 30 years," *Sensors and Actuators B-Chemical*, vol. 88, no. 1, pp. 1–20, 2003.

[30] O. S. Wolfbeis and H. Marhold, "A new group of fluorescent pH-indicators for an extended pH-range," *Fresenius Zeitschrift Für Analytische Chemie*, vol. 327, no. 3-4, pp. 347–350, 1987.

[31] J. Lin and D. Liu, "An optical pH sensor with a linear response over a broad range," *Analytica Chimica Acta*, vol. 408, no. 1-2, pp. 49–55, 2000.

[32] G. B. Harper, "Reusable glass-bound pH indicators," *Analytical Chemistry*, vol. 47, no. 2, pp. 348–351, 1975.

[33] J. I. Peterson, S. R. Goldstein, R. V. Fitzgerald, and D. K. Buckhold, "Fiber optic pH probe for physiological use," *Analytical Chemistry*, vol. 52, no. 6, pp. 864–869, 1980.

[34] L. A. Saari and W. R. Seitz, "pH sensor based on immobilized fluoresceinamine," *Analytical Chemistry*, vol. 54, no. 4, pp. 821–823, 1982.

[35] S. Hulth, R. C. Aller, P. Engstrom, and E. Selander, "A pH plate fluorosensor (optode) for early diagenetic studies of marine sediments," *Limnology and Oceanography*, vol. 47, no. 1, pp. 212–220, 2002.

[36] Z. H. Liu, J. F. Liu, and T. L. Chen, "Phenol red immobilized PVA membrane for an optical pH sensor with two determination ranges and long-term stability," *Sensors and Actuators B-Chemical*, vol. 107, no. 1, pp. 311–316, 2005.

[37] V. I. Agayn and D. R. Walt, "Fiber-optic sensor for continuous monitoring of fermentation pH," *Bio-Technology*, vol. 11, no. 6, pp. 726–729, 1993.

[38] C. M. Chan, C. S. Fung, K. Y. Wong, and W. H. Lo, "Evaluation of a luminescent ruthenium complex immobilized inside Nafion as optical pH sensor," *Analyst*, vol. 123, no. 9, pp. 1843–1847, 1998.

[39] M. F. Choi, "Spectroscopic behaviour of 8-hydroxy-1,3,6-pyrenetrisulphonate immobilized in ethyl cellulose," *Journal of Photochemistry and Photobiology A-Chemistry*, vol. 104, no. 1-3, pp. 207–212, 1997.

[40] B. M. Weidgans, C. Krause, I. Klimant, and O. S. Wolfbeis, "Fluorescent pH sensors with negligible sensitivity to ionic strength," *Analyst*, vol. 129, no. 7, pp. 645–650, 2004.

[41] R. Makote and M. M. Collinson, "Organically modified silicate films for stable pH sensors," *Analytica Chimica Acta*, vol. 394, no. 2-3, pp. 195–200, 1999.

[42] D. A. Nivens, Y. K. Zhang, and S. M. Angel, "A fiber-optic pH sensor prepared using a base-catalyzed organo-silica sol-gel," *Analytica Chimica Acta*, vol. 376, no. 2, pp. 235–245, 1998.

[43] G. J. Zhang, J. F. Lui, and M. Yuan, "Novel carbon dioxide gas sensor based on infrared absorption," *Optical Engineering*, vol. 39, no. 8, pp. 2235–2240, 2000.

[44] J. W. Severinghaus and A. F. Bradley, "Electrodes for blood pO_2 and pCO_2 determination," *Journal of Applied Physiology*, vol. 13, no. 3, pp. 515–520, 1958.

[45] D. W. Lübbers and N. Opitz, "The pCO_2-optode-pO_2-optode - new probe for measurement of pCO_2 or pO_2 in fluids and gases," *Zeitschrift Für Naturforschung*, vol. 30, no. 7-8, pp. 532–533, 1975.

[46] Z. Zhujun and W. R. Seitz, "A carbon dioxide sensor based on fluorescence," *Analytica Chimica Acta*, vol. 160, pp. 305–309, 1984.

[47] O. S. Wolfbeis, L. J. Weis, M. J. P. Leiner, and W. E. Ziegler, "Fiber-optic fluorosensor for oxygen and carbon dioxide," *Analytical Chemistry*, vol. 60, no. 19, pp. 2028–2030, 1988.

[48] M. Uttamlal and D. R. Walt, "A fiber-optic carbon dioxide sensor for fermentation monitoring," *Bio-Technology*, vol. 13, no. 6, pp. 597–601, 1995.

[49] H. Kroneis and H. Heitzmann *U.S. Patent*, no. 4,557,900, 1985.

[50] M. J. P. Leiner, "Luminescence chemical sensors for biomedical applications - scope and limitations," *Analytica Chimica Acta*, vol. 255, no. 2, pp. 209–222, 1991.

[51] G. Orellana, M. C. Moreno-Bondi, E. Segovia, and M. D. Marazuela, "Fiber-optic sensing of carbon dioxide based on excited-state proton transfer to a luminescent ruthenium(II) complex," *Analytical Chemistry*, vol. 64, no. 19, pp. 2210–2215, 1992.

[52] Y. Kawabata, T. Kamichika, T. Imasaka, and N. Ishibashi, "Fiber-optic sensor for carbon dioxide with a pH indicator dispersed in a poly(ethylene glycol) membrane," *Analytica Chimica Acta*, vol. 219, no. 2, pp. 223–229, 1989.

[53] D. B. Raemer, D. R. Walt, and C. Munkholm, "CO_2 indicator and the use thereof to evaluate placement of tracheal tubes," *U.S. Patent*, no. 5,005,572, 1991.

[54] A. Mills, Q. Chang, and N. Mcmurray, "Equilibrium studies on colorimetric plastic film sensors for carbon dioxide," *Analytical Chemistry*, vol. 64, no. 13, pp. 1383–1389, 1992.

[55] A. Mills and Q. Chang, "Modeled diffusion-controlled response and recovery behavior of a naked optical film sensor with a hyperbolic-type response to analyte concentration," *Analyst*, vol. 117, no. 9, pp. 1461–1466, 1992.

[56] A. Mills and Q. Chang, "Fluorescence plastic thin-film sensor for carbon dioxide," *Analyst*, vol. 118, no. 7, pp. 839–843, 1993.

[57] A. Mills and Q. Chang, "Colorimetric polymer film sensors for dissolved carbon dioxide," *Sensors and Actuators B-Chemical*, vol. 21, no. 2, pp. 83–89, 1994.

[58] A. Mills and Q. Chang, "Tuning colourimetric and fluorometric gas sensors for carbon dioxide," *Analytica Chimica Acta*, vol. 285, no. 1-2, pp. 113–123, 1994.

[59] Y. Amao and N. Nakamura, "An optical sensor with the combination of colorimetric change of α-naphtholphthalein and internal reference luminescent dye CO_2 in water," *Sensors and Actuators B-Chemical*, vol. 107, no. 2, pp. 861–865, 2005.

[60] Q. Chang, L. Randers-Eichhorn, J. R. Lakowicz, and G. Rao, "Steam-sterilizable, fluorescence lifetime-based sensing film for dissolved carbon dioxide," *Biotechnology Progress*, vol. 14, no. 2, pp. 326–331, 1998.

[61] M. Cajlakovic, A. Bizzarri, and V. Ribitsch, "Luminescence lifetime-based carbon dioxide optical sensor for clinical applications," *Analytica Chimica Acta*, vol. 573, pp. 57–64, 2006.

[62] B. H. Weigl and O. S. Wolfbeis, "New hydrophobic materials for optical carbon-dioxide sensors based on ion-pairing," *Analytica Chimica Acta*, vol. 302, no. 2-3, pp. 249–254, 1995.

[63] Y. Amao and T. Komori, "Optical CO_2 sensor of the combination of colorimetric change of α-naphtholphthalein in poly(isobutyl methacrylate) and fluorescent porphyrin in polystyrene," *Talanta*, vol. 66, no. 4, pp. 976–981, 2005.

[64] C. S. Burke, A. Markey, R. I. Nooney, P. Byme, and C. McDonagh, "Development of an optical sensor probe for the detection of dissolved carbon dioxide," *Sensors and Actuators B-Chemical*, vol. 119, no. 1, pp. 288–294, 2006.

[65] C. von Bültzingslöwen, A. K. McEvoy, C. McDonagh, and B. D. MacCraith, "Lifetime-based optical sensor for high-level pCO_2 detection employing fluorescence resonance energy transfer," *Analytica Chimica Acta*, vol. 480, no. 2, pp. 275–283, 2003.

[66] C. Malins and B. D. MacCraith, "Dye-doped organically modified silica glass for fluorescence based carbon dioxide gas detection," *Analyst*, vol. 123, no. 11, pp. 2373–2376, 1998.

[67] D. A. Nivens, M. V. Schiza, and S. M. Angel, "Multilayer sol-gel membranes for optical sensing applications: single layer pH and dual layer CO_2 and NH_3 sensors," *Talanta*, vol. 58, no. 3, pp. 543–550, 2002.

[68] B. H. Weigl and O. S. Wolfbeis, "Sensitivity studies on optical carbon dioxide sensors based on ion-pairing," *Sensors and Actuators B-Chemical*, vol. 28, no. 2, pp. 151–156, 1995.

[69] J. R. Lakowicz and G. Weber, "Quenching of fluorescence by oxygen - probe for structural fluctuations in macromolecules," *Biochemistry*, vol. 12, no. 21, pp. 4161–4170, 1973.

[70] R. J. Watts and G. A. Crosby, "Spectroscopic characterization of complexes of ruthenium(II) and iridium(III) with 4,4'-diphenyl-2,2'-bipyridine and 4,7-diphenyl-1,10-phenanthroline," *Journal of the American Chemical Society*, vol. 93, no. 13, pp. 3184–3188, 1971.

[71] J. N. Demas, "Photophysical pathways in metal complexes," *Journal of Chemical Education*, vol. 60, no. 10, pp. 803–808, 1983.

[72] M. J. Cook, A. P. Lewis, G. S. G. Mcauliffe, V. Skarda, A. J. Thomson, J. L. Glasper, and D. J. Robbins, "Luminescent metal complexes. Part 2. A model for the luminescence properties of the tris-chelates of substituted 2,2'-bipyridyls with ruthenium(II)," *Journal of the Chemical Society-Perkin Transactions 2*, no. 8, pp. 1303–1307, 1984.

[73] P. C. Alford, M. J. Cook, A. P. Lewis, G. S. G. Mcauliffe, V. Skarda, A. J. Thomson, J. L. Glasper, and D. J. Robbins, "Luminescent metal complexes. Part 5. Luminescence properties of ring-substituted 1,10-phenanthroline tris-complexes of ruthenium(II)," *Journal of the Chemical Society-Perkin Transactions 2*, no. 5, pp. 705–709, 1985.

[74] T. J. Meyer, "Photochemistry of metal coordination complexes: Metal to ligand charge transfer excited states," *Pure and Applied Chemistry*, vol. 58, no. 9, pp. 1193–1206, 1986.

[75] V. Balzani and A. Juris, "Photochemistry and photophysics of Ru(II)-polypyridine complexes in the Bologna group. From early studies to recent developments," *Coordination Chemistry Reviews*, vol. 211, pp. 97–115, 2001.

[76] C. S. Parmente and J. D. Rau, "Fluorescence quenching in aromatic hydrocarbons by oxygen," *Journal of Chemical Physics*, vol. 51, no. 5, pp. 2242–2246, 1969.

[77] S. V. Camyshan, N. P. Gritsan, V. V. Korolev, and N. M. Bazhin, "Quenching of the luminescence of organic compounds by oxygen in glassy matrices," *Chemical Physics*, vol. 142, no. 1, pp. 59–68, 1990.

[78] K. Kikuchi, C. Sato, M. Watabe, H. Ikeda, Y. Takahashi, and T. Miyashi, "New aspects on fluorescence quenching by molecular oxygen," *Journal of the American Chemical Society*, vol. 115, no. 12, pp. 5180–5184, 1993.

[79] J. R. Lakowicz, *Principles of Fluorescence Spectroscopy, Chapter 8 and 9.* Springer-Verlag, New York, 3rd edition, 2006.

[80] J. R. Bacon and J. N. Demas, "Determination of oxygen concentrations by luminescence quenching of a polymer-immobilized transition-metal complex," *Analytical Chemistry*, vol. 59, no. 23, pp. 2780–2785, 1987.

[81] E. R. Carraway, J. N. Demas, and B. A. DeGraff, "Luminescence quenching mechanism for microheterogeneous systems," *Analytical Chemistry*, vol. 63, no. 4, pp. 332–336, 1991.

[82] J. N. Demas and B. A. DeGraff, "Luminescence-based sensors - microheterogeneous and temperature effects," *Sensors and Actuators B-Chemical*, vol. 11, no. 1-3, pp. 35–41, 1993.

[83] W. Y. Xu, R. C. McDonough, B. Langsdorf, J. N. Demas, and B. A. DeGraff, "Oxygen sensors based on luminescence quenching - interactions of metal-complexes with the polymer supports," *Analytical Chemistry*, vol. 66, no. 23, pp. 4133–4141, 1994.

[84] I. Klimant, F. Ruckruh, G. Liebsch, C. Stangelmayer, and O. S. Wolfbeis, "Fast response oxygen micro-optodes based on novel soluble ormosil glasses," *Mikrochimica Acta*, vol. 131, no. 1-2, pp. 35–46, 1999.

[85] P. Hartmann and W. Trettnak, "Effects of polymer matrices on calibration functions of luminescent oxygen sensors based on porphyrin ketone complexes," *Analytical Chemistry*, vol. 68, no. 15, pp. 2615–2620, 1996.

[86] S. S. Lehrer, "Solute perturbation of protein fluorescence - quenching of tryptophyl fluorescence of model compounds and of lysozyme by iodide ion," *Biochemistry*, vol. 10, no. 17, pp. 3254–3263, 1971.

[87] K. A. Kneas, W. Y. Xu, J. N. Demas, and B. A. DeGraff, "Oxygen sensors based on luminescence quenching: Interactions of tris(4,7-diphenyl-1,10-phenanthroline)ruthenium(II) chloride and pyrene with polymer supports," *Applied Spectroscopy*, vol. 51, no. 9, pp. 1346–1351, 1997.

[88] A. Mills, "Response characteristics of optical sensors for oxygen: models based on a distribution in τ_0 or k_q," *Analyst*, vol. 124, no. 9, pp. 1301–1307, 1999.

[89] A. Mills, "Response characteristics of optical sensors for oxygen: a model based on a distribution in τ_0 and k_q," *Analyst*, vol. 124, no. 9, pp. 1309–1314, 1999.

[90] E. R. Carraway, J. N. Demas, B. A. DeGraff, and J. R. Bacon, "Photophysics and photochemistry of oxygen sensors based on luminescent transition-metal complexes," *Analytical Chemistry*, vol. 63, no. 4, pp. 337–342, 1991.

[91] J. Janata, "Do optical sensors really measure pH," *Analytical Chemistry*, vol. 59, no. 9, pp. 1351–1356, 1987.

[92] T. E. Edmonds, N. J. Flatters, C. F. Jones, and J. N. Miller, "Determination of pH with acid-base indicators - implications for optical fiber probes," *Talanta*, vol. 35, no. 2, pp. 103–107, 1988.

[93] M. E. Cox and B. Dunn, "Detection of oxygen by fluorescence quenching," *Applied Optics*, vol. 24, no. 14, pp. 2114–2120, 1985.

[94] O. S. Wolfbeis, H. E. Posch, and H. W. Kroneis, "Fiber optical fluorosensor for determination of halothane and/or oxygen," *Analytical Chemistry*, vol. 57, no. 13, pp. 2556–2561, 1985.

[95] W. Y. Xu, R. Schmidt, M. Whaley, J. N. Demas, B. A. DeGraff, E. K. Karikari, and B. L. Farmer, "Oxygen sensors based on luminescence quenching - interactions of pyrene with the polymer supports," *Analytical Chemistry*, vol. 67, no. 18, pp. 3172–3180, 1995.

[96] J. N. Demas and B. A. DeGraff, "Applications of luminescent transition platinum group metal complexes to sensor technology and molecular probes," *Coordination Chemistry Reviews*, vol. 211, pp. 317–351, 2001.

[97] A. Mills, "Optical oxygen sensors. Utilising the luminescence of platinum metal complexes," *Platinum Metals Review*, vol. 41, no. 3, pp. 115–127, 1997.

[98] S. K. Lee and I. Okura, "Optical sensor for oxygen using a porphyrin-doped sol-gel glass," *Analyst*, vol. 122, no. 1, pp. 81–84, 1997.

[99] M. C. Moreno-Bondi, O. S. Wolfbeis, M. J. P. Leiner, and B. P. H. Schaffar, "Oxygen optrode for use in a fiberoptic glucose biosensor," *Analytical Chemistry*, vol. 62, no. 21, pp. 2377–2380, 1990.

[100] A. K. McEvoy, C. M. McDonagh, and B. D. MacCraith, "Dissolved oxygen sensor based on fluorescence quenching of oxygen-sensitive ruthenium complexes immobilized in sol-gel-derived porous silica coatings," *Analyst*, vol. 121, no. 6, pp. 785–788, 1996.

[101] Y. Amao, K. Asai, and I. Okura, "Oxygen sensing based on lifetime of photoexcited triplet state of platinum porphyrin-polystyrene film using time-resolved spectroscopy," *Journal of Porphyrins and Phthalocyanines*, vol. 4, no. 3, pp. 292–299, 2000.

[102] S. K. Lee and I. Okura, "Photostable optical oxygen sensing material: Platinum tetrakis(pentafluorophenyl)porphyrin immobilized in polystyrene," *Analytical Communications*, vol. 34, no. 6, pp. 185–188, 1997.

[103] D. B. Papkovsky, G. V. Ponomarev, W. Trettnak, and P. Oleary, "Phosphorescent complexes of porphyrin ketones - optical-properties and application to oxygen sensing," *Analytical Chemistry*, vol. 67, no. 22, pp. 4112–4117, 1995.

[104] S. M. Borisov and I. Klimant, "Ultrabright oxygen optodes based on cyclometalated iridium(III) coumarin complexes," *Analytical Chemistry*, vol. 79, no. 19, pp. 7501–7509, 2007.

[105] R. Narayanaswamy and O. S. Wolfbeis, eds., *Optical Sensors: Industrial, Environmental and Diagnostic Applications, Chapter 13*. Springer-Verlag, Berlin, 2004.

[106] J. R. Lakowicz, ed., *Topics in Fluorescence Spectroscopy: Probe Design and Chemical Sensing, Vol. 4, Chapter 4*. Kluwer Academic Publishers Group, 1994.

[107] Z. Zhujun and W. R. Seitz, "Optical sensor for oxygen based on immobilized hemoglobin," *Analytical Chemistry*, vol. 58, no. 1, pp. 220–222, 1986.

[108] K. E. Chung, E. H. Lan, M. S. Davidson, B. S. Dunn, J. S. Valentine, and J. I. Zink, "Measurement of dissolved oxygen in water using glass-encapsulated myoglobin," *Analytical Chemistry*, vol. 67, no. 9, pp. 1505–1509, 1995.

[109] A. Mills, "Oxygen indicators and intelligent inks for packaging food," *Chemical Society Reviews*, vol. 34, no. 12, pp. 1003–1011, 2005.

[110] E. J. Wang, K. F. Chow, V. Kwan, T. Chin, C. Wong, and A. Bocarsly, "Fast and long term optical sensors for pH based on sol-gels," *Analytica Chimica Acta*, vol. 495, no. 1-2, pp. 45–50, 2003.

[111] F. Ismail, C. Malins, and N. J. Goddard, "Alkali treatment of dye-doped sol-gel glass films for rapid optical pH sensing," *Analyst*, vol. 127, no. 2, pp. 253–257, 2002.

[112] U. Kosch, I. Klimant, and O. S. Wolfbeis, "Long-lifetime based pH micro-optodes without oxygen interference," *Fresenius Journal of Analytical Chemistry*, vol. 364, no. 1-2, pp. 48–53, 1999.

[113] J. N. Liu, M. R. Shahriari, and G. H. Sigel, "Development of a porous polymer pH optrode," *Optics Letters*, vol. 17, no. 24, pp. 1815–1817, 1992.

[114] Z. H. Liu, F. L. Luo, and T. L. Chen, "Phenolphthalein immobilized membrane for an optical pH sensor," *Analytica Chimica Acta*, vol. 510, no. 2, pp. 189–194, 2004.

[115] S. H. Lee, J. Kumar, and S. K. Tripathy, "Thin film optical sensors employing polyelectrolyte assembly," *Langmuir*, vol. 16, no. 26, pp. 10482–10489, 2000.

[116] M. Cajlakovic, A. Lobnik, and T. Werner, "Stability of new optical pH sensing material based on cross-linked poly(vinyl alcohol) copolymer," *Analytica Chimica Acta*, vol. 455, no. 2, pp. 207–213, 2002.

[117] A. Lobnik, I. Oehme, I. Murkovic, and O. S. Wolfbeis, "pH optical sensors based on sol-gels: Chemical doping versus covalent immobilization," *Analytica Chimica Acta*, vol. 367, no. 1-3, pp. 159–165, 1998.

[118] K. Aslan, J. R. Lakowicz, H. Szmacinski, and C. D. Geddes, "Enhanced ratiometric pH sensing using SNAFL-2 on silver island films: Metal-enhanced fluorescence sensing," *Journal of Fluorescence*, vol. 15, no. 1, pp. 37–40, 2005.

[119] J. W. Parker, O. Laksin, C. Yu, M. L. Lau, S. Klima, R. Fisher, I. Scott, and B. W. Atwater, "Fiber-optic sensors for pH and carbon dioxide using a self-referencing dye," *Analytical Chemistry*, vol. 65, no. 17, pp. 2329–2334, 1993.

[120] A. S. Vasylevska, A. A. Karasyov, S. M. Borisov, and C. Krause, "Novel coumarin-based fluorescent pH indicators, probes and membranes covering a broad pH range," *Analytical and Bioanalytical Chemistry*, vol. 387, no. 6, pp. 2131–2141, 2007.

[121] C. R. Schröder, B. M. Weidgans, and I. Klimant, "pH fluorosensors for use in marine systems," *Analyst*, vol. 130, no. 6, pp. 907–916, 2005.

[122] Y. Clarke, W. Y. Xu, J. N. Demas, and B. A. DeGraff, "Lifetime-based pH sensor system based on a polymer supported ruthenium(II) complex," *Analytical Chemistry*, vol. 72, no. 15, pp. 3468–3475, 2000.

[123] A. P. deSilva, H. Q. N. Gunaratne, and T. E. Rice, "Proton-controlled switching of luminescence in lanthanide complexes in aqueous solution: pH sensors based on long-lived emission," *Angewandte Chemie-International Edition in English*, vol. 35, no. 18, pp. 2116–2118, 1996.

[124] O. S. Wolfbeis, E. Fürlinger, H. Kroneis, and H. Marsoner, "Fluorimetric analysis. 1. A study on fluorescent indicators for measuring near neutral (physiological) pH-values," *Fresenius Zeitschrift Für Analytische Chemie*, vol. 314, no. 2, pp. 119–124, 1983.

[125] S. G. Schulman, S. X. Chen, F. L. Bai, M. J. P. Leiner, L. Weis, and O. S. Wolfbeis, "Dependence of the fluorescence of immobilized 1-hydroxypyrene-3,6,8-trisulfonate on solution pH - extension of the range of applicability of a pH fluorosensor," *Analytica Chimica Acta*, vol. 304, no. 2, pp. 165–170, 1995.

[126] C. von Bültzingslöwen, A. K. McEvoy, C. McDonagh, B. D. MacCraith, I. Klimant, C. Krause, and O. S. Wolfbeis, "Sol-gel based optical carbon dioxide sensor employing dual luminophore referencing for application in food packaging technology," *Analyst*, vol. 127, no. 11, pp. 1478–1483, 2002.

[127] K. Ertekin, I. Klimant, G. Neurauter, and O. S. Wolfbeis, "Characterization of a reservoir-type capillary optical microsensor for pCO_2 measurements," *Talanta*, vol. 59, no. 2, pp. 261–267, 2003.

[128] M. B. Tabacco, M. Uttamial, M. McAllister, and D. R. Walt, "An autonomous sensor and telemetry system for low-level pCO_2 measurements in seawater," *Analytical Chemistry*, vol. 71, no. 1, pp. 154–161, 1999.

[129] N. Nakamura and Y. Amao, "Optical sensor for carbon dioxide combining colorimetric change of a pH indicator and a reference luminescent dye," *Analytical and Bioanalytical Chemistry*, vol. 376, no. 5, pp. 642–646, 2003.

[130] H. Segawa, E. Ohnishi, Y. Arai, and K. Yoshida, "Sensitivity of fiber-optic carbon dioxide sensors utilizing indicator dye," *Sensors and Actuators B-Chemical*, vol. 94, no. 3, pp. 276–281, 2003.

[131] A. Mills, A. Lepre, and L. Wild, "Breath-by-breath measurement of carbon dioxide using a plastic film optical sensor," *Sensors and Actuators B-Chemical*, vol. 39, no. 1-3, pp. 419–425, 1997.

[132] J. N. Demas, *Excited state lifetime measurements*. Academic Press, New York, 1983.

[133] I. Klimant, "Method and device for referencing fluorescence intensity signals," *U.S. Patent*, 2003.

[134] T. Mayr, I. Klimant, O. S. Wolfbeis, and T. Werner, "Dual lifetime referenced optical sensor membrane for the determination of copper(II) ions," *Analytica Chimica Acta*, vol. 462, no. 1, pp. 1–10, 2002.

[135] J. Lin and C. W. Brown, "Sol-gel glass as a matrix for chemical and biochemical sensing," *Trac-Trends in Analytical Chemistry*, vol. 16, no. 4, pp. 200–211, 1997.

[136] C. J. Brinker and G. W. Scherer, *Sol-Gel Science: The Physics and Chemistry of Sol-Gel Processing*. Academic Press, Boston, 1990.

[137] L. L. Hench and J. K. West, "The sol-gel process," *Chemical Reviews*, vol. 90, no. 1, pp. 33–72, 1990.

[138] J. Livage and C. Sanchez, "Sol-gel chemistry," *Journal of Non-Crystalline Solids*, vol. 145, no. 1-3, pp. 11–19, 1992.

[139] H. Schmidt, H. Scholze, and A. Kaiser, "Principles of hydrolysis and condensation reaction of alkoxysilanes," *Journal of Non-Crystalline Solids*, vol. 63, no. 1-2, pp. 1–11, 1984.

[140] J. D. Wright and N. Sommerdijk, *Sol-Gel Materials: Chemistry and Applications*. CRC Press, Boca Raton, 2000.

[141] H. Schmidt, "Chemistry of material preparation by the sol-gel process," *Journal of Non-Crystalline Solids*, vol. 100, no. 1-3, pp. 51–64, 1988.

[142] J. Y. Ying, J. B. Benziger, and A. Navrotsky, "Structural evolution of alkoxide silica-gels to glass - effect of catalyst pH," *Journal of the American Ceramic Society*, vol. 76, no. 10, pp. 2571–2582, 1993.

[143] J. Y. Ying and J. B. Benziger, "Structure tailoring of alkoxide silica," *Journal of Non-Crystalline Solids*, vol. 147, pp. 222–231, 1992.

[144] C. J. Brinker, "Hydrolysis and condensation of silicates - effects on structure," *Journal of Non-Crystalline Solids*, vol. 100, no. 1-3, pp. 31–50, 1988.

[145] C. Rottman and D. Avnir, "Effects of water/silane r-ratio and humidity on properties of sol-gel-entrapped indicators," in *Sol-Gel Optics* (V. Bruce, S. Dunn, E. J. Pope, H. K. Schmidt, and M. Yamane, eds.), vol. 3943, pp. 154–162, 2000.

[146] H. Schmidt, "New type of non-crystalline solids between inorganic and organic materials," *Journal of Non-Crystalline Solids*, vol. 73, no. 1-3, pp. 681–691, 1985.

[147] B. Lintner, N. Arfsten, H. Dislich, H. Schmidt, G. Philipp, and B. Seiferling, "A 1st look at the optical-properties of Ormosils," *Journal of Non-Crystalline Solids*, vol. 100, no. 1-3, pp. 378–382, 1988.

[148] H. Schmidt, "Organic modification of glass structure - new glasses or new polymers," *Journal of Non-Crystalline Solids*, vol. 112, no. 1-3, pp. 419–423, 1989.

[149] U. Schubert, "New materials by sol-gel processing: Design at the molecular level," *Journal of the Chemical Society-Dalton Transactions*, no. 16, pp. 3343–3348, 1996.

[150] J. D. Mackenzie and E. P. Bescher, "Structures, properties and potential applications of Ormosils," *Journal of Sol-Gel Science and Technology*, vol. 13, no. 1-3, pp. 371–377, 1998.

[151] K. H. Haas, "Hybrid inorganic-organic polymers based on organically modified Si-alkoxides," *Advanced Engineering Materials*, vol. 2, no. 9, pp. 571–582, 2000.

[152] H. S. Nalwa, ed., *Handbook of Advanced Electronic and Photonic Materials and Devices, Vol. 5, Chapter 8*. Academic Press, New York, 2001.

[153] C. Sanchez, B. Julian, P. Belleville, and M. Popall, "Applications of hybrid organic-inorganic nanocomposites," *Journal of Materials Chemistry*, vol. 15, no. 35-36, pp. 3559–3592, 2005.

[154] A. J. Salinas and M. Vallet-Regi, "Evolution of ceramics with medical applications," *Zeitschrift Für Anorganische Und Allgemeine Chemie*, vol. 633, no. 11-12, pp. 1762–1773, 2007.

[155] K. S. Finnie, D. A. Jacques, M. J. McGann, M. G. Blackford, and C. J. Barbe, "Encapsulation and controlled release of biomolecules from silica microparticles," *Journal of Materials Chemistry*, vol. 16, no. 46, pp. 4494–4498, 2006.

[156] C. Barbe, J. Bartlett, L. G. Kong, K. Finnie, H. Q. Lin, M. Larkin, S. Calleja, A. Bush, and G. Calleja, "Silica particles: A novel drug-delivery system," *Advanced Materials*, vol. 16, no. 21, pp. 1959–1966, 2004.

[157] L. Ren, K. Tsuru, S. Hayakawa, and A. Osaka, "Novel approach to fabricate porous gelatin-siloxane hybrids for bone tissue engineering," *Biomaterials*, vol. 23, no. 24, pp. 4765–4773, 2002.

[158] Y. Shirosaki, K. Tsuru, S. Hayakawa, A. Osaka, M. A. Lopes, J. D. Santos, and M. H. Fernandes, "In vitro cytocompatibility of MG63 cells on chitosan-organosiloxane hybrid membranes," *Biomaterials*, vol. 26, no. 5, pp. 485–493, 2005.

[159] O. Lev, M. Tsionsky, L. Rabinovich, V. Glezer, S. Sampath, I. Pankratov, and J. Gun, "Organically modified sol-gel sensors," *Analytical Chemistry*, vol. 67, no. 1, pp. A22–A30, 1995.

[160] M. M. Collinson, "Recent trends in analytical applications of organically modified silicate materials," *Trac-Trends in Analytical Chemistry*, vol. 21, no. 1, pp. 30–38, 2002.

[161] B. D. MacCraith, C. McDonagh, A. K. Mcevoy, T. Butler, G. O'Keeffe, and V. Murphy, "Optical chemical sensors based on sol-gel materials: Recent advances and critical issues," *Journal of Sol-Gel Science and Technology*, vol. 8, no. 1-3, pp. 1053–1061, 1997.

[162] M. E. Tess and J. A. Cox, "Chemical and biochemical sensors based on advances in materials chemistry," *Journal of Pharmaceutical and Biomedical Analysis*, vol. 19, no. 1-2, pp. 55–68, 1999.

[163] D. Avnir, D. Levy, and R. Reisfeld, "The nature of the silica cage as reflected by spectral changes and enhanced photostability of trapped rhodamine-6G," *Journal of Physical Chemistry*, vol. 88, no. 24, pp. 5956–5959, 1984.

[164] C. M. McDonagh, A. M. Shields, A. K. McEvoy, B. D. MacCraith, and J. F. Gouin, "Optical sol-gel-based dissolved oxygen sensor: Progress towards a commercial instrument," *Journal of Sol-Gel Science and Technology*, vol. 13, no. 1-3, pp. 207–211, 1998.

[165] A. K. McEvoy, C. McDonagh, and B. D. MacCraith, "Optimisation of sol-gel-derived silica films for optical oxygen sensing," *Journal of Sol-Gel Science and Technology*, vol. 8, no. 1-3, pp. 1121–1125, 1997.

[166] R. M. Bukowski, V. P. Chodavarapu, A. H. Titus, A. N. Cartwright, and F. V. Bright, "Phase fluorometric glucose biosensor using oxygen as transducer and enzyme-doped xerogels," *Electronics Letters*, vol. 43, no. 4, pp. 202–204, 2007.

[167] X. Chen, L. Lin, P. W. Li, Y. J. Dai, and X. R. Wang, "Fluorescent response of sol-gel derived ormosils for optical ammonia sensing film," *Analytica Chimica Acta*, vol. 506, no. 1, pp. 9–15, 2004.

[168] L. Yang, S. S. Saavedra, and N. R. Armstrong, "Sol-gel-based, planar waveguide sensor for gaseous iodine," *Analytical Chemistry*, vol. 68, no. 11, pp. 1834–1841, 1996.

[169] D. N. Simon, R. Czolk, and H. J. Ache, "Doped sol-gel films for the development of optochemical ethanol sensors," *Thin Solid Films*, vol. 260, no. 1, pp. 107–110, 1995.

Chapter 3

Sol-gel-derived O$_2$ sensor films

3.1 Introduction

Sol-gel-derived chemical sensors have become increasingly important for optical sensor applications. In this study, the sol-gel technology is applied to produce porous support matrices, as the versatile nature of the sol-gel process enable the matrices to be tailored to meet the requirements of the desired application. This chapter deals with the development of O$_2$-sensitive sensor films for luminescence-based sensing. A range of xerogels were prepared by encapsulating the O$_2$-sensitive ruthenium complex [Ru(dpp)$_3$]$^{2+}$ in the ORMOSIL matrices. As a small molecule, O$_2$ can diffuse into the matrix, access the complex and quench its luminescence. The luminescence is due to de-excitation from an excited state ^{3}MLCT transition back to the ground singlet state as discussed in section 2.3.2 [1]. The O$_2$ sensor sensitivity can be tailored by modifying, for example the chemical composition of the sol-gel matrix and this approach was used in this work. The sol-gel-based matrix also serves as a barrier to prevent other interfering species from interacting with the entrapped [Ru(dpp)$_3$]$^{2+}$. A phase fluorometric detection scheme was used, which yields sensors that are insensitive to various operating parameters such as photobleaching of the luminophore, fluctuations in light intensity, detector sensitivity or changes in optical alignment [2]. The focus was on combining novel, organically modified sol-gel-derived matrices with the luminescent ruthenium complex to produce stable and robust optical

O$_2$ sensor films with enhanced sensitivity and humidity-insensitive response.

3.2 Materials and methods

3.2.1 Reagents and materials

Ruthenium(III) chloride hydrate, (RuCl$_3 \times$3H$_2$O), (4,7-diphenyl-1,10-phenanthroline) ligand, absolute ethanol (EtOH), 0.1 M hydrochloric acid (HCl) and the organosilicon precursors methyltriethoxysilane (MTEOS), ethyltriethoxysilane (ETEOS) and phenyl-triethoxysilane (PhTEOS), were purchased from Aldrich Chemicals. N-propyltriethoxy-silane (PTEOS) and 3,3,3-trifluoropropyltrimethoxysilane (TFP-TMOS) were obtained from ABCR. [Ru(dpp)$_3$]Cl$_2$ was synthesised by Dr. Adrian Guckian in the School of Chemical Sciences in DCU as described in the literature [3]. All chemicals were used as received. Glass slides were purchased from VWR International, polycarbonate (PC) sheets were purchased from Radionics. Oxygen (O$_2$) and nitrogen (N$_2$) gases were purchased from BOC gases.

3.2.2 Fabrication of O$_2$ sensor films

In a typical preparation, the relevant precursor MTEOS, ETEOS, PTEOS or PhTEOS was combined with absolute EtOH, followed by dropwise addition of aqueous HCl at pH 1. The mixture was then stirred for 20 minutes. An ethanolic solution of [Ru(dpp)$_3$]$^{2+}$ was subsequently added to the sol to give a final luminophore concentration of 2.5 g/L with respect to the total volume of the solution. The final mixture was stirred under ambient conditions and aged for various times depending on the precursor used. MTEOS-derived sols were aged for 4 h, PhTEOS-derived for 24 h, ETEOS- and PTEOS-derived for 5 weeks. In order to prepare xerogels containing a fluorinated alkoxysilane, TFP-TMOS was combined with MTEOS, ETEOS, PTEOS or PhTEOS in 1:1 molar ratio. All other aspects of these sols preparation were as described above. The final molar ratio of silane:EtOH:water:HCl in all sols was 1:6.25:4:0.007.

All films were formed by dip-coating onto glass slides or PC pieces (ETEOS-derived films only) using a dip-speed of 3 mms^{-1} in a controlled environment using a computer-controlled dipping apparatus which is shown in Figure 3.1. Dip-coating is a simple deposition method suitable for planar substrates where the sample is immersed and then withdrawn at a constant speed from the coating solution. The thickness of the deposited sol-gel-based film increases with dip speed [4].
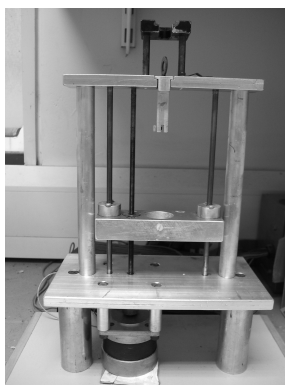

Figure 3.1: Dip-coating apparatus.

The glass slides were first treated with 30% nitric acid for 24 h and then rinsed with copious amounts of deionised water and EtOH. PC pieces were rinsed with EtOH before use. MTEOS- and PhTEOS-derived films were coated under ambient conditions, while ETEOS-, PTEOS- and all TFP-TMOS-based films were coated in a dry atmosphere (relative humidity, RH, 10%). This was achieved by flowing N_2 into the dip-coater chamber. Once coated, the samples were cured at 70 °C for 18 h and in the case of ETEOS- and PTEOS-derived sensor films, at either 70 °C or 110 °C for 18 h, depending on the experiment. All TFP-TMOS-based systems were cured at 110 °C. All fabricated sensor films were very uniform and crack-free. Samples were prepared in sextuplicate. All films were stored in the dark under ambient conditions for the long-term stability studies. All experiments were performed at room temperature.

3.2.3 Experimental characterisation systems

3.2.3.1 Phase fluorometry instrumentation

The O_2 sensor developed in this work is based on a phase fluorometric detection scheme. The experimental system used to characterise O_2 sensor films is shown in Figure 3.2. The sensor film was contained in a sealed flow cell (FC) along with a thermistor into which mixtures of O_2 and N_2 were flowed, controlled by mass flow controllers (Celerity, Ireland).
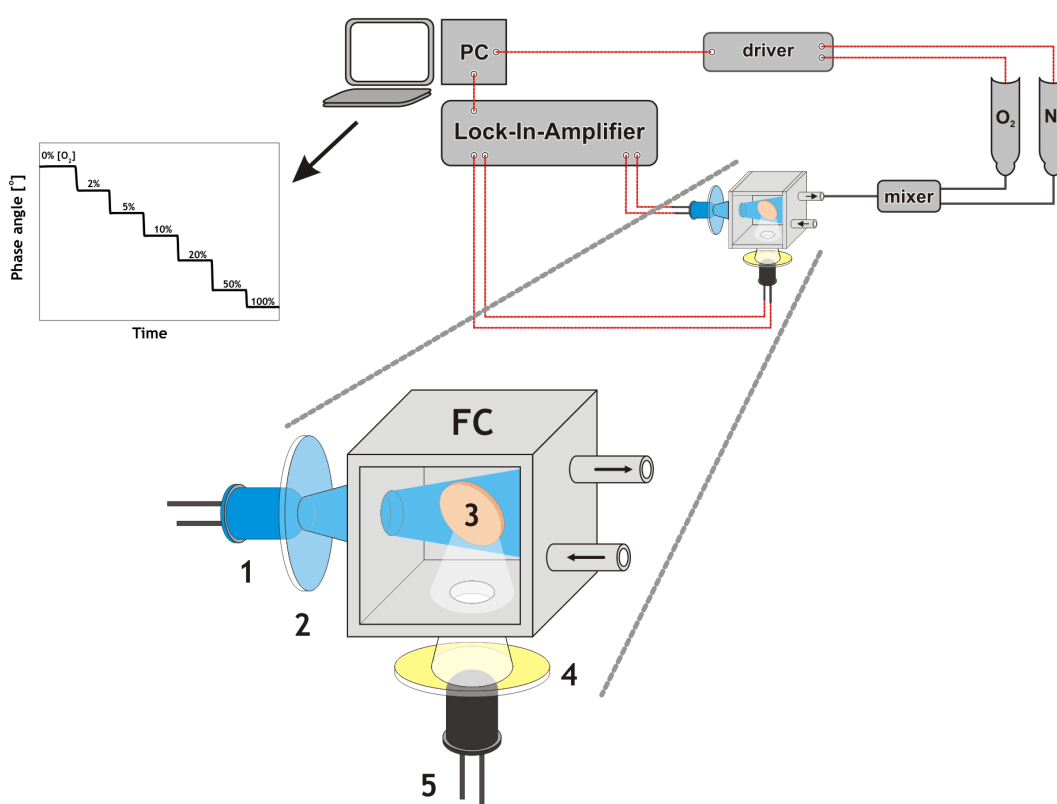

Figure 3.2: Schematic representation of the phase fluorometry experimental system. 1 - blue LED, 2 - excitation filter, 3 - O_2-sensitive sensor film, 4 - emission filter, 5 - photodiode, FC - flow cell.

The O_2 concentration was increased from 0% to 100% in predefined intervals. The duration of each interval was typically 2 min to ensure a new equilibrium point has been reached. The excitation source was a 450 nm blue LED (Roithner Lasertechnik, Austria) which was modulated at a frequency of 20 kHz using a digital dual-phase lock-in amplifier (Model 7265, Signal Recovery, UK). The modulation frequency of

the LED ideally should be matched to the luminophore lifetime via Equation 3.1:

$$2\pi f_{opt}\tau = 1 \tag{3.1}$$

where f_{opt} is the optimum frequency and τ is the lifetime of the luminophore. However, the signal-to-noise (SNR) ratio decreases as the modulation frequency increases and, therefore, the frequency has to be optimised in order to balance reduced SNR at high modulation frequency and reduced phase sensitivity at lower frequency [5].

The blue light passes through the short pass filter (ThorLabs, USA) before impinging on the sensor film, which was held at 45° to the excitation beam. The luminescence from the sample passes through a yellow dichroic filter (Edmund Optics, USA), which provides spectral discrimination of the excitation and luminescence emission, and was focused on the silicon photodiode detector (Hamamatsu, Japan). The luminescence is outputted as a voltage proportional to a phase angle. Both the excitation source and detector were operated using control electronics.

In order to test the effect of humidity on O_2 sensor sensitivity, two gas wash bottles containing deionised water were included in the gas line before the gas mixture entered the flow cell, and a commercial humidity probe (Testo 625, Germany) was employed to monitor the humidity in the cell.

The sensing of O_2 dissolved in water was accomplished by bubbling appropriate gas mixtures of O_2 in N_2 through deionised water at room temperature.

3.2.3.2 Luminescence lifetime measurements

The excited state lifetime of $[Ru(dpp)_3]^{2+}$ immobilised in sol-gel films was determined by Dr. Clare Higgins using a pulsed laser system in the School of Chemical Sciences in DCU [6]. The samples were excited with 15 ns pulses from a neodymium yttrium aluminium garnet (Nd:YAG) laser (λ_{exc} = 355 nm) from Spectron Laser Systems, United Kingdom. Samples were degassed with N_2 prior to measurements. The emitted decay was detected using a photomultiplier tube output that was connected to a digital oscilloscope. The excited state luminescence lifetime was calculated by analysing the

decay profile in Microcal Origin.

3.2.3.3 Diffusion coefficient measurements

The O$_2$ diffusion coefficient within the films was determined in order to establish the origin of the observed O$_2$ sensitivity. This was achieved by measuring the response time for films of known thickness. Diffusion coefficients were then obtained during a step change in O$_2$ concentration, using the model developed by Mills and Chang [7].

The sensor film thickness was measured using a white light interferometer (WYKO, NT1100, Veeco, USA) that provides 3D surface profile measurements without contact and is shown in Figure 3.3 (left) along with a typical X profile of the sol-gel-based film (right). Average thickness of the dip-coated O$_2$ films was in the range 450-700 nm depending on the composition of the relevant xerogel.
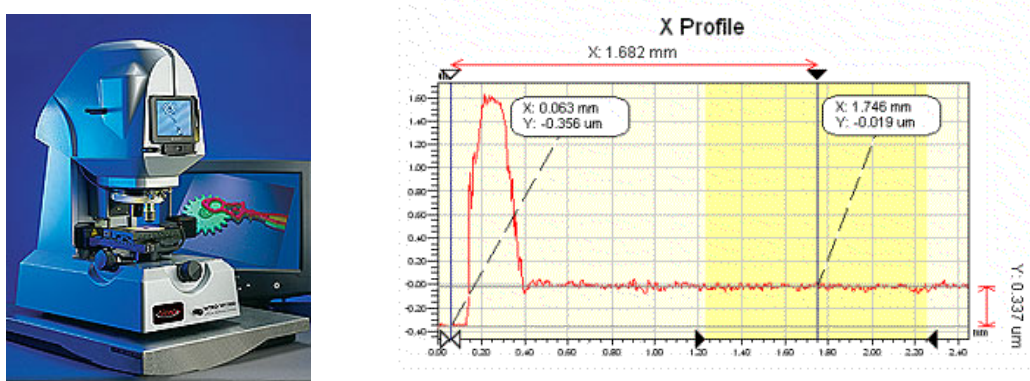
Figure 3.3: Image of interferometer WYKO, NT1100 (left). Reproduced from WYKO literature and a typical X profile of the sol-gel-derived film (right).

In order to measure the intrinsic response time of the sensor films and not that of the gas handling system (i.e., time taken to fill the gas cell and lines), the gas exchange times must be minimised. To this end, measurement instrumentation was developed that incorporated a fast solenoid valve capable of 5 ms switching times. Details of this characterisation system have been reported previously [8]. Briefly, the O$_2$ sensor film was attached to a fast solenoid valve and illuminated by the blue LED as depicted in Figure 3.4. The environment inside the solenoid valve was switched from O$_2$ to a vacuum using a LabView interface, thereby exposing the sensor to alternative
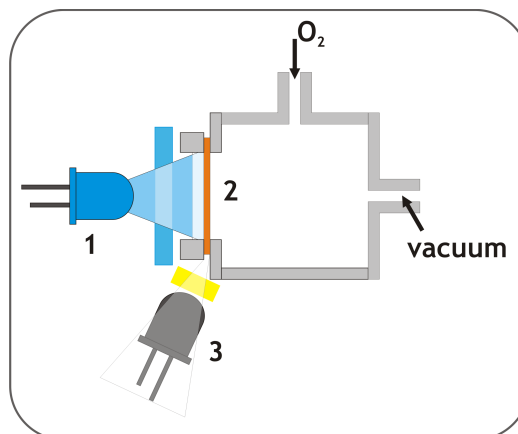
Figure 3.4: Schematic diagram of an O$_2$-sensitive film incorporated inside the solenoid valve for response time measurements. 1 - blue LED, 2 - O$_2$-sensitive sensor film, 3 - photodiode.

environments. The O$_2$-dependent luminescence was detected from the film surface by a photodiode detector. Sensing layers with a thickness of 1 μm were used as this was the minimum thickness compatible with the detection efficiency of the response time measurement apparatus. The parameter used to characterise response time in this study was t$_{90}$, which is the time taken to achieve 90% of optical signal change.

3.2.3.4 Contact angle measurements

Water contact angle measurements were made using a contact angle analyser (FTA 200, USA) shown in Figure 3.5 (left) by imaging a droplet of water that was dispensed onto the surface being characterised. The contact angle describes the shape of a liquid
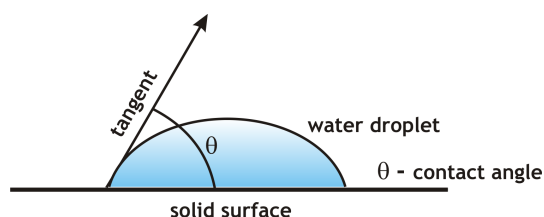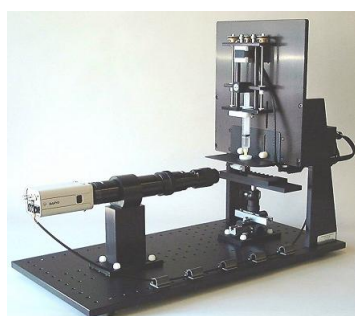
Figure 3.5: Image of FTA 200 contact analyser (left). Reproduced from FTA literature and a schematic representation of water contact angle (right).

droplet in contact with a solid. The contact angle θ is the angle between the tangent line and the solid surface as shown in Figure 3.5 (right). It was measured by imaging the drop on a CCD camera and analysing the captured images on a computer.

3.2.3.5 Other characterisation techniques

Absorption spectra were recorded using a two channel UV-Vis spectrophotometer (Cary® 50, Varian, USA) equipped with a xenon flash lamp as a light source. Solutions to be measured were contained in a quartz cuvette.

Luminescence emission spectra were acquired using a FluoroMax-2 spectrofluorometer (Horiba Jobin Yvon, USA) using a continuous wave 150 W xenon lamp as light source. The samples were contained in a quartz cuvette that was fixed at 45° with respect to the incident beam. Light emitted from the sample was guided through the monochromator and directed to the photomultiplier detector. Samples were excited at 450 nm.

Images of the film surface were taken using an optical Olympus microscope (objective lenses 4X, BX51M, United Kingdom).

AFM measurements were performed by Dr. Cedric Volcke using a Nanoscope III (Digital Instruments, USA) scanning probe microscope in ambient surroundings. Height images were obtained of sol-gel-derived O$_2$ sensor films based on ETEOS and PTEOS dip-coated on glass slides in dry environment. Films were dip-coated from sols aged for 5 weeks.

3.3   Characterisation of sol-gel-derived O$_2$ sensor films

3.3.1   Optical properties of [Ru(dpp)$_3$]$^{2+}$ in solution

As discussed in section 2.3.1.1 the luminescent O$_2$-sensitive complex of interest in this work is [Ru(dpp)$_3$]$^{2+}$. This is due to its high stability, good photostability, long-lived excited state luminescence lifetime ($\tau \sim 5$ µs), high quantum yield (0.4) and large Stokes shift as its absorption maximum is centered at 450 nm and its emission at 610 nm [9]. Strong absorption in the blue-green region of the spectrum is an attractive feature as it is compatible with low cost, commercially available blue LEDs. [Ru(dpp)$_3$]$^{2+}$ is also very soluble in typical sol-gel precursors and its optical properties remain much the same upon immobilisation in the sol-gel matrix [10]. Figure 3.6 displays absorption and emission spectra of [Ru(dpp)$_3$]$^{2+}$ dissolved in EtOH (c = 1.3×10^{-5} mol/L) along with emission profile of the blue LED and transmission spectrum of the emission filter used in this work.
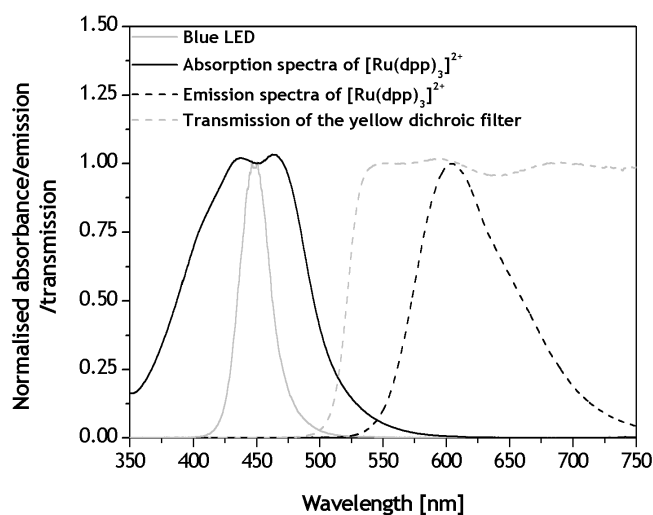
Figure 3.6: Normalised absorption and emission spectra of [Ru(dpp)$_3$]$^{2+}$ ($\lambda_{exc} = 450$ nm) dissolved in EtOH along with emission profile of the blue LED and transmission spectrum of the emission filter.

These attractive features of [Ru(dpp)$_3$]$^{2+}$ make it an ideal choice of luminophore for use in reliable, robust O$_2$ sensor platforms.

3.3.2   Performance of O$_2$ sensor films

ORMOSIL-based sensor films give enhanced O$_2$ sensitivity compared to TEOS-based films [11]. The degree of enhancement is related to the non-bridging R' bonds that act as network modifiers, increasing the film hydrophobicity and terminating the silicate network. Figure 3.7 shows the phase response for MTEOS- and PhTEOS-derived O$_2$ sensor films dip-coated on glass and cured at 70 °C for 18 h. As expected, the phase angle decreases ($[Ru(dpp)_3]^{2+}$ lifetime decreases) as the O$_2$ concentration increases.
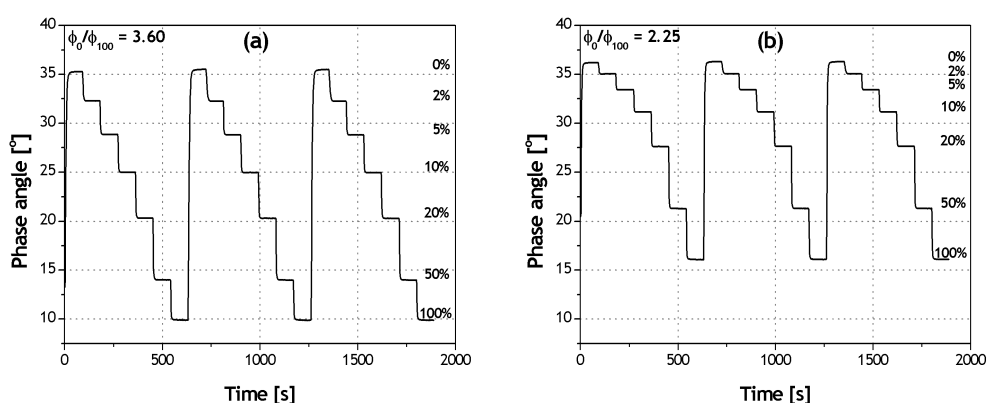
Figure 3.7: Phase response for (a) MTEOS- and (b) PhTEOS-derived O$_2$ sensor films cured at 70 °C.

As can be seen from the above figures, these sensors exhibit excellent repeatability from cycle to cycle, reversibility and short response times (less than 1 s). It is clear that PhTEOS-based sensor films are less sensitive ($\phi_0/\phi_{100} = 2.25$ where ϕ_0/ϕ_{100} is used as a measure of maximum O$_2$ sensitivity) towards O$_2$ than MTEOS-based O$_2$ films ($\phi_0/\phi_{100} = 3.60$). This is due to the steric hindrance of the bulky phenyl group.

Figure 3.8 presents typical Stern-Volmer plots (ϕ_0/ϕ versus $[O_2]$) for MTEOS- and PhTEOS-derived O$_2$ sensor films. The curves were evaluated using both the classical Stern-Volmer model and the Demas two-site model (Equation 2.2 and Equation 2.5 in section 2.3.2). The Demas model gave an excellent correlation ($r^2 = 0.999$) over the full O$_2$ concentration range when compared with the Stern-Volmer linear fit (see data in Table 3.1). This means that there are two independent luminophore

microdomains with different accessibilities (both are quenched at different rates).

PhTEOS-derived O$_2$ films are also well described by the simple Stern-Volmer model

($r^2 = 0.992$). In this case, it is not necessary to use the more complicated Demas

model for these xerogels, as the linear Stern-Volmer plot facilitates the use of simple

two-point calibration strategies. The calibration is based on the performance of 3
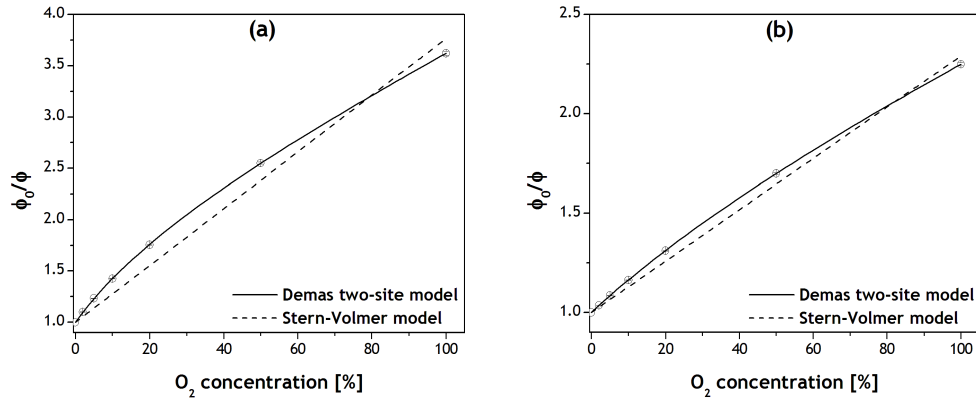

Figure 3.8: Best fit to the Stern-Volmer and Demas model for (a) MTEOS- and (b) PhTEOS-derived O$_2$ sensor films cured at 70 °C.

samples (n = 3). The error bars (Figure 3.8) associated with the films are very small.

This demonstrates that the film to film reproducibility is excellent for MTEOS- and

PhTEOS-based O$_2$ sensor films cured at 70 °C.

Table 3.1: Fit parameters for the Stern-Volmer and Demas models. Terms from Equation 2.5, r^2 - regression.

	Stern-Volmer	
Precursor	$K_{SV}[O_2]^{-1}$	r^2
MTEOS	0.0276 ± 0.0013	0.977
PhTEOS	0.0129 ± 0.0003	0.992

	Demas			
Precursor	f_1	$K_{SV1}[O_2]^{-1}$	$K_{SV2}[O_2]^{-1}$	r^2
MTEOS	0.65 ± 0.02	0.0724 ± 0.0027	0.0076 ± 0.0005	0.999
PhTEOS	0.59 ± 0.02	0.0262 ± 0.0006	0.0044 ± 0.0002	0.999

The data in the Table 3.1 also confirms that the Stern-Volmer constant associated

with the most readily quenched site, K_{SV1}, of PhTEOS-derived films is around 3

times lower than that of MTEOS-derived O_2 films. The recovered value for f_1 for MTEOS- and PhTEOS-derived films is 0.65 ± 0.02 and 0.59 ± 0.02, respectively, which means that 65% and 59% of $[Ru(dpp)_3]^{2+}$ molecules that are immobilised within the sol-gel matrix are entrapped within the microenvironment that makes these molecules about 10 fold (MTEOS) and 6 fold (PhTEOS) more sensitive to O_2 than the microenvironment occupied by $[Ru(dpp)_3]^{2+}$ molecules at site 2 entrapped in the same sensor film.

3.3.3   Influence of relative humidity

A key issue in the development of effective O_2 sensors for use in applications such as bioprocess monitoring is the effect of humidity on sensor response as there is a high degree of environmental humidity during the fermentation process (minimum 80% RH). Hydrophobic O_2 sensor films should have a reduced sensitivity to ambient moisture compared to hydrophilic matrices, for example matrices based on TEOS. For MTEOS- and PhTEOS-based films the methyl and phenyl group, respectively, render the xerogel surface hydrophobic (water contact angle of MTEOS-based xerogels is $87° \pm 1°$, PhTEOS-based films $92° \pm 1°$) The humidity dependence for MTEOS- and PhTEOS-derived O_2 xerogels is shown in Figure 3.9. The more hydrophobic
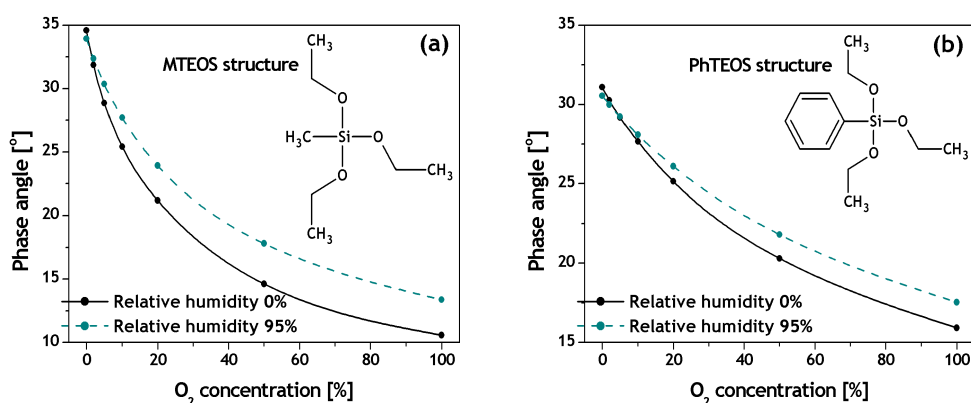
Figure 3.9: Effect of humidity on O_2 sensitivity for (a) MTEOS- and (b) PhTEOS-derived films cured at 70 °C.

PhTEOS-based film is clearly less sensitive to humidity than the MTEOS-based film.

Humidity reduced the film sensitivity by 10% and 17% at 100% of O$_2$ for PhTEOS- and MTEOS-derived sensor films, respectively.

It is proposed that the mechanism for this humidity interference is the partial blocking of the sol-gel matrix pores by the water molecules, which adsorb on the film surface. This will reduce the O$_2$ diffusion coefficient due to the relatively low solubility of O$_2$ in water. This increases the response times and decreases the observed sensitivity of the sensor films.

3.4 Development of humidity-insensitive sol-gel-based O$_2$ sensor films

3.4.1 Performance of hydrophobic O$_2$ sensor films

MTEOS- and PhTEOS-derived O$_2$ sensor films exhibited humidity-sensitivity as shown in Figure 3.9. The next task in this work was to design a matrix formulation that was completely insensitive to moisture. It was decided to develop O$_2$ sensor films using silanes that would form more hydrophobic matrices. ETEOS and PTEOS were the precursors of choice. Such materials should exhibit increased hydrophobicity and, therefore, be less prone to humidity interference.
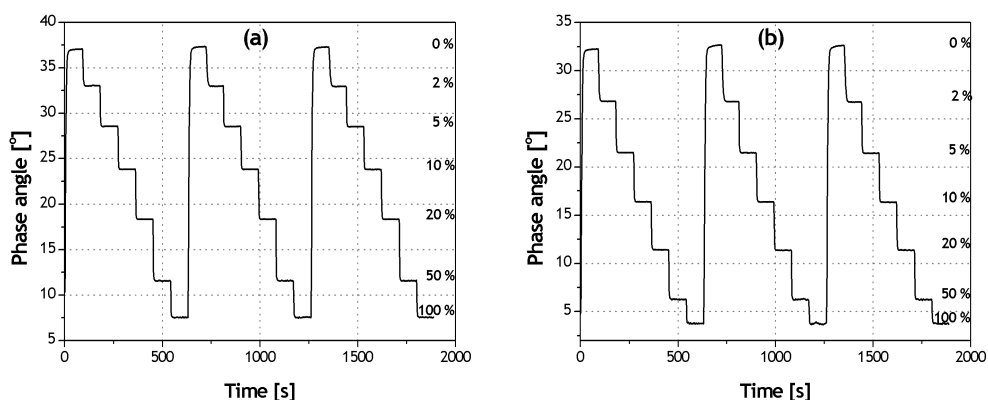
Figure 3.10: Phase response for (a) ETEOS- and (b) PTEOS-derived O$_2$ sensor films cured at 70 °C.

Figure 3.10 shows the phase response of ETEOS- and PTEOS-based O$_2$ films dip-

coated on glass and cured at 70 °C for 18 h. As for MTEOS- and PhTEOS-derived films, ETEOS- and PTEOS-based xerogels show excellent repeatability from cycle to cycle, reversibility and short response times (less than 1 second). The data for the novel films was also fitted to both the Demas two-site model and the Stern-Volmer model (Figure 3.11). The recovered fitting parameters are compiled in Table 3.2.
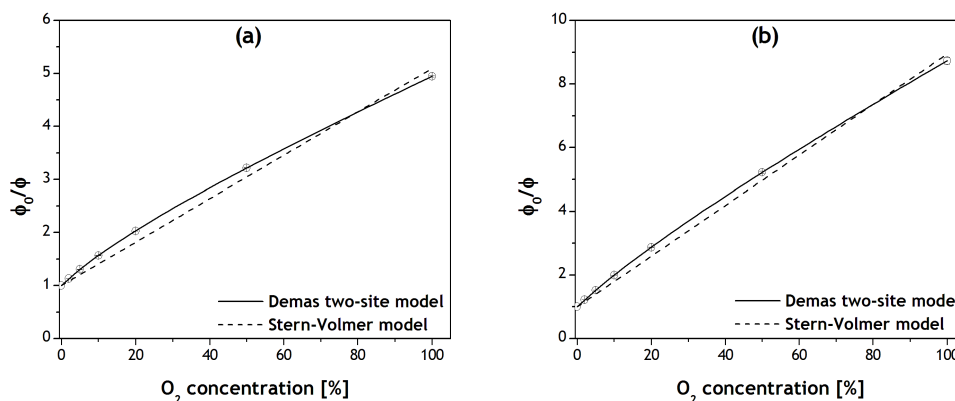

Figure 3.11: Best fit to the Stern-Volmer and Demas model for (a) ETEOS- and (b) PTEOS-derived O$_2$ sensor films cured at 70 °C.

Table 3.2: Fit parameters for the Stern-Volmer and Demas models. Terms from Equation 2.5, r^2 - regression

Precursor	Stern-Volmer	
	$K_{SV}[O_2]^{-1}$	r^2
ETEOS	0.0409 ± 0.0013	0.989
PTEOS	0.0794 ± 0.0018	0.995

Precursor	Demas			
	f_1	$K_{SV1}[O_2]^{-1}$	$K_{SV2}[O_2]^{-1}$	r^2
ETEOS	0.72 ± 0.02	0.0860 ± 0.0028	0.0123 ± 0.0007	0.999
PTEOS	0.90 ± 0.01	0.1192 ± 0.0019	0.0131 ± 0.0010	0.999

The Demas two-site model yields a superior correlation for both films (r^2_{ETEOS} = 0.999, r^2_{PTEOS} = 0.999), but they are also well described by the linear Stern-Volmer model (r^2_{ETEOS} = 0.989, r^2_{PTEOS} = 0.995). This means that the $[Ru(dpp)^3]^{2+}$ microenvironment is more homogeneous than in MTEOS-derived films described in section 3.3.2. In addition, a simple two-point calibration procedure can be used for

both ETEOS- and PTEOS-derived O$_2$ sensor films. Further inspection of the data in Table 3.2 reveals that ETEOS-based films are less O$_2$ sensitive ($\sim$ 2 times) than PTEOS-derived xerogels as they possess a lower value of K$_{SV}$. Both new sensor compositions are more sensitive towards O$_2$, especially at low O$_2$ concentration, than the MTEOS- and PhTEOS-based sensor films. Again, small error bars, shown within the data points (n = 3) in Figure 3.11, demonstrate excellent film to film reproducibility.

3.4.2 Humidity interference

Figure 3.12 illustrates the humidity sensitivity of ETEOS- and PTEOS-derived sensor films cured at 70 °C. As can be seen from the figures, the films show slightly higher sensitivity (7% for ETEOS- and 5% for PTEOS-based films at 100% of O$_2$, respectively) in 95% relative humidity. The effect was more pronounced for films dip-coated on PC. The effect of the substrate on sensor performance remains to be addressed. The drying treatment at 70 °C proved insufficient for the ETEOS- and PTEOS-derived films that remained sticky. These sensor films also exhibited relatively poor surface quality when compared to the MTEOS- and PhTEOS-based sensor films, cured with the same temperature programme.
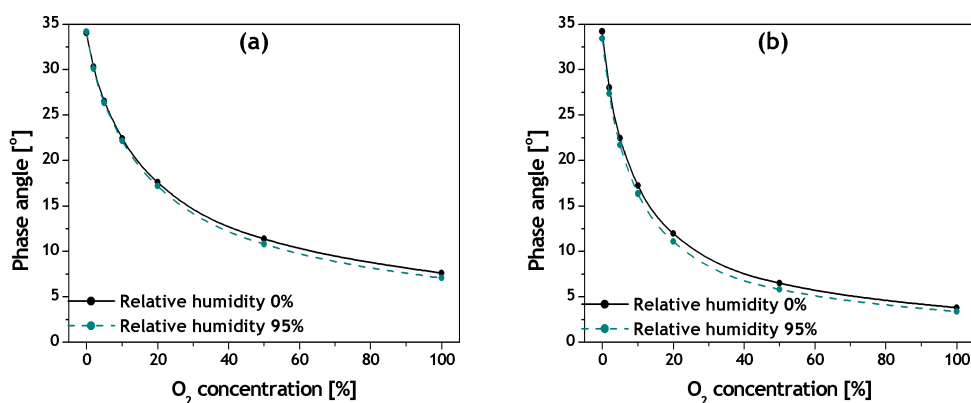

Figure 3.12: Effect of humidity on O$_2$ sensitivity for (a) ETEOS- and (b) PTEOS-derived films cured at 70 °C.

3.4.3 Tailoring of the response of hydrophobic O$_2$ sensor films

It was noticed that sensor films looked uniform and transparent only for a short time ($\sim$ 5 s) after dipping, subsequently turning cloudy upon exposure to the surrounding atmosphere. This effect was not observed for MTEOS- and PhTEOS-derived films, indicating that this effect is precursor-dependent. To improve the optical quality of the ETEOS- and PTEOS-derived O$_2$ films, it was decided to decrease the ambient humidity while coating. A series of ETEOS- and PTEOS-based films were dip-coated in both ambient and dry environments for comparison purposes. Figure 3.13 shows PTEOS-derived oxygen sensor films that were dip-coated in (a) dry ($\sim$10% RH) and (b) ambient ($\sim$40% RH) conditions. A significant improvement was achieved for both ETEOS- and PTEOS-derived O$_2$ films when using a dry atmosphere during dip-coating. The films showed excellent surface quality as shown in Figure 3.13a. Coating under ambient conditions caused the formation of droplets on the film surfaces. The water vapor in the atmosphere affects the microstructure of the thin films. It is proposed that increased humidity in the surroundings (ambient humidity is usually about 40%) of the film lead to separation of the liquid components and/or uncontrolled hydrolysis. The resulting coatings exhibit a cloudy appearance with crater-like structures (Figure 3.13b). By modifying the dip-coating process, it was possible to reduce the susceptibility of the wet film to humidity, thereby improving coating quality and reproducibility, both on glass and polymer substrates.
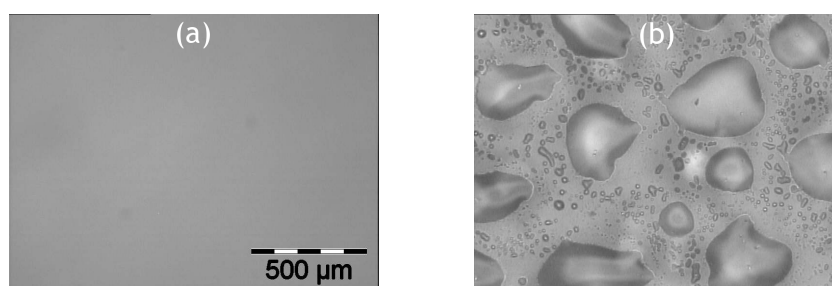

Figure 3.13: Surface of PTEOS-derived films dip-coated (a) in dry and (b) in ambient conditions. Photographs taken through an optical microscope. The same magnification was used for both images.

The ageing time of the sols is also an important factor when dip-coating ETEOS- and PTEOS-derived O$_2$ films. It was established that ETEOS-based sols require at least 3 weeks of ageing, whilst PTEOS-based sols should be aged for 4 weeks in order to obtain uniform thin films. This is due to the slow condensation rates of such precursors under the conditions employed. Distinct differences can be seen for ETEOS-derived film surfaces when using sols aged for (a) 24 h and (b) 3 weeks (see Figure 3.14).
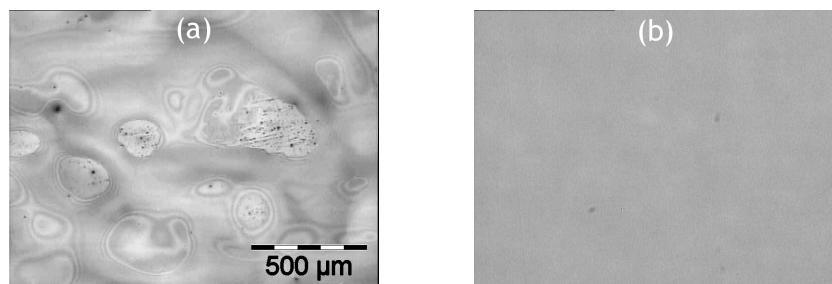

Figure 3.14: Surface of ETEOS-based films aged for (a) 24 h and (b) 3 weeks. Photographs taken through an optical microscope. The same magnification was used for both images.

Height AFM images also confirm good quality of ETEOS- and PTEOS-based sensor films surface properties on a nanoscopic scale as shown in Figure 3.15. Both
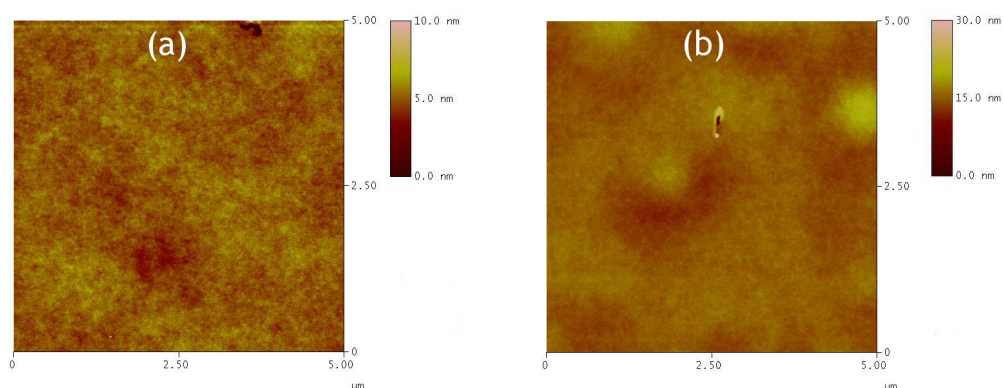
Figure 3.15: AFM height images of (a) ETEOS-based and (b) PTEOS-based O$_2$ sensor films dip-coated in dry conditions and cured at 110 °C. Sols were aged for 5 weeks.

samples exhibit smooth and relatively featureless surface. Surface roughness was

measured to be around 2 nm.

3.4.4 Influence of relative humidity

ETEOS- and PTEOS-derived O$_2$ sensor films were coated in dry conditions and cured at 110 °C (these films were not dry enough when cured at 70 °C) and then were scanned in dry ($\sim$ 10% RH) and humid ($\sim$ 95% RH) conditions in order to examine their humidity sensitivity. Figure 3.16 shows the influence of humidity on ETEOS- and PTEOS-based O$_2$ sensor films cured at 110 °C for 18 h. Figure 3.16 clearly shows that humidity-sensitivity was eliminated for ETEOS- and PTEOS-derived xerogels cured at 110 °C.
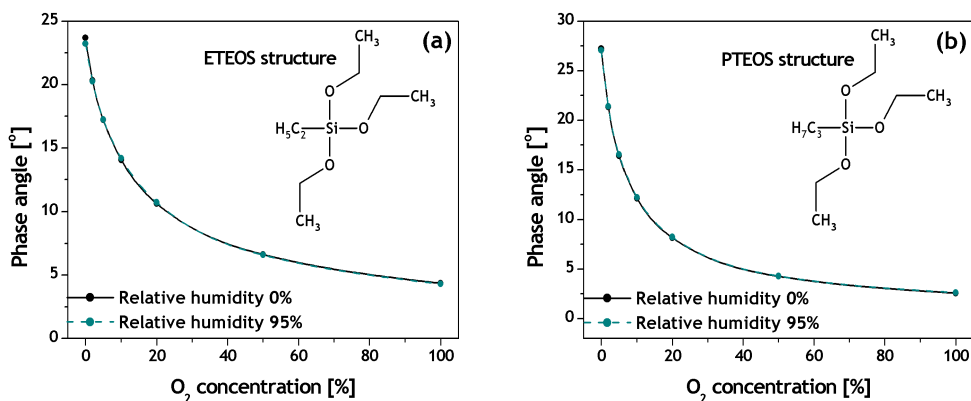
Figure 3.16: Effect of humidity on O$_2$ sensitivity for (a) ETEOS- and (b) PTEOS-derived films cured at 110 °C.

The water contact angles of films dip-coated on glass were measured and are shown in Table 3.3. The measurements show that these coatings have a hydrophobic

Table 3.3: Water contact angles of ETEOS- and PTEOS-derived xerogels.

	Water contact angle [°]	
Sensor platform	glass 70 °C	glass 110 °C
ETEOS-based xerogels	95 $\pm$ 1	97 $\pm$ 2
PTEOS-based xerogels	100 $\pm$ 1	100 $\pm$ 1

surface and are highly water-repellent. In general, if the contact angle of water is less than 30°, the surface is designated hydrophilic and water spreads over the surface

without the formation of droplets. On a hydrophobic surface, water forms distinct droplets. Surfaces with contact angle greater than 80° are designated as hydrophobic [12]. Figure 3.17 presents the capture images of drop of water on (a) PTEOS-derived film surface cured at 110 °C and for comparison on (b) plain microscope glass slide surface. The water contact angle of PTEOS-based film surface was found to be 100° and that of a plain microscope glass surface was 13°. There is no significant
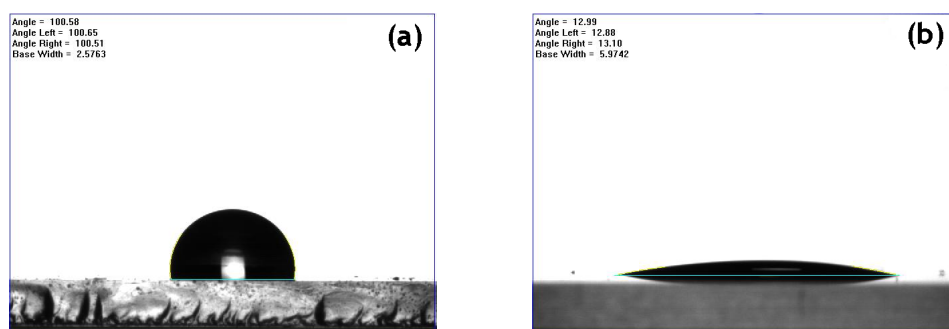

Figure 3.17: Image of drop of water on a (a) PTEOS-derived film and (b) glass slide surface.

difference in water contact angle values for films dip-coated on glass as the curing temperature is increased, indicating thermal stability of the films. The heat treatment seems not to influence the surface enrichment of the ethyl and propyl groups. However, it is expected that it improves the material connectivity and hardness. Measured water contact angles for ETEOS- and PTEOS-derived xerogels are higher than those measured for MTEOS- and PhTEOS-derived films, which is consistent with the increase in the hydrophobicity of the films as the length of the non-hydrolysable alkyl group is increased.

Sol-gel-based O$_2$ sensor films, which are insensitive to humidity, were successfully implemented by fabricating matrices using ETEOS and PTEOS precursors, which form more hydrophobic matrices than those derived from MTEOS or PhTEOS. Increasing the curing temperature of the films from 70 °C to 110 °C, prolonging the ageing time of these sols, and consequently improving the surface morphology of the xerogels are important factors that helped to yield humidity-insensitive materials.

3.5 Comparison of performance of different sensor formulations

Figure 3.18 shows an example of the phase response of six PTEOS-derived O_2 sensors. All O_2 sensor films dip-coated on glass and cured at 110 °C exhibited excellent repeatability, reversibility and reproducibility. The response in Figure 3.18 is typical of each of the pure ORMOSIL sensor elements produced in this work.
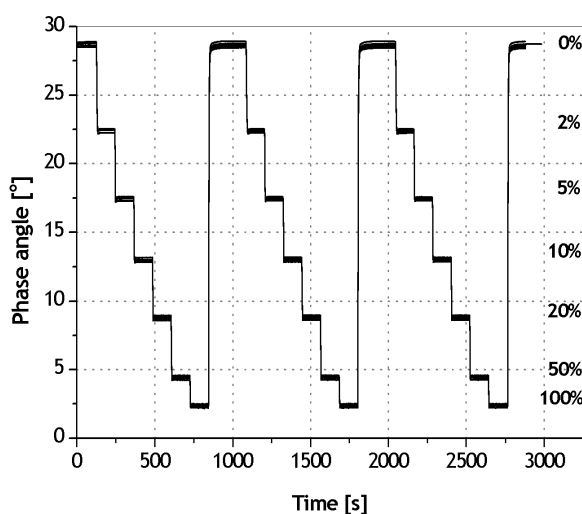

Figure 3.18: Phase response of six PTEOS-derived O_2 sensor films cured at 110 °C.

All sensors also exhibited very short response times. The shortest t_{90} was found for ETEOS- and PTEOS-based sensors. The response times of these sensors were 232 ms and 223 ms, respectively. The response time of MTEOS-based film was 432 ms. The longest t_{90} was found for the PhTEOS-based sensor platforms ($t_{90} = 2687$ ms) due to the relatively low value of diffusion coefficient (D) for this film (see Table 3.5). This response time was an order of magnitude greater than that of any of the other materials tested. Short response time is an important consideration in medical applications such as in O_2 breath monitoring.

3.5.1   O$_2$ sensitivity

Figure 3.19 presents the best fit to the Stern-Volmer and Demas two-site models for

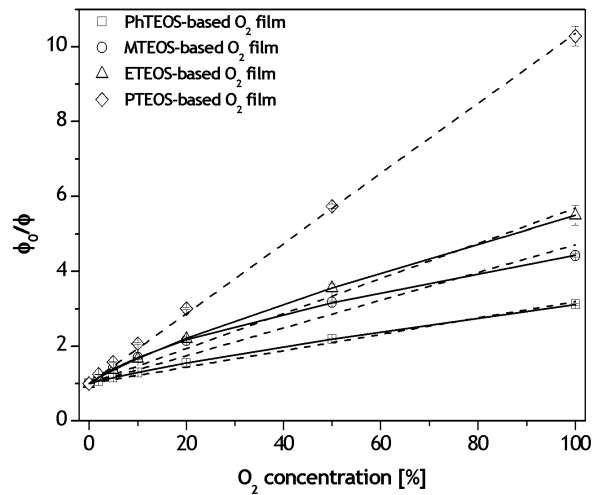a set of O$_2$ sensor films cured at 110 °C which were 6 weeks old.

Figure 3.19: Best fit to the Stern-Volmer (dashed lines) and Demas model (solid lines) for MTEOS-, ETEOS-, PTEOS- and PhTEOS-based sensor platforms cured at 110 °C. The slope represents K$_{SV}$, O$_2$ sensitivity.

Table 3.4 compares the recovered fitting parameters for the data from this figure.

There is a very good fit to a linear Stern-Volmer model over the full O$_2$ concentration

Table 3.4: Fit parameters for the Stern-Volmer and Demas models. Terms from Equation 2.5, r^2 - regression

.

Precursor	Stern-Volmer	
	K$_{SV}$[O$_2$]$^{-1}$	r^2
MTEOS	0.0371 ± 0.0026	0.944
ETEOS	0.0468 ± 0.0017	0.986
PTEOS	0.0936 ± 0.0009	0.999
PhTEOS	0.0219 ± 0.0007	0.990

Precursor	Demas			
	f$_1$	K$_{SV1}$[O$_2$]$^{-1}$	K$_{SV2}$[O$_2$]$^{-1}$	r^2
MTEOS	0.70 ± 0.02	0.1273 ± 0.0076	0.0073 ± 0.0197	0.999
ETEOS	0.74 ± 0.02	0.1181 ± 0.0052	0.0123 ± 0.0011	0.999
PhTEOS	0.61 ± 0.04	0.0485 ± 0.0030	0.0081 ± 0.0390	0.999

range (0-100% O$_2$) for PTEOS-derived sensor platforms, which means that it is not

necessary to use the more complex Demas two-site model for these films. Stern-Volmer plots for ETEOS-, PTEOS- and PhTEOS-derived sensor platforms are very well described by Equation 2.2 ($r^2_{ETEOS} = 0.986$, $r^2_{PTEOS} = 0.999$, $r^2_{PhTEOS} = 0.990$). Such a response simplifies calibration and demonstrates that the environment of $[Ru(dpp)_3]^{2+}$ molecules is more homogeneous than within MTEOS-based films. The fit to the Demas model was excellent for MTEOS-, ETEOS- and PhTEOS-derived films ($r^2 = 0.999$). The error bars associated with the films shown in Figure 3.19 are very small (0.04° for MTEOS- and PhTEOS-derived films and 0.26° for ETEOS- and PTEOS-based O_2 films at 100% O_2) and demonstrate that film to film reproducibility is very good. Inspection of Figure 3.19 also provides evidence that the more hydrophobic xerogels are more sensitive to lower levels of O_2. All sensors exhibit different sensitivities as indicated by the K_{SV} values shown in Table 3.4. PTEOS-based films exhibit the greatest sensitivity, ETEOS- and MTEOS-derived xerogels similar sensitivities and PhTEOS-based O_2 sensor is the least sensitive due to the steric effect of the phenyl group. Figure 3.20 presents the influence of alkyl chain length on the Stern-Volmer constant, K_{SV}. These results show that K_{SV} increases as the alkyl chain length of the sol-gel precursor increases.
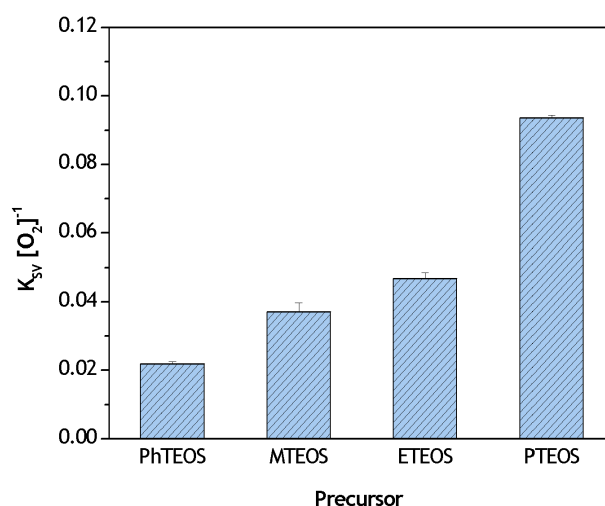

Figure 3.20: Effect of ORMOSIL alkyl chain length on the Stern-Volmer constant, K_{SV}.

In order to understand the origin of improved O_2 sensitivity, more experiments were carried out. As mentioned earlier, O_2 sensitivity is dependent on both τ_0 and D. To elucidate the origins of the improved sensitivity of O_2 films D, τ_0 and water contact angle were determined for each xerogel. Table 3.5 reports on the effect of the organosilicon precursor on the properties for the O_2 sensor elements. There is

Table 3.5: Influence of organosilicon precursor on xerogel properties. Accuracy of lifetime measurements $\pm$ 10%.

Precursor	Sensitivity ϕ_0/ϕ_{100}	D$\times$ 10^{-6} [cm^{2}s^{-1}]	Water contact angle [°]	τ_0 [µs]
MTEOS	5.45 $\pm$ 0.29	9.86	91 $\pm$ 3	4.92
ETEOS	6.35 $\pm$ 0.16	62.1	97 $\pm$ 2	4.91
PTEOS	10.27 $\pm$ 0.27	67.3	100 $\pm$ 1	5.11
PhTEOS	3.12 $\pm$ 0.03	0.03	93 $\pm$ 1	5.81

a good correlation between sensor sensitivity, ϕ_0/ϕ_{100}, and both measured D and water contact angle. The parameters ϕ_0/ϕ_{100}, D and water contact angle increase in magnitude as the alkyl chain length increases. From Table 3.5, τ_0 was found to remain essentially constant for MTEOS-, ETEOS- and PTEOS-based sensor materials. While all samples were stored in a N_2 environment, minor deviations in the lifetime data are thought to be due to slight fluctuations in O_2 concentration within the measuring environment due to leaks in the sample cell. Therefore, we can attribute the enhanced sensitivity to the increase of O_2 transport within the ETEOS- and PTEOS-based O_2 films, as evidenced by the D values recorded for these films. Moreover, organic groups that act as network modifiers increase the hydrophobicity of the xerogels as evidenced by high values of water contact angle. PhTEOS-based sensor elements exhibit a longer excited state lifetime (ca. 18%) than other materials tested but exhibit ca. 5 times lower sensitivity than the most sensitive PTEOS-based films, which is due to the steric effect of the bulky phenyl group. It is also worth pointing out that films cured at 110 °C are more sensitive towards O_2 than those films cured at 70 °C. When an elevated curing temperature programme was employed, O_2 sensitivity increased by 43%, 15%, 15% and 45% for MTEOS- ETEOS-, PTEOS- and PhTEOS-

derived xerogels, respectively. Increased thermal curing caused the remaining water and solvent to evaporate, thereby increasing the population of accessible luminophore molecules. It is also well known that ageing and thermal treatment result in increased pore size of sol-gel glasses and this may also account for the observed increase in O_2 sensitivity [13].

3.5.2 Long-term stability

Stability over time is a very important parameter for any sensor. Figure 3.21 shows the effect of storage time on the response stability of O_2 sensors. The results show
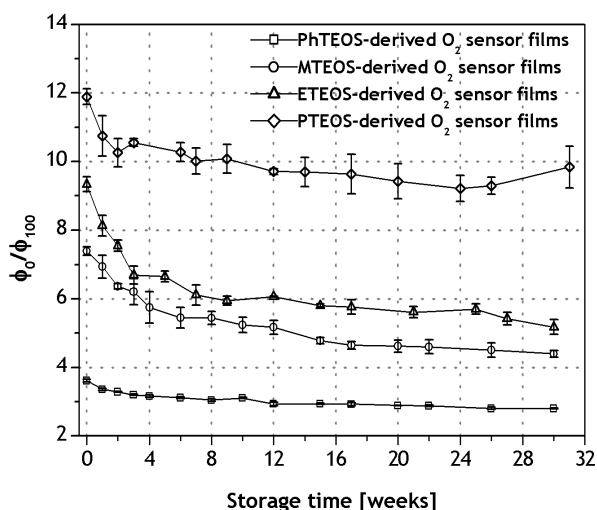
Figure 3.21: Effect of storage time on O_2 sensors sensitivity.

changes in sensitivity during the first few weeks following sensor films fabrication. MTEOS-, ETEOS- and PTEOS-derived sensor responses stabilise after around 4 weeks. PhTEOS-based material stabilses after 2 weeks of storage. Over seven months of long-term stability study, MTEOS-, ETEOS-, PTEOS- and PhTEOS-derived xerogels exhibit ϕ_0/ϕ_{100} values of: 4.88 ± 0.40 (RSD = 8.2%), 5.83 ± 0.40 (RSD = 6.9%), 9.72 ± 0.34 (RSD = 3.5%) and 3.01 ± 0.15 (RSD = 5.0%), respectively. These results show that ORMOSIL-based O_2 sensor films exhibit very good long-term stability. Previous experiments in our laboratory showed that TEOS-based O_2 films

significantly lose sensitivity with time [14]. Such a good stability of ORMOSIL-based films arises from the flexibility of these xerogels and the presence of non-hydrolysable organic groups [11].

3.5.3 Photostability

Luminescence-based sensors are susceptible to photodegradation when exposed to the excitation source for prolonged time and thus optical sensors often exhibit limited long-term stability [15]. Photodegradation of the luminophore alters luminescence intensity and therefore such sensors are not reliable. Photobleaching should not affect decay time parameters. However, Klimant et al. have indicated that the photoproducts may exhibit their own lifetime and also quench O_2-sensitive dye luminescence [16].

In order to minimise the photobleaching effect, it is recommended to reduce the excitation source intensity or use a pulsed LED. Hartmann et al. investigated the use of some tertiary amines, which act as singlet O_2 quenchers as it is known that destructive singlet O_2 is formed as a by-product of dynamic quenching of O_2 [17]. They showed that photobleaching associated with both luminescence intensity and lifetime can be significantly reduced by employing singlet O_2 scavengers.

Some of these approaches have been investigated in our laboratory by others and the details of this work are not presented here [18].

3.6 Characterisation of the optimum O_2 sensor film for bioprocess monitoring

Glass is the optimum substrate for use with the sol-gel coatings due to the close compatibility between the materials and most data shown so far described only films dip-coated on glass as a substrate. However, glass is not easily mouldable and can not be used when moulded sensor windows or non-planar sensor platforms are required. Plastics can be moulded to produce disposable sensor platforms and are the required substrate for some bioprocess applications. Polymer substrates allow for flexibility in

designing sensor platforms in a variety of configurations.

The objective of this phase of my study was to develop a humidity-insensitive O$_2$ optical, plastic sensor with enhanced sensitivity for use in bioprocess monitoring. ETEOS-derived O$_2$ sensor films, dip-coated on PC and cured at 110 °C for 18 h, were chosen as the optimum O$_2$ sensor films for bioprocess applications. PTEOS-based films were, in fact, too O$_2$ sensitive, 80% of the $[Ru(dpp)_3]^{2+}$ luminescence being quenched under ambient conditions (O$_2$ range specified for bioprocess monitoring was 0-25% O$_2$ with a typical operation conditions between 15-21% O$_2$).

Figure 3.22 presents (a) the phase response of 6 sensors of choice and (b) the influence of humidity on O$_2$ films response. The sensor performance can be char-
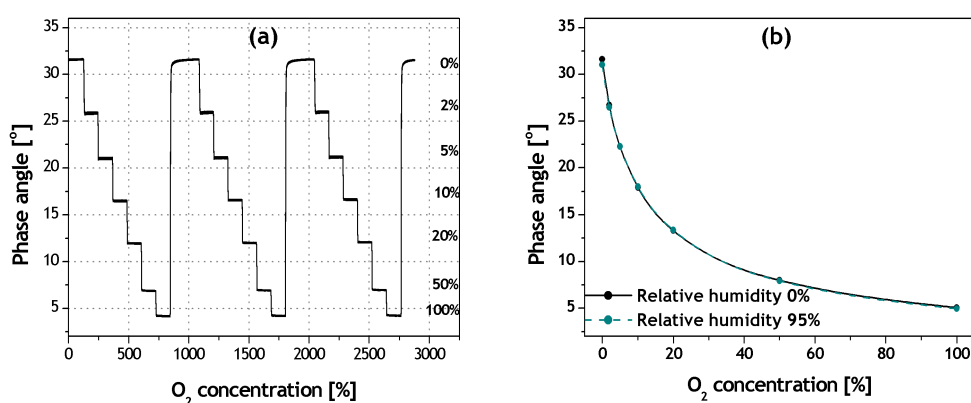
Figure 3.22: (a) Phase response of 6 ETEOS-derived O$_2$ sensor films and (b) influence of humidity on O$_2$ response for films dip-coated on PC and cured at 110 °C.

acterised by excellent repeatability from cycle to cycle, reversibility, short response times, enhanced O$_2$ sensitivity and humidity-insensitivity (water contact angle for ETEOS-based films coated on PC was found to be 98° ± 2°).

Figure 3.23 shows the best fit to the Demas and Stern-Volmer model for 6 week old sensor films. From this figure, it can be seen that good correlation was obtained for the two models, the Demas two-site model ($r^2 = 0.999$) and the Stern-Volmer model ($r^2 = 0.990$). This result indicates that ETEOS-based O$_2$ films dip-coated on PC are compatible with a two-point calibration procedure.
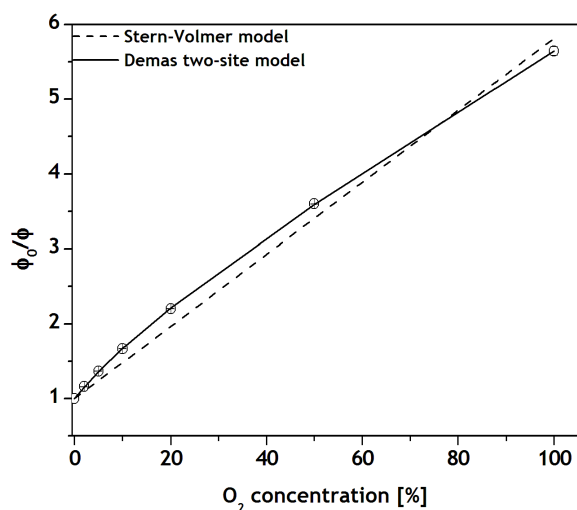
Figure 3.23: Best fit to the Stern-Volmer and Demas model for ETEOS-derived films coated on PC.

Figure 3.24 illustrates the long term stability of such sensor films. The stability of these films is very good over a 9 months period. Again, it takes around 4 weeks for the films to stabilise. Over this 9 month period of stability study the films exhibit
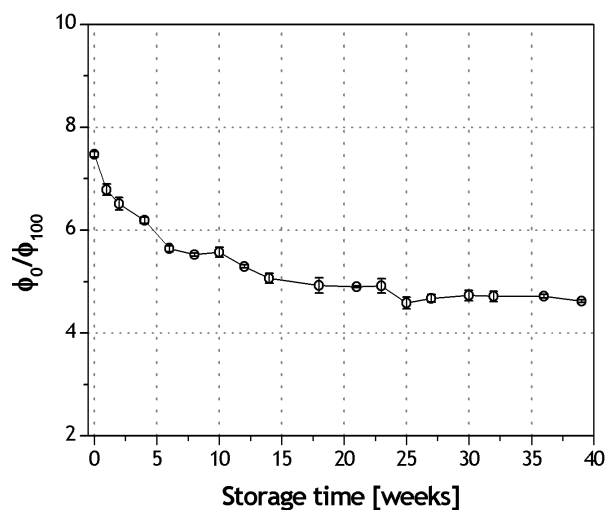
Figure 3.24: Effect of storage time on ETEOS-derived O$_2$ sensor coated on PC.

ϕ_0/ϕ_{100} value of 4.99 ± 0.4 (RSD = 7.4%). The calculated limit of detection (LOD) for these sensor films in the flow-cell-based instrumentation in this laboratory yielded 0.006% ± 0.001% of O$_2$ and a resolution of 0.015% ± 0.003% (in the range 0-20%

O$_2$), which compares favorably with previously reported sensors [19].

The sensors for bioprocess applications have to be capable of withstanding steam-sterilisation without the need of sensor recalibration after the sterilisation cycle. This study was pursued by others in our laboratory and it was shown that the ETEOS-based sensor response remains stable after 6 autoclave cycles [5]. However, alternatively, O$_2$ sensor films for such applications can be gamma-sterilised, which is a less demanding process than autoclaving, and this approach will be investigated in the future work.

3.7   Performance of O$_2$ sensor films based on fluorinated sol-gel precursor

In the last phase of my study on O$_2$ sensor films, the fluorinated sol-gel precursor, TFP-TMOS (Figure 3.25) was used to develop highly O$_2$-sensitive materials. $[Ru(dpp)_3]^{2+}$ was entrapped within the xerogels composed of TFP-TMOS and organosilicon precursors, MTEOS, ETEOS, PTEOS- and PhTEOS in the 1:1 molar ratio. The O$_2$ sensitivity of these films was compared to the pure

Figure 3.25: Chemical structure of TFP-TMOS.

ORMOSIL-based sensors described in section 3.5. The influence of humidity and stability of these films were also investigated.

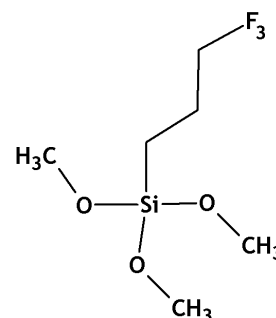Figure 3.26 displays a phase response of six PTEOS/TFP-TMOS-derived xerogels which are the most O$_2$-sensitive sensor films fabricated in the course of this study. These films exhibit much higher O$_2$ sensitivity at low O$_2$ concentration as shown in Figure 3.26 ($\Delta\phi$ from 0-5% O$_2$ = 16.4°, for PTEOS-based films = 10.9°), which makes them suitable for applications where continuous O$_2$ measurements are required at very low O$_2$ concentration. Moreover, film to film reproducibility is excellent.
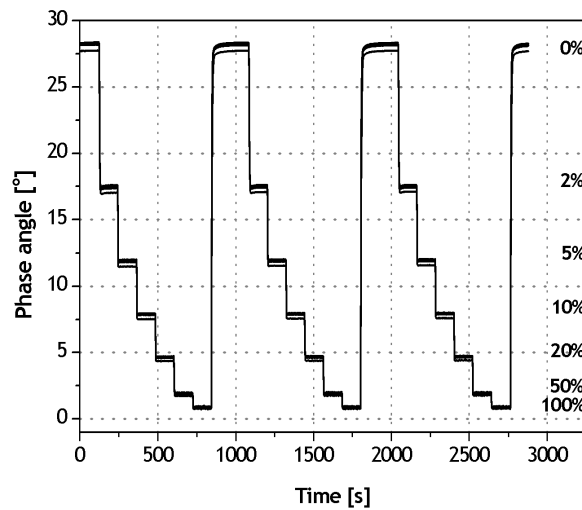
Figure 3.26: Phase response of six PTEOS/TFP-TMOS-derived O_2 sensor films cured at 110 °C.

3.7.1 O_2 sensitivity

Figure 3.27 represents typical Stern-Volmer plots for films derived from MTEOS/TFP-TMOS, ETEOS/TFP-TMOS, PTEOS/TFP-TMOS and PhTEOS/TFP-TMOS, which had been stored for 6 weeks. The Stern-Volmer plots for all the films tested ap-
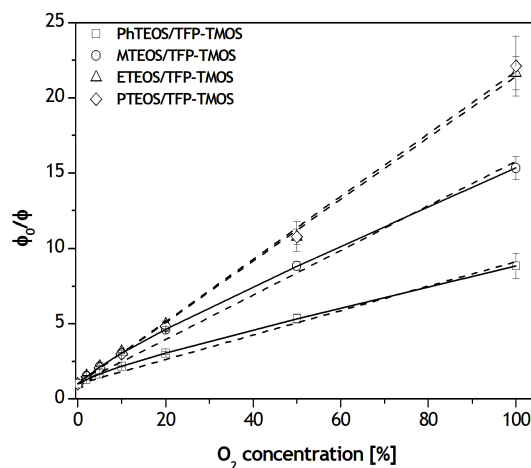

Figure 3.27: Best fit to the Stern-Volmer (dashed lines) and Demas model (solid lines) for MTEOS/TFP-TMOS-, ETEOS/TFP-TMOS-, PTEOS/TFP-TMOS- and PhTEOS/TFP-TMOS-based sensor films cured at 110 °C.

pear to be linear with the best linear fit for ETEOS/TFP-TMOS and PTEOS-TFP-

TMOS ($r^2 = 0.999$) over the full O_2 concentration range. MTEOS/TFP-TMOS and PhTEOS/TFP-TMOS were fitted to both Stern-Volmer and two-site Demas models. As expected, the Demas model gave excellent correlation with $r^2 = 0.999$. These xerogels are also quite well described by the Stern-Volmer equation ($r^2 = 0.991$ and $r^2 = 0.988$ for MTEOS/TFP-TMOS and PhTEOS/TFP-TMOS, respectively). These sensor films exhibit much greater O_2 sensitivity than observed for pure ORMOSIL-based films described in the previous section (see Table 3.5). Table 3.6 presents the ϕ_0/ϕ_{100} values for sensor films based on the composite of the MTEOS, ETEOS, PTEOS and PhTEOS with TFP-TMOS.

Table 3.6: ϕ_0/ϕ_{100} values for sensor films based on the fluorinated precursor TFP-TMOS.

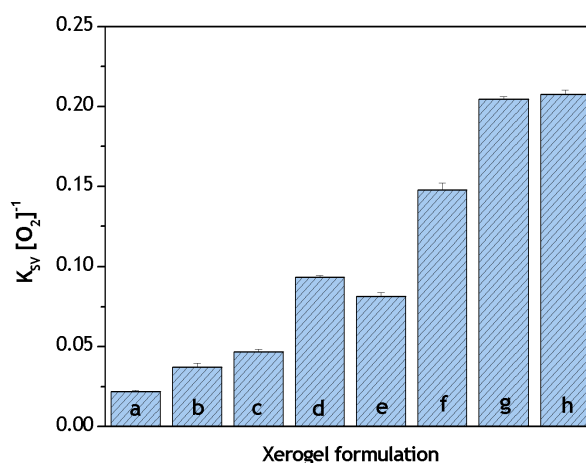| Sensor platform	ϕ_0/ϕ_{100}
MTEOS/TFP-TMOS	15.34 ± 0.77
ETEOS/TFP-TMOS	21.65 ± 1.11
PTEOS/TFP-TMOS	22.12 ± 1.99
PhTEOS/TFP-TMOS	8.85 ± 0.84

Figure 3.28: Effect of xerogel formulation on the Stern-Volmer constant, K_{SV}: (a) PhTEOS-, (b) MTEOS-, (c) ETEOS-, (d) PTEOS-, (e) PhTEOS/TFP-TMOS-, (f) MTEOS/TFP-TMOS-, (g) ETEOS/TFP-TMOS- and (h) PTEOS/TFP-TMOS-based sensor elements cured at 110 °C.

Figure 3.28 presents the effect of all $[Ru(dpp)_3]^{2+}$ doped xerogels compositions produced in this study on O_2 sensitivity, K_{SV}. K_{SV} for the PhTEOS/TFP-TMOS-

based material increased by 2 fold and for other systems increased by 4 fold when compared to pure ORMOSIL-based films. Such an increase in sensitivity arises from better O_2 transport within these types of xerogels [20].

3.7.2   Influence of relative humidity

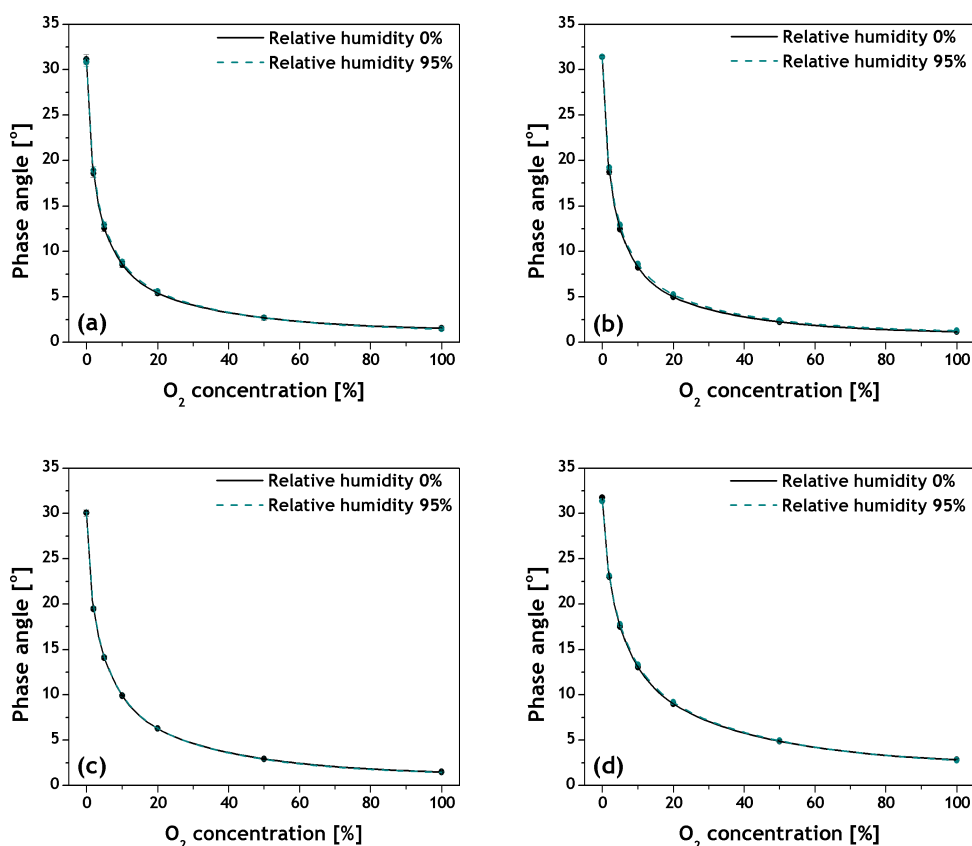Figure 3.29 shows the influence of humidity on sensor films response. As can be seen

Figure 3.29: Influence of humidity on O_2 response for (a) MTEOS/TFP-TMOS-, (b) ETEOS/TFP-TMOS-, (c) PTEOS/TFP-TMOS- and (d) PhTEOS/TFP-TMOS-based sensor xerogels cured at 110 °C.

from these figures all films that contained a fluorinated precursor are humidity insensitive. This is consistent with the water contact angle measured for these xerogels, which are reported in Table 3.7. Such high values of water contact angles are due to the addition of fluorinated organosilane TFP-TMOS that forms sol-gel coatings with a strong hydrophobic character. The small atomic radius and high electronegativity of fluorine makes it an ideal atom to form a covalent bond with carbon to generate low

surface energy [21]. The drawback is that the van der Waals forces of such coatings are very weak against the glass substrate and it is necessary to mix them with other organosilicon precursors in order to improve adhesion.

Table 3.7: Water contact angle for sensor films based on the fluorinated precursor TFP-TMOS.

Sensor platform	Water contact angle [°]
MTEOS/TFP-TMOS	100 ± 1
ETEOS/TFP-TMOS	102 ± 1
PTEOS/TFP-TMOS	103 ± 1
PhTEOS/TFP-TMOS	100 ± 2

Sensor films composed of monoalkoxysilane and TFP-TMOS formed robust O_2 sensors with enhanced sensitivity and a humidity-insensitive O_2 response.

3.7.3 Long-term stability

Sensor response was monitored for 7 months in order to examine long-term stability. The results are shown in Figure 3.30 and demonstrate that the response of these sensor xerogels is reasonably stable. Generally, for MTEOS/TFP-TMOS-
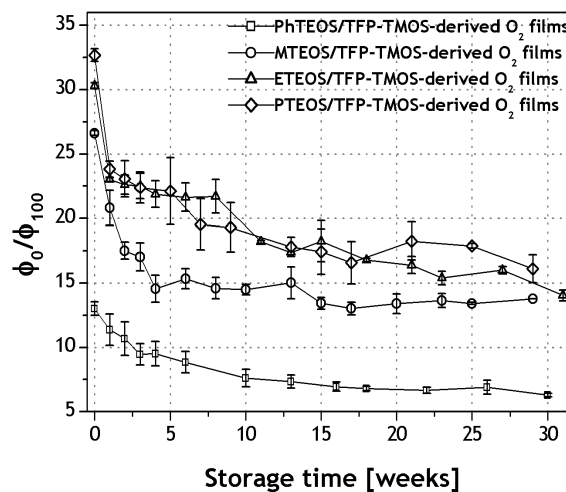

Figure 3.30: Effect of storage time on MTEOS/TFP-TMOS-, ETEOS/TFP-TMOS-, PTEOS/TFP-TMOS and PhTEOS/TFP-TMOS-derived O_2 sensor films.

and PhTEOS/TFP-TMOS-based sensor films the results show that the sensor re-

sponse stabilises after 4 weeks. After this time, the average value of ϕ_0/ϕ_{100} for MTEOS/TFP-TMOS- and PhTEOS/TFP-TMOS-derived xerogels was 14.02 ± 0.79 (RSD = 5.6%) and 7.18 ± 0.79 (RSD = 11.0%), respectively. Different behavior was found for ETEOS/TFP-TMOS- and PTEOS/TFP-TMOS-based materials. The original ϕ_0/ϕ_{100} value drops significantly after 1 week of storage (by 24% and 27% for ETEOS/TFP-TMOS- and PTEOS/TFP-TMOS-based sensors, respectively). After this time, average ϕ_0/ϕ_{100} value for ETEOS/TFP-TMOS was 19.37 ± 2.88 (RSD = 14.9%) and for PTEOS/TFP-TMOS 19.14 ± 2.40 (RSD = 12.5%).

3.7.4   Dissolved O$_2$ sensing

Figure 3.31 presents (a) the phase response to O$_2$ dissolved in water and (b) corresponding calibration curve for ETEOS/TFP-TMOS-derived sensor film. The calculated LOD for this sensor film was estimated to be less than 1 ppb which compares very well with other optical O$_2$ sensors. This experiment demonstrates that all O$_2$ films are also suitable for dissolved O$_2$ sensing, for example, in waste water treatment or water quality monitoring.
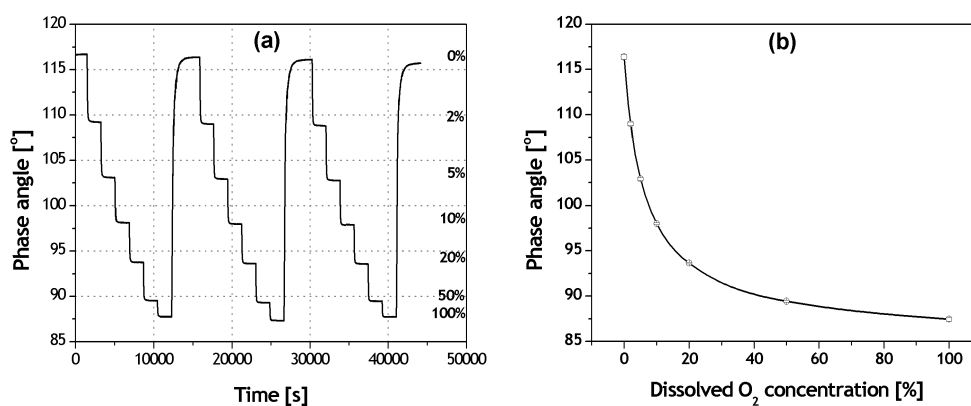

Figure 3.31: (a) Phase response to O$_2$ dissolved in water and (b) corresponding calibration curve for ETEOS/TFP-TMOS-derived O$_2$ sensor film.

3.8 Conclusions

In this chapter, the performance of ORMOSIL-based O$_2$ sensor xerogels, namely MTEOS-, ETEOS-, PTEOS-, PhTEOS-, MTEOS/TFP-TMOS, ETEOS/TFP-TMOS, PTEOS/TFP-TMOS and PhTEOS/TFP-TMOS, based on luminescence quenching, was characterised. All sensors displayed short response times, excellent repeatability, reversibility, film to film reproducibility and very good long-term stability. It was demonstrated that one can successfully tune the sensor sensitivity by using organosilicon precursors with different alkyl chain length (C$_1$-C$_3$), by incorporating fluorinated precursor into the sol-gel matrix and by using elevated curing temperatures.

The optimised ETEOS-, PTEOS- and TFP-TMOS-derived O$_2$ sensor films developed in this work demonstrated enhanced O$_2$ sensitivity and were humidity insensitive. If necessary, two-point calibration procedures can be used for most of these sensors (beside MTEOS-derived), as Stern-Volmer plots appear to be linear. The linear response suggests that the encapsulated luminophore emits from similar environments and that each microenvironment is equally accessible to O$_2$ molecules.

The characterisation and optimisation of sol-gel-derived O$_2$ sensor films coated on plastic substrates for bioprocess applications has also been presented. The design of a sol-gel-based matrix formulation, completely insensitive to humidity, and its application as a matrix for O$_2$ sensor films was implemented. An optimum sensing film has been identified. Humidity insensitivity is an extremely significant result for bioprocess monitoring applications as it facilitates the development of a system that does not require the integration of gas drying strategy into its design in order to eliminate the effects of the high environmental humidity during the fermentation process.

Finally, it was demonstrated that the O$_2$ films developed in this work are also suitable for dissolved O$_2$ monitoring.

References

[1] J. N. Demas and B. A. DeGraff, "Applications of luminescent transition metal complexes to sensor technology and molecular probes," *Journal of Chemical Education*, vol. 74, no. 6, pp. 690–695, 1997.

[2] C. McDonagh, C. Kolle, A. K. McEvoy, D. L. Dowling, A. A. Cafolla, S. J. Cullen, and B. D. MacCraith, "Phase fluorometric dissolved oxygen sensor," *Sensors and Actuators B-Chemical*, vol. 74, no. 1-3, pp. 124–130, 2001.

[3] R. J. Watts and G. A. Crosby, "Spectroscopic characterization of complexes of ruthenium(II) and iridium(III) with 4,4'-diphenyl-2,2'-bipyridine and 4,7-diphenyl-1,10-phenanthroline," *Journal of the American Chemical Society*, vol. 93, no. 13, pp. 3184–3188, 1971.

[4] C. McDonagh, F. Sheridan, T. Butler, and B. D. MacCraith, "Characterisation of sol-gel-derived silica films," *Journal of Non-Crystalline Solids*, vol. 194, no. 1-2, pp. 72–77, 1996.

[5] C. Higgins, "Characterisation and optimisation of novel sol-gel materials for luminescence-based O₂ sensing," *Ph.D. Thesis, Dublin City University*, 2007.

[6] B. S. Creaven, M. W. George, A. G. Ginzburg, C. Hughes, J. M. Kelly, C. Long, I. M. Mcgrath, and M. T. Pryce, "Laser-pulse photolysis and transient infrared investigation into the effect of solvent or substituents (X) on the reactivity of photogenerated (η-C$_6$H$_{6-y}$X$_y$)Cr(CO)$_2$ intermediates," *Organometallics*, vol. 12, no. 8, pp. 3127–3131, 1993.

[7] A. Mills and Q. Chang, "Modelled diffusion-controlled response and recovery behavior of a naked optical film sensor with a hyperbolic-type response to analyte concentration," *Analyst*, vol. 117, no. 9, pp. 1461–1466, 1992.

[8] C. McDonagh, P. Bowe, K. Mongey, and B. D. MacCraith, "Characterisation of porosity and sensor response times of sol-gel-derived thin films for oxygen sensor applications," *Journal of Non-Crystalline Solids*, vol. 306, no. 2, pp. 138–148, 2002.

[9] R. Narayanaswamy and O. S. Wolfbeis, eds., *Optical Sensors: Industrial, Environmental and Diagnostic Applications, Chapter 13*. Springer-Verlag, Berlin, 2004.

[10] K. Mongey, "The photophysical properties of ruthenium(II) polypyridyl complexes immobilised in sol-gel matrices," *Ph.D. Thesis, Dublin City University*, 1996.

[11] Y. Tang, E. C. Tehan, Z. Y. Tao, and F. V. Bright, "Sol-gel-derived sensor materials that yield linear calibration plots, high sensitivity, and long-term stability," *Analytical Chemistry*, vol. 75, no. 10, pp. 2407–2413, 2003.

[12] "Hydrophobicity, hydrophilicity and silane surface modification," *http://www.gelest.com/Library/*.

[13] C. J. Brinker and G. W. Scherer, *Sol-Gel Science: The Physics and Chemistry of Sol-Gel Processing*. Academic Press, Boston, 1990.

[14] A. K. McEvoy, "Development of an optical sol-gel-based dissolved oxygen sensor," *Ph.D. Thesis, Dublin City University*, 1996.

[15] O. S. Wolfbeis, ed., *Fiber Optic Chemical Sensors and Biosensors, Vol. 1*. CRC Press, Boca Raton, 1991.

[16] I. Klimant, F. Ruckruh, G. Liebsch, C. Stangelmayer, and O. S. Wolfbeis, "Fast response oxygen micro-optodes based on novel soluble ormosil glasses," *Mikrochimica Acta*, vol. 131, no. 1-2, pp. 35–46, 1999.

[17] P. Hartmann, M. J. P. Leiner, and P. Kohlbacher, "Photobleaching of a ruthenium complex in polymers used for oxygen optodes and its inhibition by singlet oxygen quenchers," *Sensors and Actuators B-Chemical*, vol. 51, no. 1-3, pp. 196–202, 1998.

[18] P. M. Moore, "Ongoing Ph.D. research project by J. P. Moore,"

[19] A. N. Watkins, B. R. Wenner, J. D. Jordan, W. Y. Xu, J. N. Demas, and F. V. Bright, "Portable, low-cost, solid-state luminescence-based O$_2$ sensor," *Applied Spectroscopy*, vol. 52, no. 5, pp. 750–754, 1998.

[20] A. M. Morin, W. Y. Xu, J. N. Demas, and B. A. DeGraff, "Oxygen sensors based on a quenching of tris-(4,7-diphenyl-1,10-phenanthroline)ruthenium(II) in fluorinated polymers," *Journal of Fluorescence*, vol. 10, no. 1, pp. 7–12, 2000.

[21] K. C. Chang, H. Chen, C. K. Huang, and S. I. Huang, "Preparation of super-hydrophobic film with fluorinated-copolymer," *Journal of Applied Polymer Science*, vol. 104, no. 3, pp. 1646–1653, 2007.

Chapter 4

Dual-excitation sol-gel-derived pH sensor films

4.1 Introduction

It is well known that hybrid sol-gel-based films fabricated from organically modified precursors can produce better sensor performance for some applications compared to xerogels fabricated from TEOS [1]. In addition, the microstructure of the sol-gel materials can be carefully tailored for specific, high performance sensor materials.

A key step in the development of optical pH sensors is immobilisation of a pH-sensitive dye in a suitable, solid matrix. Such a matrix dictates the characteristics of the sensor. pH dyes are typically either covalently bound or physically entrapped in the matrix [2]. The covalent binding method is reliable as the pH dye is strongly linked to the matrix and cannot leach out. However, this approach is usually complex and time consuming. In contrast, chemical doping using a sol-gel approach is easy to implement and reliable but slow indicator leaching can be a problem depending on the efficiency of the entrapment.

In this study, the pH-sensitive dye, HPTS, which was ion paired with cetyltrimethylammonium bromide (HPTS-IP), was physically entrapped in a range of proton-permeable sol-gel matrices to produce a pH sensor. Novel pH materials have been developed based on a composite of the hybrid precursors 3-glycidoxypropyltrimethoxysilane and ethyltriethoxysilane (GPTMS/ETEOS). The sensor films were optimised for fast

and reversible pH determination in the physiological pH range. The polar GPTMS precursor provides a hydrophilic matrix which promotes proton permeability while the ETEOS precursor improves the adhesion and mechanical stability of the resulting sol-gel-derived layers. The microstructure of the optimum film has been tailored to completely encapsulate the dye thereby eliminating leaching.

HPTS-IP exhibits pH-dependent changes in excitation maxima which allow for dual excitation measurements as a robust measure of the pH. Such measurements are insensitive to changes in dye concentration, leaching and photobleaching of the fluorophore and instrument fluctuations, unlike unreferenced fluorescence intensity-based measurements. This sensor is also compatible with the DLR sensing technique, described in section 2.4.3, an advantage of which is its ability to provide a referenced sensor output using a single excitation source.

This chapter presents the development of a sol-gel-derived pH sensor and high-lights how the versatile nature of the sol-gel process has been employed to produce a high performance pH sensor material that prevents leaching, yields a short response time and has long-term stability.

4.2   Materials and methods

4.2.1   Reagents and materials

Tetraethoxysilane (TEOS), ethyltriethoxysilane (ETEOS), 3-aminopropyltrimethoxy-silane (APTMS), 3-glycidoxypropyltrimethoxysilane (GPTMS), 1-methylimidazole (MI) and potassium chloride were purchased from Fluka. N-propyltriethoxysilane (PTEOS) was obtained from ABCR. 8-hydroxypyrene-1,3,6-trisulfonic acid trisodium salt (HPTS), 0.1 M hydrochloric acid (HCl), sodium hydroxide and hexadecyltrimethylammonium bromide (CTAB) were purchased from Aldrich Chemicals. Phosphate buffer solutions of defined pH were prepared from potassium salts of hydrogen phosphate (K_2HPO_4) and dihydrogen phosphate (KH_2PO_4) and were purchased from Sigma Aldrich Chemicals. Absolute ethanol (EtOH), standard buffer solutions (pH 4.0, 7.0 and 10.0)

for pH meter calibration and glass slides were purchased from VWR International. Polystyrene bottomless 96-well microplates were obtained from Cruinn Ltd. Silicon wafers were purchased from Silicon Inc. Aqueous solutions were prepared from deionised (DI) water. All chemicals were of analytical grade and used without further purification.

4.2.2 Buffer preparation

10 mM phosphate buffers were prepared by mixing two stock solutions. Acidic and basic stock solutions were prepared by dissolving 1.36 g of KH_2PO_4 and 1.74 g of K_2HPO_4 in 1 L of DI water, respectively. Potassium chloride was used as a background electrolyte to adjust the ionic strength. The stock solutions of defined ionic strength were combined to obtain buffer solutions of the desired pH. The pH of such solutions was controlled using a pH meter calibrated with standard buffer solutions of pH 4.0, 7.0 and 10.0. The ionic strength (IS) of the buffer solutions was calculated using the equation:

$$IS = \frac{1}{2} \sum_{i=1}^{n} c_i \cdot z_i^2 \qquad (4.1)$$

where c_i is the concentration of each ionic species and z_i is its charge. In order to prepare a buffer solution at pH 10.0, sodium hydroxide was added to the buffer solution and pH was controlled with a pH meter.

4.2.3 Synthesis of HPTS(CTA)$_2$ ion pair

278 mg of CTAB (0.76 mmol) was dissolved in 25 ml of DI water at 50 °C and mixed with a solution comprising 200 mg of HPTS (0.38 mmol) in 25 ml of DI water. The precipitate of the ion pair (HPTS-IP) was subsequently filtered and dried in the oven at 70 °C for 12 h.

4.2.4   Fabrication of pH sensor films

pH sensor films were prepared using a variety of silicon alkoxides such as: TEOS, APTMS and GPTMS and mixtures of APTMS/PTEOS and GPTMS/ETEOS. The TEOS-, ETEOS- and PTEOS-based sols were prepared by mixing the relevant sol-gel precursor with absolute EtOH and 0.1 M aqueous HCl (catalyst). The final molar ratio of silane:EtOH:water:HCl was 1:6.25:4:0.007. The APTMS- and GPTMS-based sols were prepared by mixing the relevant precursor, absolute EtOH, DI water and MI (catalyst) in 1:6.25:4:0.69 molar ratio. As all precursors have different hydrolysis and condensation rates, different ageing times were employed. TEOS-based sols were aged for 24 h, APTMS-based sols for 1 h and GPTMS-based sols for 4.5 h. After an appropriate sol ageing time, an ethanolic solution of HPTS-IP was added to the sol to give a final HPTS-IP/silane molar ratio of 10^{-2}. For optimised pH sensor films, a HPTS-IP/silane molar ratio of 10^{-3} was used.

The APTMS/PTEOS and GPTMS/ETEOS hybrid sols were prepared by combining two separate sols to achieve the desired molar ratio: 0.1:0.9, 0.3:0.7, 0.5:0.5 and 0.7:0.3, respectively and then they were allowed to stir for 24 h after an ethanolic solution of HPTS-IP was added.

All sensor films were fabricated by dip-coating onto glass slides using a dip-speed of 3mms^{-1} in a controlled environment using a computer-controlled dipping apparatus described in section 3.2.2. Films were deposited after either 24 h, 3 days and 7 days of sol ageing. The glass slides were cleaned as described in section 3.2.2. After deposition, the films were cured at either 70 °C or 140 °C for 4 h and 24 h. 140 °C is the highest curing temperature and was necessary, as pH sensor films for bioprocess monitoring should be autoclavable, usually at 121 °C. Curing them at a temperature higher than that used during sterilisation minimises any structural changes of the sol-gel material. All experiments were performed at room temperature.

4.2.5 Experimental characterisation systems

4.2.5.1 Absorbance and fluorescence measurements

Absorption spectra were recorded using a UV-Vis spectrophotometer described in section 3.2.3.5.

pH-dependent fluorescence measurements were acquired using a FluoroMax-2 fluorometer described in section 3.2.3.5. All spectra were recorded from pH films dip-coated on glass contained in a quartz cuvette that was fixed at 45° with respect to the incident beam. Films were immersed in phosphate buffer solutions that were adjusted to pH values ranging from 4.0 to 10.0. The fluorometer collected the emission intensity at 515 nm, employing excitation wavelengths of 405 nm and 455 nm or 460 nm depending on matrix formulation. 2 nm passbands were used for both the excitation and emission monochromators.

For the long-term stability study, sensor films were placed in a custom-made flow cell and buffer solutions at the desired pH were pumped at a rate of 8 mms^{-1} using a Minipuls-3 peristaltic pump (Gilson, France). In general, for the fluorescence measurements, phosphate buffers of IS = 150 mM were used in order to approximate the IS of isotonic phosphate buffered saline and many cell culture media preparations. All experiments were performed at room temperature.

For ionic strength experiments, a Safire II microplate reader from Tecan Systems Inc., (Austria) was employed. The emission wavelength was set to match the maximum emission of the HPTS-IP at 515 nm. The excitation wavelength was varied from 380 nm to 485 nm. Temperature was set to 25 ± 1°C. Optimum pH xerogel films were dip-coated on glass slides, cured at 140 °C for 4 h and then attached to the underside of the bottomless microplates. 150 μl of phosphate buffers of IS = 50, 100, 150, 200 and 300 mM were added to the wells. The same experiments were performed at different temperatures (25 °C, 37 °C and 42 °C) in order to investigate the influence of temperature on the sensor response. Measurements were taken 10 min after filling. Mean values and standard deviations were calculated from at least

five samples.

4.2.5.2   Raman measurements

In order to study the influence of sol ageing time on the chemical microstructure of the pH films, Raman spectroscopy was used. An InVia Raman microscope (Renishaw, UK) was used with a diode laser (emitting at 785 nm) as an excitation source. Optimum undoped sol-gel-derived pH ETEOS/GPTMS-derived films were used which were dip-coated on glass from sols aged for 24 h, 3 and 7 days.

In this work, Raman measurements using thin pH films were performed by Mr. Krzysztof Skrzypiec under the supervision of Dr. Ewaryst Mendyk using a Raman microscope in the University of Marie Curie-Skłodowska in the Chemistry Department in Lublin, Poland. Raman measurements using organosilicon precursors solutions were performed by Dr. Ute Neugebauer in the School of Chemical Sciences in DCU. The Raman spectra were recorded on a Horiba Jobin Yvon (USA) spectrometer equipped with a confocal microscope. A 633 nm excitation line was employed from an air-cooled HeNe laser.

4.2.5.3   Other characterisation techniques

A digital Orion Benchtop 420 A+ pH meter was used to measure pH values. This was calibrated with three standard buffers of pH 4.0, 7.0 and 10.0 at room temperature.

For Dual Lifetime Referencing (DLR) measurements, a digital dual phase lock-in-amplifier (Model 7265, Signal Recovery, UK) was used for sinusoidal modulation of the 460 nm LED and for phase-shift detection of the photodiode output signal. The pH-sensitive film was immersed in solutions of the desired pH in a quartz cuvette.

SEM images of the pH film dip-coated on silicon wafer were taken using an S-3000N Hitachi (Hitachi Science Systems, Ltd., Japan) instrument. The operating voltage of 20 kV was used.

AFM measurements were performed by M.Sc. Krzysztof Skrzypiec in the University of Marie Curie-Skłodowska in the Chemistry Department in Lublin, Poland. A

NanoScope III (Digital Instruments, USA) scanning probe microscope was used to obtain high resolution (300 nm $\times$ 300 nm) AFM images of undoped sol-gel-derived pH films dip-coated on glass. Topography and phase images were obtained simultaneously. Samples were scanned at ambient temperature.

Film thickness measurements were obtained using a white light interferometer (WYCO N1100 Optical Profiling System, Veeco, USA) as described in section 3.2.3.3.

4.3 Development of the dual-excitation pH sensor films

4.3.1 Optical properties of HPTS-IP in solution

HPTS is a very photostable, highly fluorescent pH indicator with a pKa around 7.3 that has been extensively used for fluorescence-based pH and carbon dioxide detection [3]. In this study, HPTS was ion paired with hexadecyltrimethylammonium bromide, CTAB, to form a HPTS derivative, HPTS-IP (Figure 4.1). This was then entrapped in a sol-gel matrix to produce a
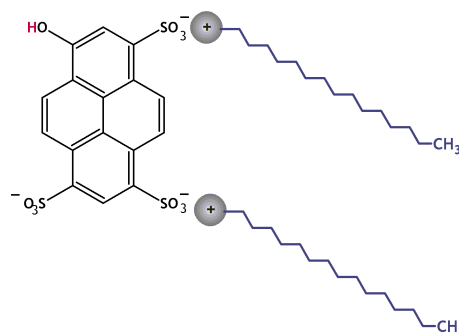
Figure 4.1: Chemical structure of HPTS-IP.

pH sensor. HPTS-IP is more hydrophobic than HPTS and displays poor water solubility but is very soluble in a typical sol-gel precursor. By using such a dye, one can expect minimised leaching and improved sensor film stability. It exhibits the same pH-dependent absorption and emission maxima as the unmodified HPTS. The pH-dependent excitation and emission spectra of HPTS-IP are illustrated in Figure 4.2. Depending on the pH, HPTS-IP exhibits two different pH-dependent excitation
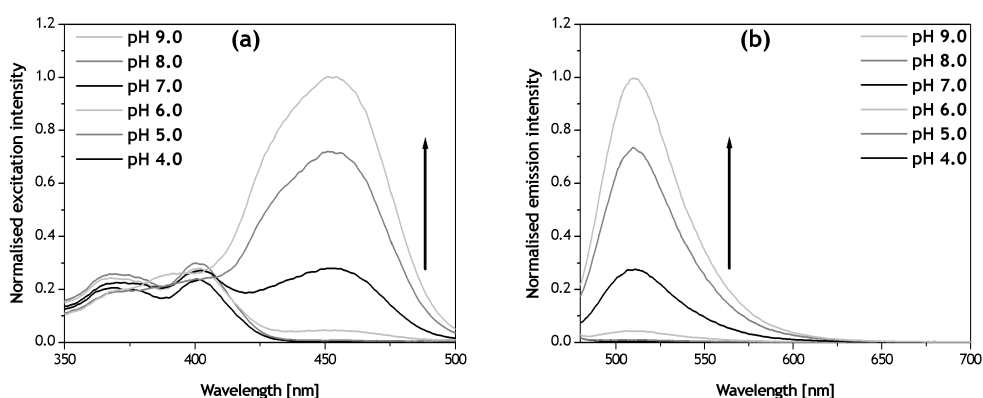

Figure 4.2: Normalised (a) excitation spectra ($\lambda_{em} = 515$ nm) and (b) fluorescence emission spectra ($\lambda_{exc} = 460$ nm) of HPTS-IP in 0.15 M phosphate buffers at different pH values. Concentration of HPTS-IP = 5.7×10^{-4} mol/L.

bands, one at 401 nm corresponding to the protonated (acidic) form, the other at 455 nm corresponding to the deprotonated (basic) form. The emission spectrum shows one maximum at 515 nm. The presence of the dual excitation bands facilitates the use of excitation ratiometric detection. The excitation intensity ratio defined here as the emission intensity with 455 nm (blue) excitation divided by the emission intensity with 405 nm (UV) excitation (I_{455nm}/I_{405nm}), is related to pH. Figure 4.3 shows the characteristic calibration plot of a 10^{-4} mol/L HPTS-IP in buffer solutions. The dynamic range extends from pH 6.0 to 8.5 and the pKa calculated from the point of inflection is equal to 7.43.
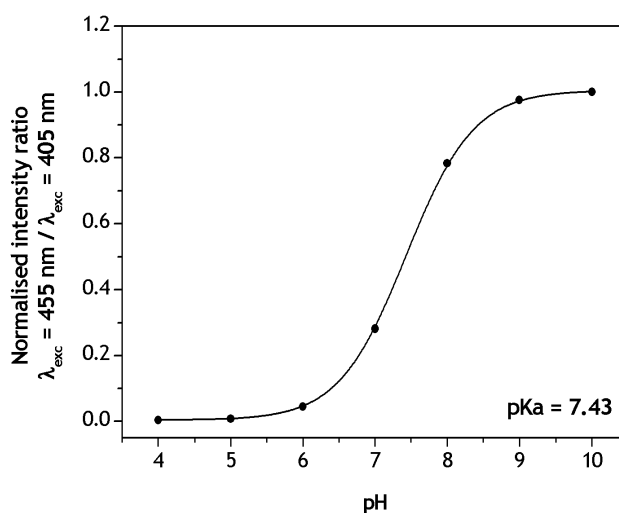
Figure 4.3: Normalised calibration curve of HPTS-IP in 0.15 M phosphate buffer solutions at different pH values.

4.3.2   Investigation of sol-gel-derived matrices for pH sensing

This section describes an extensive study on a wide range of sol-gel-derived matrices doped with HPTS-IP and their suitability for use as pH sensors. The focus was on tailoring the properties of the sol-gel-based pH films by using different starting sol-gel precursors and their mixtures and by applying various curing temperatures. The HPTS-IP was entrapped within: TEOS-, APTMS- and GPTMS-based matrices and APTMS/PTEOS- and GPTMS/ETEOS-derived binary systems. Chemical structures

of TEOS, APTMS and GPTMS are shown in Figure 4.4. Binary systems represent a much better alternative than that of a single precursor as they can favorably combine the often dissimilar properties of two components in one material. Compositional variations were carried out in order to gradually tune the material properties.
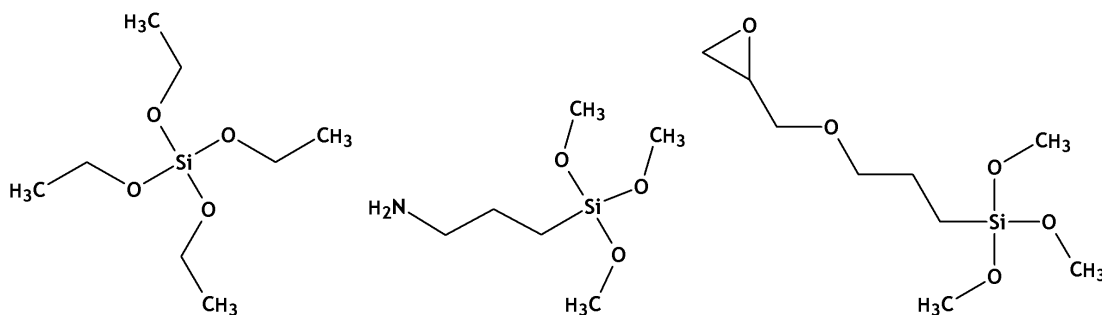

Figure 4.4: Chemical structures of TEOS, APTMS and GPTMS (from left to right).

TEOS is the most widely used silicon precursor that forms an inorganic SiO_2 network. APTMS in an organically modified alkoxysilane with a $-(CH_2)_3NH_2$ functional group. During hydrolysis of the methoxy groups, silanol groups are formed which condense to form a silicate network. In this case, APTMS modifies the silica network without supplying additional functional groups intended to undergo further chemical reactions. The final structure is modified only by the organic $-(CH_2)_3NH_2$ groups. GPTMS is a different type of organically modified alkoxide whose organic group contains an epoxy ring that can be cross-linked to form a poly(ethylene oxide) chain and acts therefore as network former [4]. The organic polymerisation is simultaneously achieved with the formation of the inorganic network. Epoxy groups react via basic or acidic catalysis or via thermal- or photo-induced polymerisation. In this work, the basic catalyst 1-methylimidazol was employed. It acts at the same time as a catalyst of the siloxane inorganic polymerisation at room temperature and an initiator of organic polymerisation (epoxy ring opening) at elevated temperatures. However, it does not directly contribute to the formation of the network [5]. Figure 4.5 shows a schematic model of the polymerised GPTMS-based hybrid material.

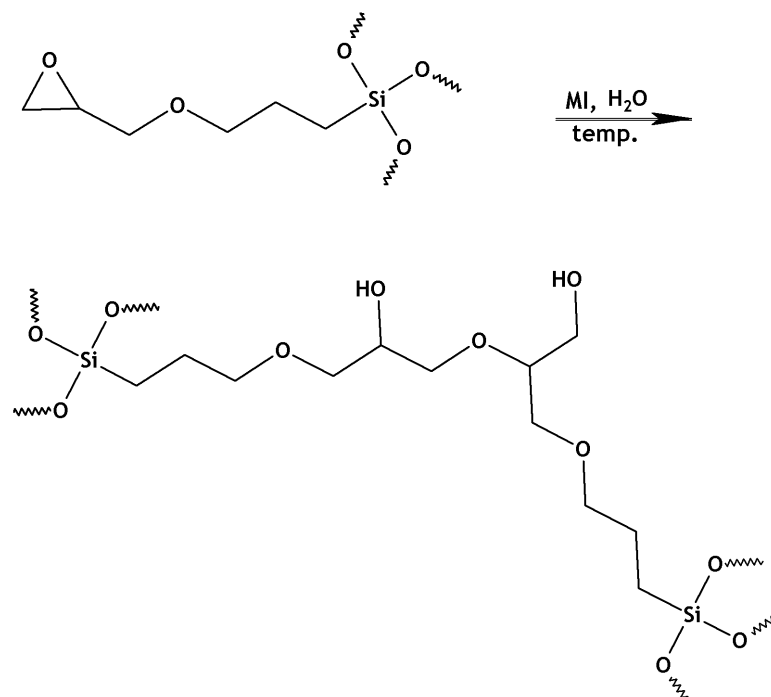Preliminary results showed that all films, beside TEOS-based, which were cured

Figure 4.5: Structure of GPTMS-derived network after epoxy ring opening.

at 70 °C showed very poor adhesion to glass when immersed in buffer solutions for 15 minutes. Curing at 140 °C for 24 h resulted in a significant decrease in sensor sensitivity and increased response times. The sensor materials cured at these temperatures were consequently eliminated as a possible sensor matrix for this application. pH films cured at 140 °C for 4 h were selected for further investigations and were also characterised in terms of :

- Optical transparency
- Adhesion to glass
- Leaching
- pH sensitivity.

A summary of these investigations are shown in Table 4.1. From Table 4.1 it is clearly seen that a number of formulations are unsuited for pH sensing applications due to poor adhesion to glass when immersed in buffer solutions for 24 h and due to leaching. All films based on a single precursor exhibited poor adhesion and extensive leaching.

These preliminary results were promising only for composite pH film formulations,

Table 4.1: Characterisation data of the pH sensor films cured at 140 °C for 4 h (besides TEOS-based films that were cured at 70 °C for 4 h). Sols aged for 3 days before dip-coating. A - APTMS, P - PTEOS, G - GPTMS, E - ETEOS, numbers indicate percentage of APTMS or GPTMS in the sol.

Film formulation	Optical transparency	Adhesion to glass	Leaching after 24 h	pH sensitivity
TEOS	good	good	Yes	low
APTMS	poor	poor	Yes	high
AP10	good	good	No	No sensitivity
AP30	good	good	No	good
AP50	good	good	No	high
AP70	poor	poor	Yes	high
GPTMS	good	poor	Yes	good
GE10	good	good	No	low
GE30	good	good	No	good
GE50	good	good	No	good
GE70	good	poor	Yes	good

namely AP30, AP50, GE30 and GE50. These pH sensor materials demonstrated good adhesion to glass, good pH sensitivity and insignificant or no leaching after soaking them in buffer solutions at pH 7.0 for an extended period of time. These film compositions were then investigated in more detail and results are given in the following sections. Results for the most widely used TEOS-derived materials are discussed for comparison purposes.

4.3.3   TEOS-derived pH sensor films

The real time response and calibration plot of a TEOS-based sensor film, which was dried at 70 °C, are shown in Figure 4.6. Calibration plots were determined from a series of time traces measured at a fixed emission wavelength of 515 nm and excited at 405 nm and 455 nm and the ratio of the intensity with two excitation wavelengths (I_{455nm}/I_{405nm}) was calculated.

pKa is mainly dictated by the properties of the indicator, but interactions of the host material with the entrapped dye can also shift the pKa. Changes in pKa observed
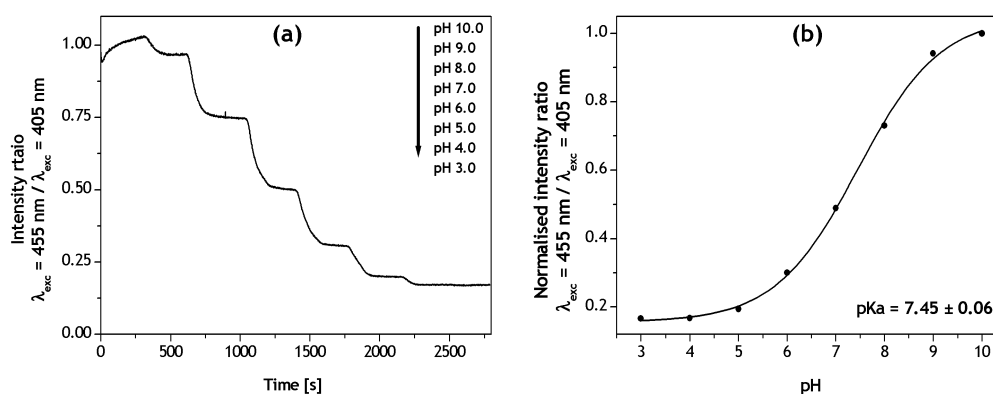
Figure 4.6: Normalised (a) real time pH response and (b) calibration plot of TEOS-derived sensor film. IS of a buffer solutions = 150 mM.

upon immobilisation of the dye can be attributed to the changes in the polarity of the microenvironment. The apparent pKa (pKa') value of HPTS-IP entrapped in a TEOS-based matrix calculated from the calibration plot was measured to be 7.45 which is very close to the pKa of HPTS-IP in buffer solutions (pKa = 7.43). This indicates that the HPTS-IP microenvironment in the TEOS-based matrix is much the same as in water. The dynamic range of the TEOS-based sensor extends from pH 6.0 to 9.0.

Unfortunately, absorption spectra revealed that approximately 40% of the dye leached out of the matrix after 2 pH cycles. Curing at a higher temperature resulted in a significant decrease in sensor sensitivity and increased response times ($\geq$ 10 min, results not shown). Accordingly, the TEOS-based sensor films were deemed to be unsuited for this application and were not investigated further.

4.3.4   Composite pH sensor films

This section presents characterisation of the pH sensor films AP30, AP50, GE30 and GE50 which were dip-coated from sols aged for 3 days and then cured at 140 °C for 4 h. Figure 4.7 shows typical pH-dependent excitation spectra for AP50 and GE50 xerogels measured at 515 nm and normalised to the intensity at 405 nm. As in the solution, the entrapped HPTS-IP exhibited pH dependence with more than a
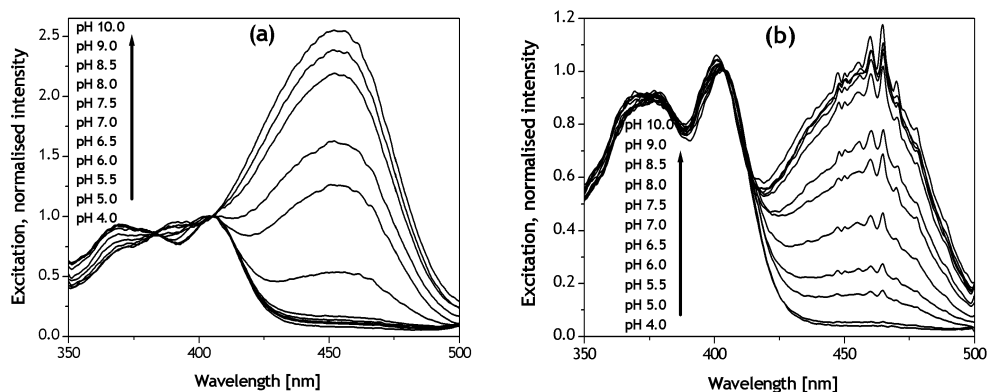
Figure 4.7: Normalised (a) pH-dependent excitation spectra for AP50 and (b) GE50 sensor films. IS of a buffer solutions = 150 mM.

17-fold and 20-fold increase between pH 5.0 and 8.5 for AP50 and GE50, respectively. HPTS-IP immobilised in sol-gel host matrices preserves both characteristic pH-dependent wavelengths, however the excitation band for GE50 film is slightly red shifted (to 460 nm).

Figure 4.8 represents calibration plots for pH sensor films, namely, AP30, AP50, GE30 and GE50. The pKa' of entrapped HPTS-IP was measured to be 7.95 ± 0.04
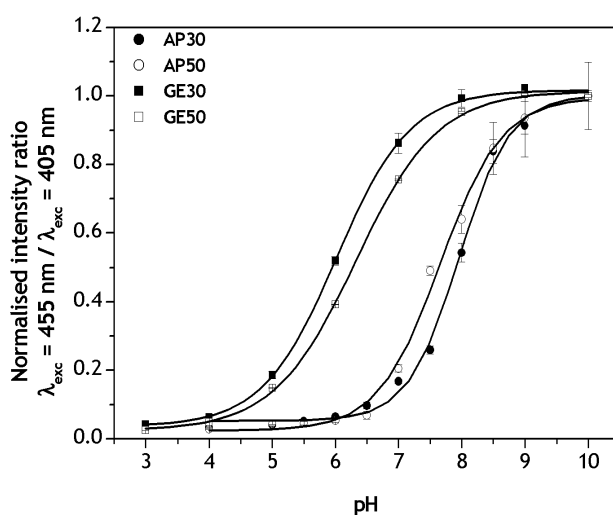

Figure 4.8: Calibration curves of AP30, AP50, GE30 and GE50 pH sensor films.

for AP30, 7.66 ± 0.06 for AP50, 6.01 ± 0.03 for GE30 and 6.35 ± 0.03 for GE50. A significant difference in pKa' values between APTMS/PTEOS- and GPTMS/ETEOS-

based sensor films was observed. The pKa' of HPTS-IP in AP30 and AP50 was 7.95 and 7.66, respectively which is slightly higher than that for HPTS-IP in solution (pKa = 7.43). This indicates a small change in the local indicator microenvironment, which is slightly less polar than in water-based solutions or in a TEOS-based matrix (pKa' = 7.45). The dynamic range of these sensor films extends from pH 6.5 to 8.5, which is suitable for bioprocess monitoring applications. Leaching studies showed that when films were soaked in pH 7.0 buffer solutions for a period of 2 weeks no significant leaching was observed, with the exception of the first 24 hours during which 19% of the loosely incorporated dye leached out as verified using UV-Vis absorption studies (results not shown). However, after keeping these sensor films in buffer solution for an extended period of time, the matrix became optically opaque and thus unsuitable for optical measurements. It is worth noting that single ORMOSIL compositions based only on TEOS, APTMS or GPTMS showed a much higher degree of leaching within shorter periods of time.

The lower pKa' value observed for HPTS-IP entrapped in the GPTMS/ETEOS-derived matrices was attributed to the influence of the matrix (specific chemical interactions between the dye and the host matrix) on the pH response of the indicator and not to the presence of the IP as the pKa' of HPTS in the sol-gel matrix was also measured and was similar to that of HPTS-IP (data not shown). The dynamic range of these sensors films extends from pH 5.0 to 8.0, which still matches the physiological pH range. In order to understand the shift in pKa' value, micro-Raman spectroscopy was employed and the results are discussed in section 4.3.5. For GE30 and GE50 sensor films no leaching was observed as verified by absorbance measurements. In addition, these films exhibited excellent mechanical and optical properties even after soaking them in buffer solutions for an extended period of time.

To conclude, two main potential candidates were identified as optimum pH sensors, namely GE30 and GE50 films as they exhibited excellent adhesion to the glass substrate, good pH sensitivity, were optically transparent and leaching was not observed. GE50 pH films exhibit slightly higher pKa' value of 6.32 than GE30 films

(pKa' = 6.01), which more closely matches the physiological pH range necessary for some bioprocess applications. This composition was selected as the optimum pH sensor material formulation and is characterised in the next sections.

4.3.5 Influence of ageing time on optimum pH sensor characteristics

At the start, all hybrid composite sols were aged for 24 h before dip-coating. However, GPTMS/ETEOS-derived pH sensors dip-coated from sols aged for this time did not exhibit pH sensitivity. During the experiment it was noticed that ageing time of these sols had an influence on the sensitivity of the deposited sensor films. Figure 4.9 shows calibration plots for GE50 films dip-coated from sols aged for 24 h, 72 h and 7 days.
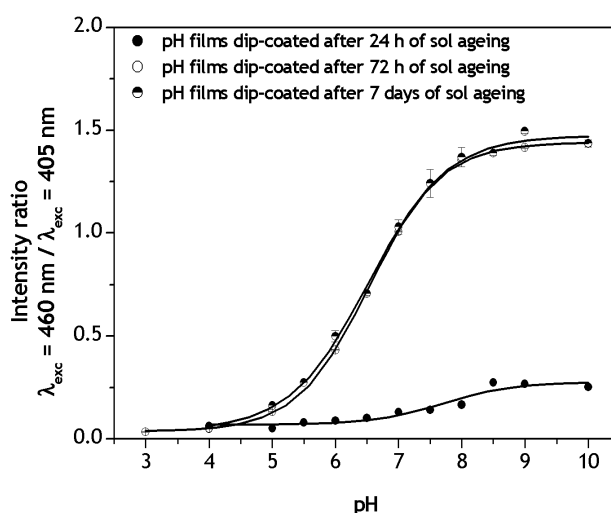

Figure 4.9: Calibration plots obtained for pH sensor films coated from sols aged for different times.

It is clear that after 24 h, the films were pH insensitive and that the optimum ageing time was 72 h. Longer ageing time did not influence the dynamic range and sensitivity of the pH sensor. In addition, films dip-coated from sols aged for 1 week were too thick and less uniform than films coated after 72 h.

    Figure 4.10 presents the absorption spectra of pH GE50 films coated from sols aged for 24 h, 72 h and 7 days. The results demonstrate that if longer sol ageing

time was employed, the basic form of HPTS-IP ($\lambda_{max} = 460$ nm) was predominant within the matrix.
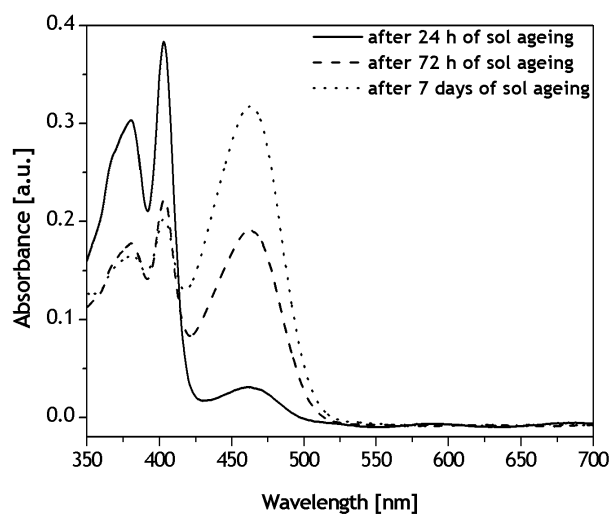

Figure 4.10: Absorption spectra of pH sensor films coated from sols aged for different times.

As Raman spectroscopy is a powerful tool for the analysis of the chemical structure of the sol-gel-derived materials, it was employed to investigate changes in the chemical structure of GE50 films when different sol ageing times were used. GE50 films were dip-coated from sols aged for 24 h, 72 h and 7 days and cured at 140 °C for 4 h. Figure 4.11a shows the Raman spectra of ETEOS and GPTMS precursors. The spectra were recorded for comparison purposes. Figure 4.11b presents Raman spectra recorded for undoped GE50 films with varying ageing times.

The GPTMS precursor exhibits a strong Raman signal, which is a doublet at 610 cm^{-1} and 641 cm^{-1} due to the $\nu(SiO_3)$ stretching vibrations (symmetric and asymmetric) of the $Si(OCH_3)_3$ groups (Figure 4.11a) [6, 7]. The band at 624 cm^{-1} in the ETEOS spectrum is assigned to the $\nu(SiO_3)$ stretching of the $Si(OC_2H_5)_3$ groups. These bands in GPTMS and ETEOS spectra are characteristic of unhydrolysed trimethoxysilane and triethoxysilane molecules, respectively. The spectra in Figure 4.11b does not show these peaks, indicating a high degree of hydrolysis of the methoxy and ethoxy groups in the films. In addition, the bands at 2842 cm^{-1} and
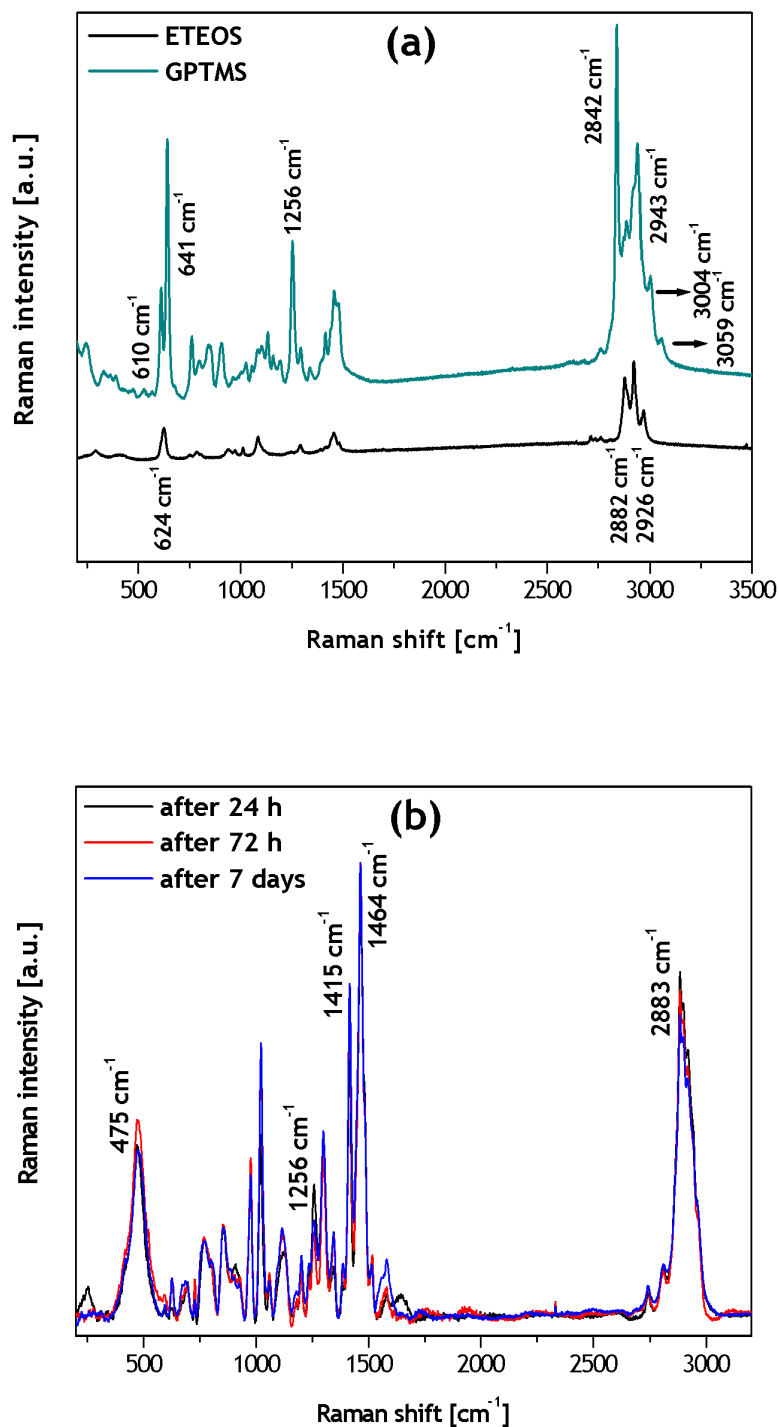
Figure 4.11: (a) Raman spectra of ETEOS and GPTMS precursors and (b) Raman spectra of hybrid ETEOS/GPTMS-derived films dip-coated from sols aged for 24 h, 72 h and 7 days and cured at 140 °C for 4 h.

$2943\ cm^{-1}$ present in the GPTMS spectrum are absent in Figure 4.11b also indicating

a significant rate of hydrolysis of the $O\text{-}CH_3$ groups. Another characteristic peak in

the GPTMS spectrum is at 1256 cm^{-1} corresponding to the breathing mode of the epoxy ring. The bands at 3004 cm^{-1} and 3059 cm^{-1} are attributed to the epoxy group CH stretching and their absence in the Raman spectra of the films (Figure 4.11b) confirms that most of the epoxy rings were opened. The spectra of the films show a significant decrease of the intensity band at 1256 cm^{-1} after 72 h of ageing. After 7 days of ageing, this band is still detected in the film indicating that some rings were not opened. This suggests that the silica network was formed much faster than the organic polymer and hindered the formation of the organic chains [5]. The strongest ETEOS bands, at 2882 cm^{-1} and 2926 cm^{-1}, are assigned to stretching vibrations of -CH$_3$ and -CH$_2$, respectively. The band at 475 cm^{-1} in Figure 4.11b has appeared and is attributed to Si-O-Si bending confirming the inorganic network formation. Extensive formation of the inorganic network was already achieved after 24 h of sol ageing which is demonstrated by the well-defined peak. These results can be correlated with changes in the pKa' value of HPTS-IP entrapped in the GE50 films. When organic polymerisation starts, the ring opening occurs (see Figure 4.5) and an oxygen - hydrogen bond is formed because of the excess of charge in the oxygen atom that attracts the hydrogen in the HPTS-IP molecule and, consequently, the dye becomes deprotonated (as confirmed by absorption spectra in Figure 4.10). Its dissociation constant K$_a$ is then shifted towards higher values (and pKa'shifts towards lower values).

To conclude, the influence of sol ageing time on pH sensor sensitivity was identified and optimised. GE50 sensor films coated from sols aged for 72 h and cured at 140 °C for 4 h were selected as the optimum pH films and their performance as pH sensors is described in detail in the coming sections.

A detailed study is necessary in the future to elucidate the exact mechanism of the hybrid film formation. Further investigations are needed to assign all the bands that appeared in the Raman spectra after the temperature programme, such as bands at 1415 cm^{-1} and 1464 cm^{-1}, and to understand the influence of sol ageing time on sensor sensitivity. However, it is known that ageing time influences the pore size

of sol-gel-derived materials and this may account for the observed increase in pH sensitivity [8]. Future work will include characterisation of the optimum pH film using infrared spectroscopy (IR), ^{29}Si and ^{13}C solid state nuclear magnetic resonance spectroscopy (NMR) and porosity of xerogels will be also determined via ellipsometric porosimetry.

4.3.6 Morphology of the optimum pH films

The homogeneity and surface morphology of the dip-coated pH sensor films was investigated by employing absorbance measurements, scanning electron microscopy (SEM) and atomic force microscopy (AFM). It is important that sensor layers are uniform as heterogeneity has an impact on a number of factors, such as the optical transparency and mechanical properties of the material. It is also important in mass production of these materials as reproducibility is a critical factor in sensor materials development. The pH sensor films were optically transparent as judged by the eye, which is indicative of no phase separation which can cause instability in sensor performance.

Figure 4.12 presents the absorption spectra of 6 randomly picked optimum pH sensor films dip-coated on glass. Each film was measured 4 times in different po-
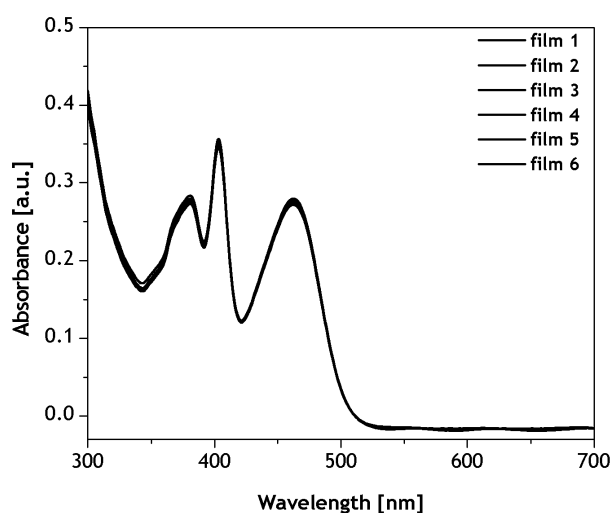

Figure 4.12: Absorption spectra of the optimum pH sensor films illustrating excellent homogeneity of sol-gel material on the glass substrate.

sitions and then the average was taken. The data shows that an excellent uniform coverage of sol-gel material on the glass substrate was achieved.

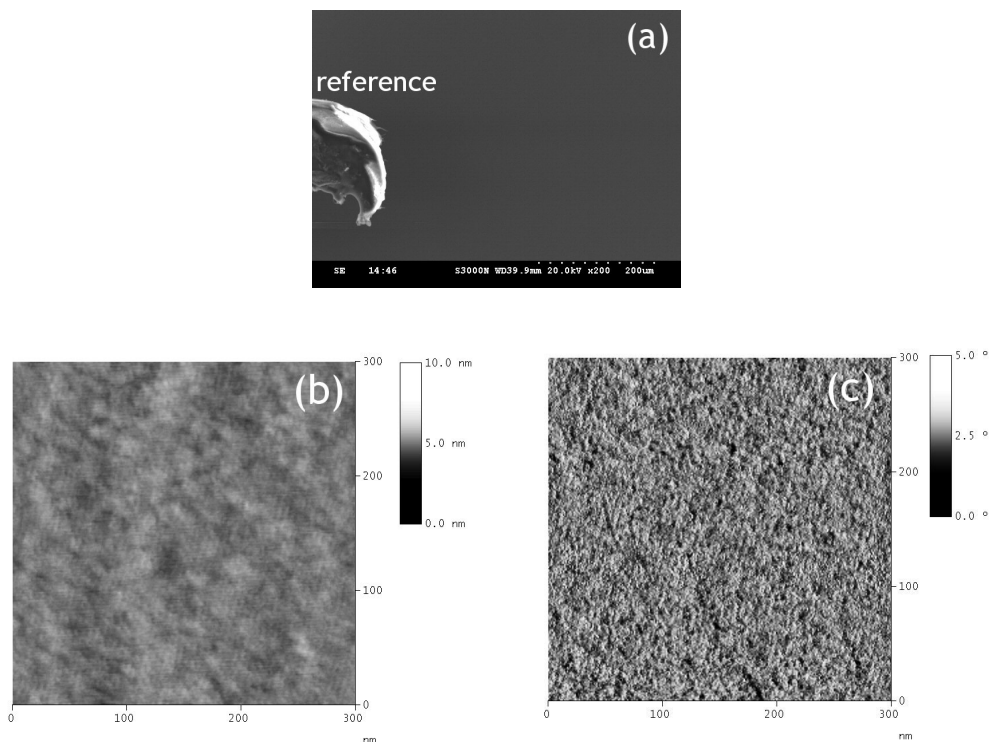Figure 4.13 shows images of pH films taken by SEM and AFM microscopes. SEM

Figure 4.13: (a) SEM image of optimised pH sensor film. Scale bar is 200 μm, 200 × magnification. (b) Height AFM image (Z-range is 0-10 nm) and (c) phase AFM (Z-range 0-5°) image of undoped GE50 pH sensor films. All films were dip-coated on silicon wafers and cured at 140 °C for 4 h.

was performed to evaluate alternations in morphology of the films as a result of phase separation at the submicrometer level. Height and phase AFM images refer to surface properties on the nanoscale level. Topography images show changes in height across the sample where phase images indicate differences in mechanical properties. Differences in phase translate into differences in hardness and cross-linking of the sol-gel-derived films [9]. The films did not show any features when imaged with SEM, which demonstrates a homogeneous material at the micrometer scale. Heterogeneity occurred at a very fine level as shown by AFM images. However, the variation in height and phase was very uniform throughout the sample area with surface roughness of 0.26 nm. This demonstrates that ETEOS and GPTMS precursors were well combined and

the synthesis of hybrid ETEOS/GPTMS-derived materials has led to homogeneous films at the microscopic and nanoscopic scale.

4.3.7   Optimum pH sensor performance

Figure 4.14 shows the pH-dependent excitation (normalised to intensity at 405 nm) and emission spectra (λ_{exc} = 460 nm) of the optimum GE50 xerogel. The sensor
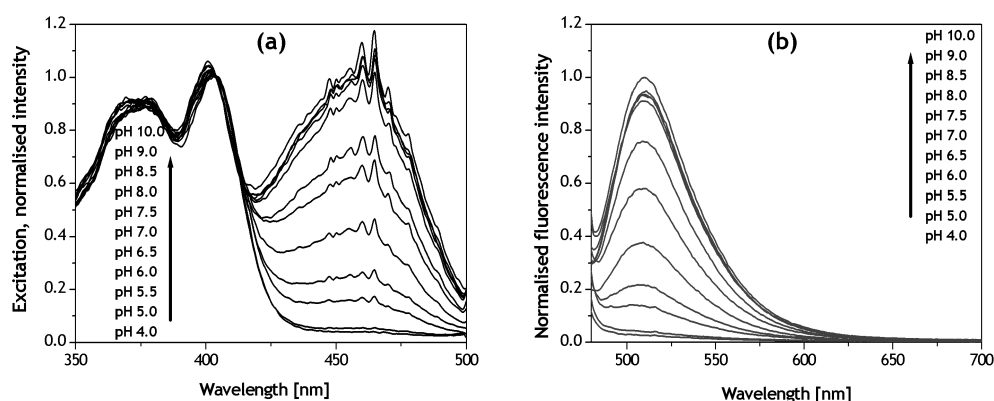

Figure 4.14: Normalised (a) pH-dependent excitation (λ_{em} = 515 nm) and (b) emission spectra (λ_{exc} = 460 nm) for GE50 sensor films. IS of a buffer solutions = 150 mM.

film is suitable for dual excitation and single intensity measurements as it exhibits 2 pH-dependent excitation bands, one at 405 nm and one at 460 nm while the emission occurs at 515 nm. For ratiometric detection, the excitation intensity ratio is defined as the emission intensity at 515 nm with 460 nm excitation divided by the emission intensity with 405 nm excitation (I_{460nm}/I_{405nm}).

The pKa' value was determined from the calibration plot shown in Figure 4.15 and was measured to be 6.40 ± 0.02. The dynamic range extends from pH 5.0 to 8.0, which allows for use of the sensor in neutral-range bioprocesses. The sensor resolution measured under the conditions of IS = 150 mM and at room temperature, was calculated to be 0.01 pH unit at pH 7.0 and 0.005 pH units at pH 5.0.

Figure 4.16 shows the sensor response over 7 measurement cycles demonstrating very good reversibility of the response for pH transitions from pH 5.0 to 7.0 and back.
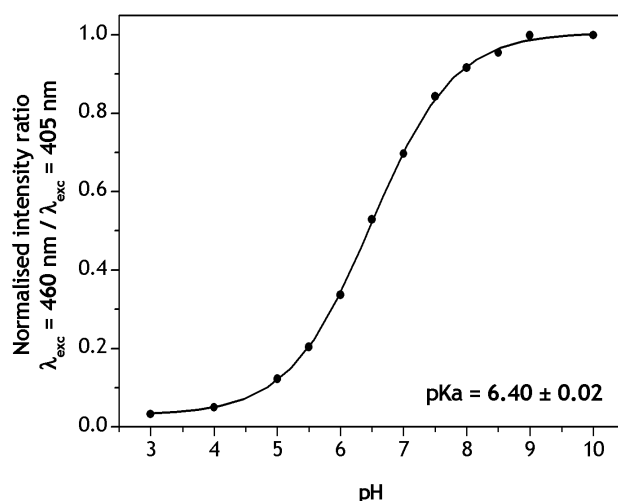
Figure 4.15: Calibration curve of GE50 pH sensor film. IS of buffer solutions = 150 mM.
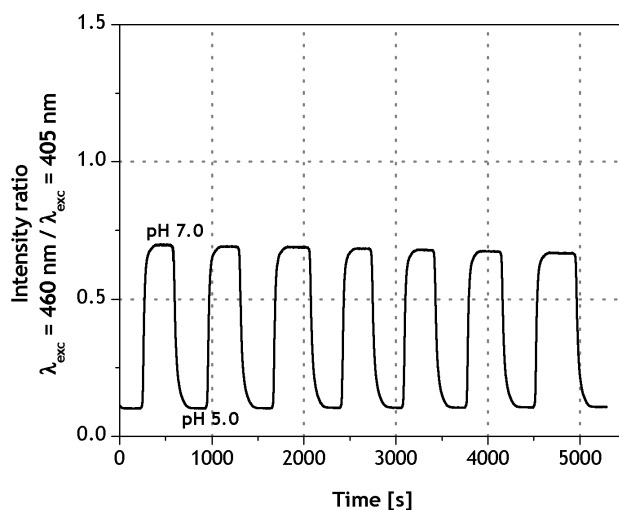

Figure 4.16: Reversibility of pH GE50 pH sensor film for pH changes from pH 5.0 to 7.0 and back. IS of buffer solutions = 150 mM.

The sensor response time, the so-called t_{90}, which was the time taken for the intensity to achieve 90% of the final value when the pH is changed from pH 5.0 to pH 7.0, was calculated to be 60 s from pH 5.0 to 7.0 and 90 s from pH 7.0 to 5.0. However, the response time is dependent on sensor film thickness and the flow rate of the buffer solutions. In order to eliminate the fill time of the flow cell, buffer solutions at pH 5.0 and 7.0 were injected directly into the flow cell through a short section

of tubing. A typical response under these conditions for a film thickness of 1 μm is shown in Figure 4.17 from which data a response time (t_{90}) of 12 s was measured. The response time can be further improved by fabricating thinner sol-gel films (i.e., by using a slower dip-coating speed).
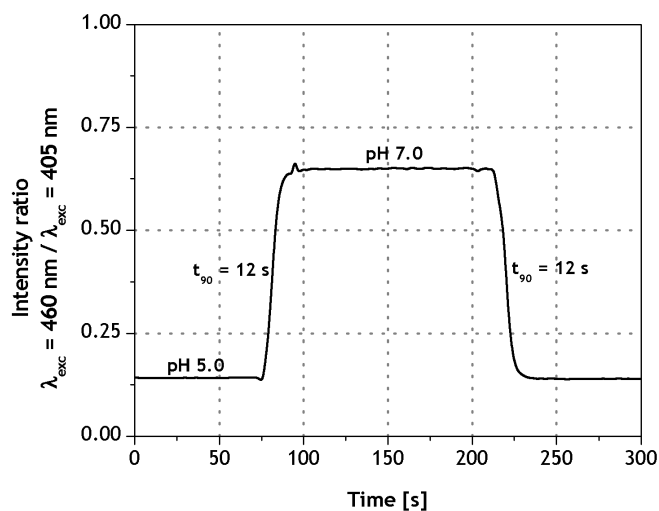

Figure 4.17: Real response time (t_{90}) of GE50 pH sensor film. IS of buffer solutions = 150 mM.

In order to study reproducibility, the pH sensor films were attached to the underside of the bottomless microplates. Then 150 μl of buffer solutions of IS = 150 mM were added to the wells. Figure 4.18 presents the average response for a set of 5 pH sensor films. The error bars associated with these films are very small (0.02) and the calculated relative standard deviation (RSD) of the pKa' values for these films was 0.32% which demonstrates the high level of reproducibility in pH response.

The photostability of GE50 sensor films was tested at pH 10.0. The sensor film was placed in a quartz cuvette filled with buffer solution and was continuously irradiated with λ = 460 nm for 1 h using a 150 W xenon light. Buffer solutions at pH 10.0 were used here as at this pH, HPTS-IP exists only in the deprotonated form yielding maximum fluorescence signal. After 1 h of illumination, the direct fluorescence intensity was reduced to 97%. However, the ratiometric signal changed insignificantly (less than 1%) after the experiment which demonstrates the benefits of using ratiometric
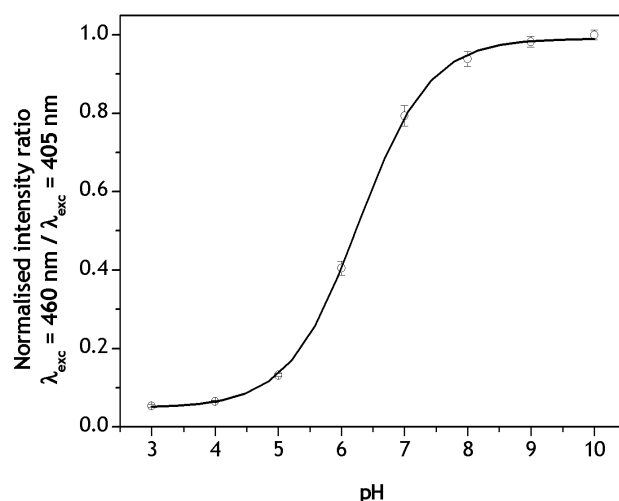
Figure 4.18: Calibration plot for 5 sensor elements. IS of buffer solutions = 150 mM, temperature 25 °C.

detection. Results are presented in Figure 4.19, and they indicate that HPTS-IP is a very photostable molecule compared to fluorescein that was reported to undergo considerable photobleaching for example, after 1 h of illumination in similar conditions the direct intensity of fluorescence dropped by 91% [10].
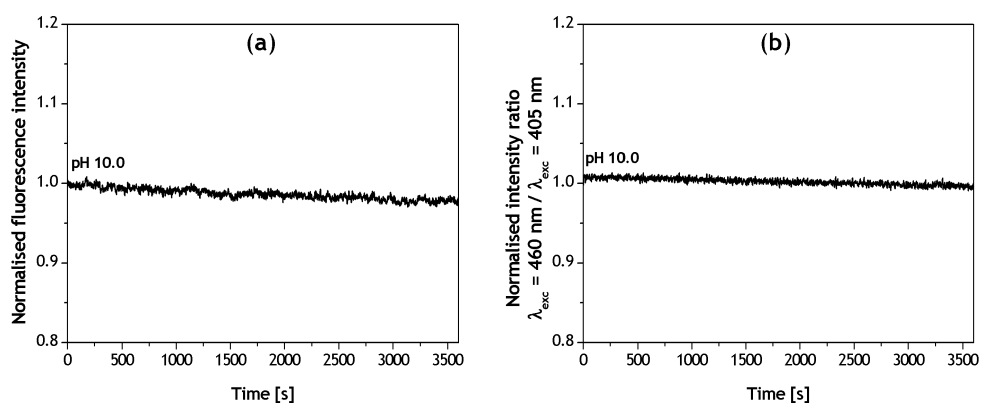

Figure 4.19: Photostability of the GE50 sensor films. (a) decay of the fluorescence intensity (b) intensity ratio. IS of a buffer solution = 150 mM.

4.3.7.1   Leaching study

Dye leaching is a problem for pH sensors where the dye is physically entrapped in the solid matrix. In this investigation, two different experiments were carried out. In each case, basic conditions were selected where the more soluble deprotonated form of the HPTS-IP was dominant. In the first experiment, sensor films were soaked in pH 7.0 buffer solutions for 1 month. Absorption spectra of these films and the excitation spectra of the phosphate buffer solutions were monitored weekly. There was no change in optical absorption of the films and no dye fluorescence detected in the buffer solution as presented in Figure 4.20a and Figure 4.20b.
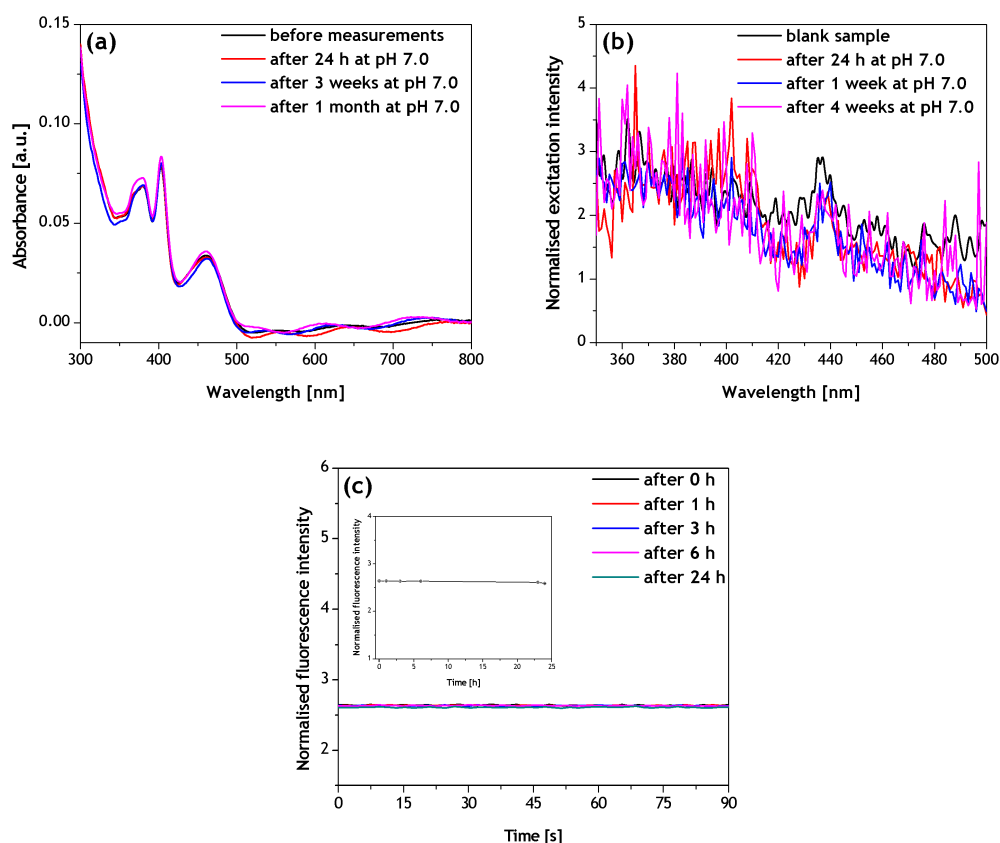
Figure 4.20: Leaching study of the GE50 sensor film. (a) Absorption spectra of HPTS-IP entrapped in GE50 xerogel film after immersion in pH 7.0 phosphate buffer for 1 month. (b) Normalised excitation spectra of phosphate buffer solution at pH 7.0. (c) Fluorescence intensity of the GE50 xerogel film after 0 h, 1 h, 3 h, 6 h and 24 h in phosphate buffer flow. Pump speed 1 mm/s. IS of a buffer solutions = 150 mM.

In the second experiment, a phosphate buffer solution at pH 7.0 was pumped for

24 h with a flow rate of 1 ml/min through the flow cell containing the pH sensor film. The fluorescence intensity of the film was recorded (λ_{exc} = 460 nm) at time intervals of 1 h, 3 h, 6 h and 24 h. The results of these experiments are shown in Figure 4.20c. Clearly, no leaching was observed for films exposed to phosphate buffer flow indicating a complete physical entrapment of HPTS-IP in GE50 matrix. In contrast to these results, other authors reported complete loss of dye within 12-48 h from TEOS-derived matrix [11]. The enhanced stability can be partly attributed to the liphophilic nature of HPTS-IP which minimised leaching from the host matrix. However, it is considered that the predominant effect is the dense sol-gel network resulting from the inorganic-organic polymerisation and cross-linking which occur in the GPTMS/ETEOS-based matrix and which form an interconnected epoxy and silica network compared to the somewhat less dense, more open structure formed by pure organically modified alkoxides such as ETEOS or APTMS [12].

4.3.7.2 Temporal stability

In order to test sensor temporal stability, two pH sensor elements were stored for 1 month under two different conditions: one in ambient conditions in the dark and the other in phosphate buffer solution at pH 7.0. The sensor response was monitored weekly for 1 month. Table 4.2 compares pKa' values calculated during the experiment. There was no significant pKa' change over the 1 month period. The standard

Table 4.2: pKa' values recorded during temporal stability experiment.

Storage	Start	After 1 week	After 2 weeks	After 3 weeks	After 4 weeks
In air	6.55 ± 0.01	6.53 ± 0.01	6.54 ± 0.01	6.53 ± 0.02	6.52 ± 0.02
In buffer	6.49 ± 0.02	6.51 ± 0.01	6.55 ± 0.01	6.58 ± 0.02	6.56 ± 0.01

deviation of the pKa' value was 0.01 for the sensor stored in air and 0.04 for the film stored in buffer solution. This indicates that pH sensor films display very good temporal stability when kept both in dry and aqueous conditions.

Figure 4.21 presents typical superimposed calibration curves for the pH sensor kept

in air. The curves in Figure 4.21 confirm very good pH sensor stability. In addition, direct emission intensities (λ_{exc} = 460 nm) for these sensors decreased by less than 1% during this time.
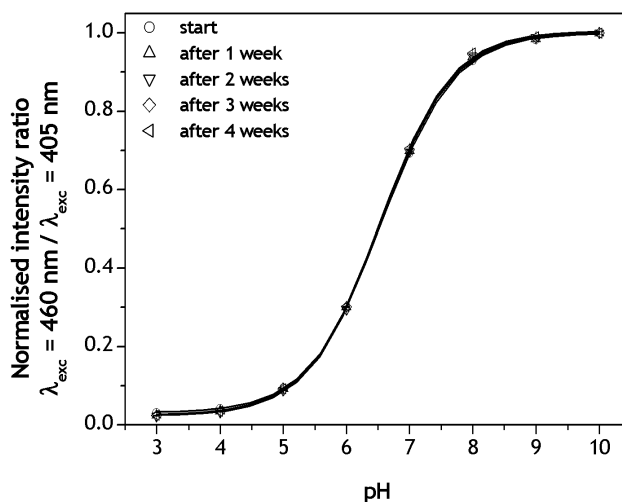

Figure 4.21: Superimposed calibration curves for GE50 pH sensor films kept in air during 1 month study. IS of a buffer solutions = 150 mM.

4.3.7.3   Influence of temperature on sensor response

Temperature influences both pKa of the pH indicator and the pH of buffer solutions. pH buffer temperature dependence is due to the ionisation of the buffer components with temperature. The phosphate buffer changes pH by -0.0028 pH units per °C. In order to compare sensor performance at different temperatures, the pH must be corrected.

pH sensor films were attached to the underside of the bottomless microplates and the microplate reader was employed to investigate the influence of temperature on sensor response. Figure 4.22 presents the corrected calibration plots obtained at 25 °C, 37 °C and 42 °C, which is the temperature range most useful for bioprocesses [13]. It is clear that there is a negligible influence of temperature on sensor response when it changes from 25 °C to 37 °C and finally to 42 °C. A pH error of 0.06 pH units was measured for a temperature change between 25 °C and 37 °C and 0.11 pH
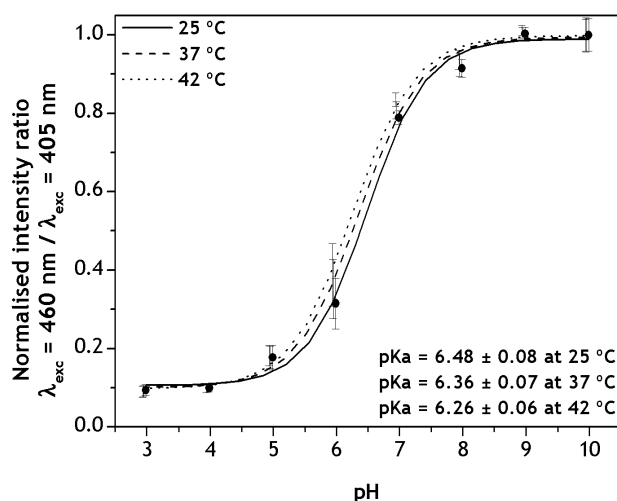
Figure 4.22: Corrected calibration curves for GE50 xerogel films at different temperatures. IS of buffer solutions = 150 mM.

units when temperature was changed from 25 °C to 42 °C. Therefore, small changes in temperature that occur during the fermentation process should have a negligible influence on pH sensor measurement accuracy.

4.3.7.4 Influence of ionic strength on sensor response

A factor that is commonly underestimated in the case of optical pH sensors is the cross-sensitivity towards IS because it affects accuracy of pH sensors [14]. This cross-sensitivity is due to the measurement of the concentration of the hydrogen ions, where the pH value is related to their activity (as described in section 2.3.2).

In this work, the influence of IS was investigated by monitoring the sensor response at different ionic strengths: 50 mM, 100 mM, 150 mM, 200 mM and 300 mM, and potassium chloride was employed as a background electrolyte. Figure 4.23 clearly shows that there is a small dependence of the pH response on the IS. The response is affected by IS mostly due to the fact that HPTS-IP is negatively charged. The largest variation, when IS was varied from 50 mM to 300 mM, yielded a pH error of 0.2 pH units. The relevant range of IS in bioprocess monitoring is between 135 mM and 170 mM. Such a change would cause a much smaller pH error. In this study, a change

Figure 4.23: Calibration curves for HPTS-IP doped xerogel films (GE50) measured at different IS. Temperature = 25 °C.

from 150 mM to 200 mM yielded a pH error of 0.09 pH units. For accurate pH measurements a simultaneous determination of IS using conductivity measurements would be necessary.

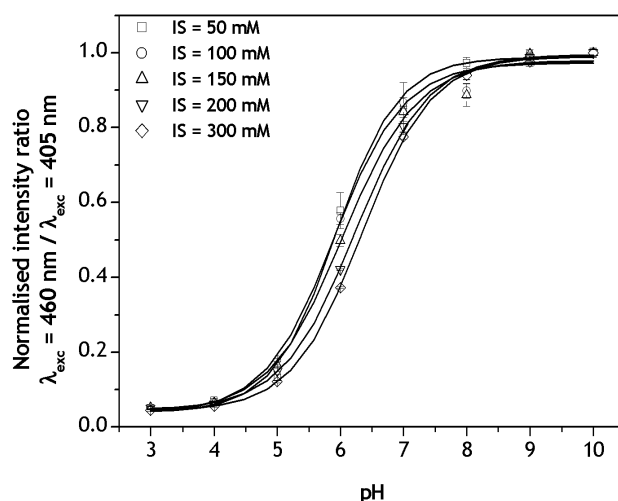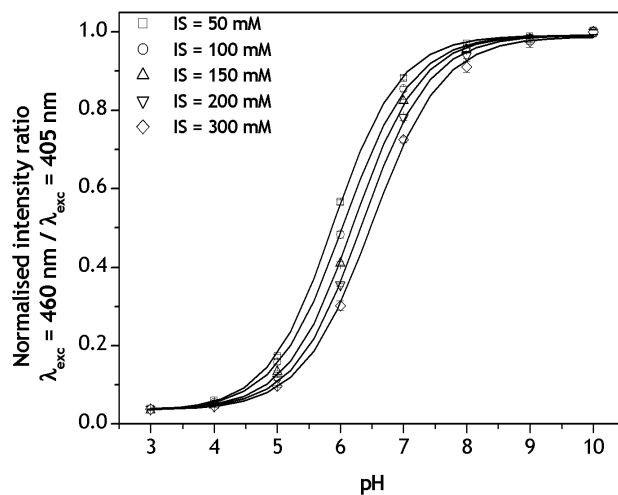
Figure 4.24: Calibration curves for HPTS doped xerogel films (GE50) measured at different IS. Temperature = 25 °C.

The influence of IS on the pH sensor doped with HPTS was also investigated for comparison purposes (see Figure 4.24). The calculated pH error when IS was varied

from 50 mM to 300 mM was 0.3 pH units. The pH error is higher than for HPTS-IP doped sensor films because HPTS has a highly charged structure in its acidic (-3) and basic form (-4). IS influence on sensor response is minimised for HPTS-IP doped films due to the ion-pairing process. A positively charged ammonium group in CTAB compensates the negatively charged groups in the HPTS molecule.

pKa' values calculated for both, HPTS and HPTS-IP indicators entrapped in GE50 matrix increase as the IS increases. The pKa of negatively charged pH indicators usually decreases with increasing IS [10]. It seems that the sol-gel matrix has a strong influence on the dissociation constant of the pH dyes and causes the opposite changes. The same behavior for modified HPTS entrapped in a hydrogel was observed by other authors [15].

4.3.8   DLR-based optical pH sensor

The aim of this study was to investigate the compatibility of the pH sensor with both detection techniques: dual excitation and DLR. The DLR technique can be advantageous over the dual excitation technique as it requires a single LED excitation source. The principle of DLR involves the use of two luminophores (an indicator and a reference) with different decay times and similar spectral properties to obtain a referenced, phase-based measurement of an analyte. This is described in detail in section 2.4.3 [16].

In this study, the short-lived pH sensitive fluorophore, HPTS-IP, was combined with the long-lived standard, $[Ru(dpp)_3]^{2+}$, in a sol-gel matrix. Figure 4.25 displays the pH-dependent phase shifts of TEOS-derived films cured at 70 °C and 140 °C for 24 h. The overall phase shift of 18.7° and 12.2° was achieved for TEOS-derived pH sensor films cured at 70 °C and 140 °C, respectively. The dynamic range of the film cured at 140 °C is about 1.5 times lower than that cured at 70 °C. This is due to the fact that, curing at higher temperatures produces a denser oxide network and the encapsulated pH dye is therefore less accessible to protons. A resolution of 0.02 pH unit (film dried at 70 °C) and 0.16 pH unit (film dried at 140 °C) was calculated for
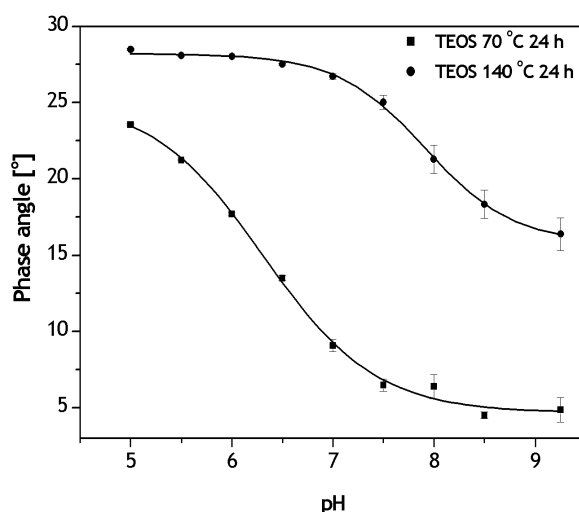
Figure 4.25: Calibration plot of TEOS-based pH sensor films measured using the DLR technique. IS of a buffer solutions = 150 mM.

both sensors.

4.4   Conclusions

Novel sol-gel-derived, ratiometric pH sensor films have been developed and their performance have been characterised. The fluorescent, pH-sensitive, liphophilic dye HPTS-IP, that allows for dual excitation ratiometric detection was entrapped in a wide range of sol-gel matrices to produce the pH sensor film.

It was demonstrated that, by fine tuning of the sol-gel-derived matrix, it is possible to achieve the desired sensor performance. Novel pH materials have been developed and are based on GPTMS/ETEOS hybrid xerogel films which were optimised for fast and reversible pH determination. The dynamic range of the sensor extends from pH 5.0 to pH 8.0 which is compatible with pH detection during bioprocess monitoring. In addition, optimised sensor films exhibit excellent reproducibility, reversibility, photo-stability, temporal stability, no leaching and short response times (12 s). The use of a liphophilic dye, which minimised leaching from the host matrix, resulted in stable pH sensor films with excellent sensor resolution (0.01 pH unit at pH 7.0, IS = 150 mM, temperature = 25 °C). The influence of temperature on sensor response was negligi-

ble. The pH error caused by temperature change from 25 °C to 42 °C was calculated to be 0.11 pH units change. The pH sensor is affected by IS of the buffer solutions with the maximum error of 0.2 pH units when IS was varied from 50 mM to 300 mM. Variation of IS in the range from 150 mM to 200 mM (relevant range in bioprocess monitoring) caused a small pH error of 0.09 pH units. The sensor is also compatible with DLR detection scheme. This method requires a single LED excitation source, but it is more complex (fabrication method requires using two luminophores, pH dye and fluorescence particles that act as a reference) than the ratiometric technique used in this study.

References

[1] B. D. MacCraith, C. McDonagh, A. K. McEvoy, T. Butler, G. O'Keeffe, and V. Murphy, "Optical chemical sensors based on sol-gel materials: Recent advances and critical issues," *Journal of Sol-Gel Science and Technology*, vol. 8, no. 1-3, pp. 1053–1061, 1997.

[2] J. Lin, "Recent development and applications of optical and fiber-optic pH sensors," *Trac-Trends in Analytical Chemistry*, vol. 19, no. 9, pp. 541–552, 2000.

[3] D. A. Nivens, M. V. Schiza, and S. M. Angel, "Multilayer sol-gel membranes for optical sensing applications: single layer pH and dual layer CO_2 and NH_3 sensors," *Talanta*, vol. 58, no. 3, pp. 543–550, 2002.

[4] S. R. Davis, A. R. Brough, and A. Atkinson, "Formation of silica/epoxy hybrid network polymers," *Journal of Non-Crystalline Solids*, vol. 315, no. 1-2, pp. 197–205, 2003.

[5] P. Innocenzi, G. Brusatin, and F. Babonneau, "Competitive polymerization between organic and inorganic networks in hybrid materials," *Chemistry of Materials*, vol. 12, no. 12, pp. 3726–3732, 2000.

[6] U. Posset, M. Lankers, W. Kiefer, H. Steins, and G. Schottner, "Polarized raman spectra from some sol-gel precursors and micro-raman study of one selected copolymer," *Applied Spectroscopy*, vol. 47, no. 10, pp. 1600–1603, 1993.

[7] D. Bersani, P. P. Lottici, M. Casalboni, and P. Prosposito, "Structural changes induced by the catalyst in hybrid sol-gel films: a micro-Raman investigation," *Materials Letters*, vol. 51, no. 3, pp. 208–212, 2001.

[8] C. J. Brinker and G. W. Scherer, *Sol-Gel Science: The Physics and Chemistry of Sol-Gel Processing*. Academic Press, Boston, 1990.

[9] G. L. G. Goring and J. D. Brennan, "Effect of ormosil and polymer doping on the morphology of separately and co-hydrolyzed silica films formed by a two-step aqueous processing method," *Chemistry of Materials*, vol. 19, no. 22, pp. 5336–5346, 2007.

[10] B. M. Weidgans, "New fluorescent optical pH sensors with minimal effects to ionic strength," *Ph.D. Thesis, University of Regensburg*, 2004.

[11] R. Makote and M. M. Collinson, "Organically modified silicate films for stable pH sensors," *Analytica Chimica Acta*, vol. 394, no. 2-3, pp. 195–200, 1999.

[12] P. Innocenzi, G. Brusatin, M. Guglielmi, and R. Bertani, "New synthetic route to (3-glycidoxypropyl)trimethoxysilane-based hybrid organic-inorganic materials," *Chemistry of Materials*, vol. 11, no. 7, pp. 1672–1679, 1999.

[13] V. I. Agayn and D. R. Walt, "Fiber-optic sensor for continuous monitoring of fermentation pH," *Bio-Technology*, vol. 11, no. 6, pp. 726–729, 1993.

[14] F. Baldini, "Critical review of pH sensing with optical fibers," *Proceedings of SPIE, Chemical, Biochemical and Environmental Fiber Sensors X, Boston, Massachusetts*, vol. 3540, 1998.

[15] H. R. Kermis, Y. Kostov, and G. Rao, "Rapid method for the preparation of a robust optical pH sensor," *Analyst*, vol. 128, no. 9, pp. 1181–1186, 2003.

[16] C. von Bültzingslöwen, A. K. McEvoy, C. McDonagh, B. D. MacCraith, I. Klimant, C. Krause, and O. S. Wolfbeis, "Sol-gel-based optical carbon dioxide sensor employing dual luminophore referencing for application in food packaging technology," *Analyst*, vol. 127, no. 11, pp. 1478–1483, 2002.

Chapter 5

Fluorescence-based sol-gel-derived dCO$_2$ sensor films

5.1 Introduction

Environmental dCO$_2$ is normally monitored either using infrared absorption analysis or electrochemical methods. The infrared absorption method is suitable for CO$_2$ determination in the gas phase and it is difficult to adapt the technique to dCO$_2$ analysis. Electrochemical measurements are suitable for dCO$_2$ monitoring and are performed using modified pH electrode (Severinghaus electrode) where CO$_2$ diffuses through the membrane and changes the pH of the aqueous sodium bicarbonate solution, which is trapped on the electrode surface by a thin gas-permeable membrane such as silicone rubber. Unfortunately, the electrode suffers from significant drawbacks such as: long response and recovery times, electrical and chemical interferences, it is expensive and is difficult to miniaturise. Other problems include effects of osmotic pressure and reference electrode contamination [1].

Optical dCO$_2$ sensors are attractive as they facilitate the use of low-cost opto-electronic components, can be easily miniaturised, offer high detection sensitivity, short response time and do not consume the analyte of interest. The most frequently reported solid optical dCO$_2$ sensors rely on the detection of intensity changes of a fluorescent, pH-sensitive dye encapsulated in a solid host matrix, as described in section 2.3.1.

In this study, a fluorescent pH dye, HPTS-IP (described in section 4.3.1) with low water solubility was entrapped in a sol-gel-derived matrix along with the liphophilic organic base to produce a dCO$_2$ sensor. The sol-gel-derived layer was coated with a thin teflon membrane. Consequently, cross-sensitivity to pH and electrolytes was eliminated. HPTS-IP has a very short excited state lifetime (in the range of nanoseconds) and therefore is not suitable for phase fluorometry measurements.

In this work dCO$_2$ experiments were based on direct fluorescence intensity-based measurements. An optical probe had already been designed in this laboratory for use in dissolved O$_2$ sensing that combines effective fluorescence excitation and detection with low-cost instrumentation [2]. The probe is compatible with both ratiometric and phase domain measurements that are superior to purely intensity-based measurements with regard to sensor performance and stability as explained in section 2.4. For the dCO$_2$ work, the probe was used to measure direct intensity of fluorescence. However, ratiometric detection will be implemented in the next phase of sensor development. The probe is also compatible with O$_2$ sensing, introducing the possibility of a multianalyte probe, where O$_2$ and CO$_2$ are detected simultaneously.

5.2 Materials and methods

5.2.1 Reagents and materials

8-hydroxypyrene-1,3,6-trisulfonic acid trisodium salt (HPTS), hexadecyltrimethylammonium bromide (CTAB), tetraoctylammonium bromide (TOAB), benzyltrimethylammonium bromide (BenzylTMAB), 0.1 M hydrochloric acid (HCl), methanol (MeOH, 99.8%), silver(I) oxide (Ag$_2$O), sodium hydrogen carbonate (NaHCO$_3$) and methyltriethoxysilane (MTEOS) were purchased from Sigma-Aldrich Chemicals. Absolute ethanol (EtOH) was purchased from VWR International. N-propyltriethoxysilane (PTEOS) was obtained from ABCR. Teflon AF 1601 was obtained from DuPont. Carbon dioxide (CO$_2$) and nitrogen (N$_2$) gases were purchased from BOC gases. Circular microscope coverslips (16 mm in diameter, thickness 1.5 mm) were obtained

from Lennox Laboratories Supplies. HPTS-IP and buffer solutions (c = 10 mM, IS = 150 mM) were prepared as described in section 4.2. All chemicals were of analytical grade and were used without further purification. Aqueous solutions were prepared from deionised (DI) water.

5.2.2   Synthesis of bases

Hexadecyltrimethylammonium hydroxide (CTAOH), tetraoctylammonium hydroxide (TOAOH) and benzyltrimethylammonium hydroxide (BenzylTMAOH) were synthesised in the following manner: the relevant bromide was stirred with Ag$_2$O in MeOH in a molar ratio $3.93 \times 10^{-3} : 3.93 \times 10^{-3} : 0.148$, respectively. The solution was left to stir for 5 h in the dark and then filtered through a 0.2 μm PTFE syringe filter.

5.2.3   Fabrication of dCO$_2$ sensor films

MTEOS- and PTEOS-based sols were prepared as described in section 3.2.2 with one modification to the protocol, namely the preparation of PTEOS-based sol without the addition of absolute EtOH. MTEOS- and PTEOS-derived sols were aged for 4 h and 3 weeks, respectively. 0.01 g of HPTS-IP was dissolved in 0.85 g of a relevant organic base and was added to 1 g of PTEOS-based sol and left stirring for 15 minutes before deposition.

    The fabrication of a typical dCO$_2$ sensor film was achieved as follows:

1. A glass cover slip was spin-coated with a thin, MTEOS-derived sol-gel film (1000 rpm, 30 s). It was cured at 110 °C for 18 h.

2. A 5 μl volume of the PTEOS-derived sensor formulation was deposited onto the centre of the MTEOS-coated coverslip by micropipetting. Sensor films were cured at 70 °C for 3 days.

3. A thin teflon layer was then deposited over the entire coverslip by spin-coating (1000 rpm, 30 s).

The purpose of the MTEOS-based layer was to promote adhesion of the Teflon film to the coverslip, while the Teflon film itself served as a proton-impermeable membrane, thereby reducing the pH-dependence of the sensor. All samples were stored in a desiccator over sodium hydroxide solution. All experiments were performed at room temperature.

5.2.4 Experimental characterisation systems

5.2.4.1 Optical probe design

As discussed in section 2.4, unreferenced luminescence intensity measurements are susceptible to effects such as source and detector drift, leaching and photobleaching. In this thesis, these effects were avoided by employing phase fluorometry for O$_2$ sensing and by ratiometric detection for pH sensing. Since fluorescence-based CO$_2$ sensing uses the same dye and sensing principles as that of pH, in principle ratiometric detection is the optimum detection technique. However, due to the difficulties associated with sample handling for dCO$_2$ testing, it was not possible to use the same experimental setup as that used for the pH sensor film development. Hence, an optical probe which was previously developed for dissolved O$_2$ sensing [2], was modified for use as a dCO$_2$ probe, but without the implementation of ratiometric detection. The probe measured unreferenced fluorescence intensity which represents a compromise situation whereby it was not possible to properly quantify long-term stability of the dCO$_2$ sensor films. The probe consists of a plastic parabolic lens element and detachable sensor cap as depicted in Figure 5.1. The parabolic element effectively captures the emitted fluorescence from the dCO$_2$ sensor element by exploiting supercritical angle fluorescence [2]. The combination of focused excitation and efficient fluorescence collection facilitates the production of a highly-sensitive sensor probe using low-cost optoelectronic components. A reference channel has also been incorporated into the control electronics in order to eliminate temperature-induced fluctuations from the detected signal. Due to the unique mechanical design of the probe, the chemical sensor is easily accessible making its replacement and maintenance straightforward.

The probe enclosure is rugged and fully submersible and the parabolic light collection element can be produced through mass production techniques like injection moulding.
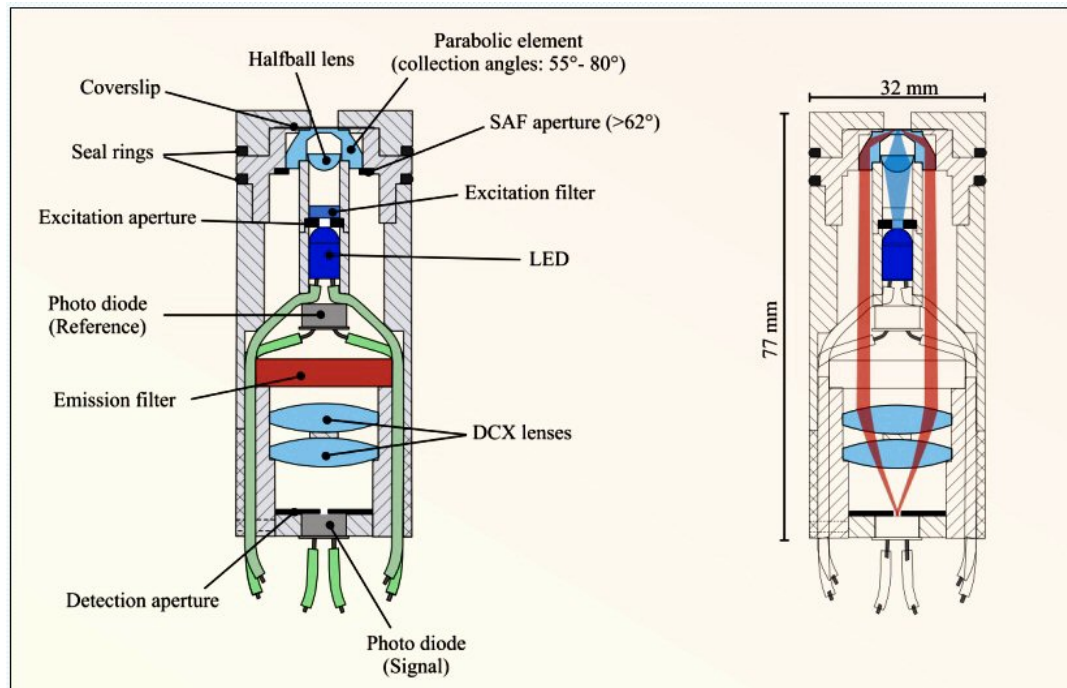

Figure 5.1: Schematic representation of dCO$_2$ probe.

During typical operation, the cap that houses the sensor sample was attached to the probe via a threaded connection. The sensor probe was then immersed in a reservoir filled with DI water, which was saturated with CO$_2$ at various concentrations delivered via mass flow controllers (MFC's - Celerity, Ireland). In addition, the reservoir was placed in a water bath and the temperature was maintained at 20 °C. The sensor film was then excited using a blue LED ($\lambda_{max} = 460$ nm, Nichia, Japan) and the fluorescence emission was collected and focused onto a Si-PIN photodiode (Hamamatsu, Japan). The data were then sent to a computer and recorded using dedicated Labview software. For CO$_2$ gas measurements, CO$_2$ was humidified by bubbling through two gas wash bottles containing DI water before it was delivered to the sensor film.

5.2.4.2   Absorbance and fluorescence measurements

Absorption spectra were recorded using a UV-Vis spectrophotometer described in section 3.2.3.5.

Fluorescence spectra were acquired using a FluoroMax-2 fluorometer described in section 3.2.3.5. The sensor films were contained in a sealed flow cell into which mixtures of CO_2 and N_2 were flowed, controlled by MFC's. Samples were excited at 470 nm.

5.3 Development of the fluorescence-based optical dCO$_2$ sensor

5.3.1 Introduction

In this work, HPTS-IP with pKa $\sim$ 7.4 was used as a pH indicator suitable for dCO$_2$ sensing and was entrapped in a PTEOS-derived matrix. The optical properties of this pH dye were described in section 4.3.1. Figure 5.2a displays absorption spectrum of HPTS-IP entrapped in a PTEOS-derived matrix along with an ammonium organic base, TOAOH. The presence of the base within the matrix is necessary in order to keep the dye in the deprotonated form as discussed in section 2.3.2. The absorption spectrum of the deprotonated form of the dye (absorption maximum at 470 nm) exhibited a red shift of 15 nm compared with that measured in the solution (absorption maximum at 455 nm) but still matches the emission spectrum of the blue LED. This shift indicates that close ion-pairs are formed between HPTS-IP and TOAOH [3]. Figure 5.2b shows an emission spectra of these films in the presence of various CO$_2$
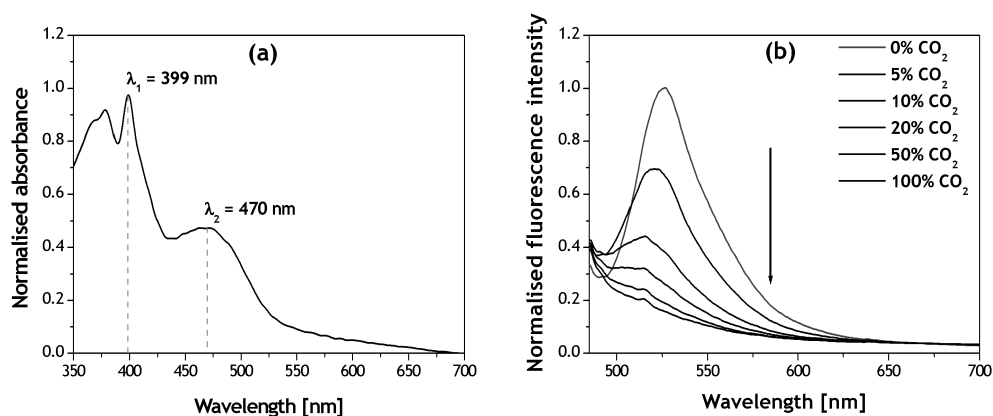
Figure 5.2: Normalised (a) absorption spectrum (λ_1 and λ_2 - protonated and deprotonated form of the dye, respectively) and (b) emission spectra ($\lambda_{exc} = 470$ nm) of HPTS-IP entrapped in the PTEOS-derived sol-gel matrix along with TOAOH. Emission spectra were recorded in the presence of different CO$_2$ concentrations.

concentrations. The fluorescence intensity of HPTS-IP decreases with increasing CO$_2$ concentration as CO$_2$ diffuses within the film, forms carbonic acid that dissociates giving protons and eventually protonates the dye, hence decreasing the intense green

fluorescence.

5.3.2   Organic bases and their influence on dCO$_2$ sensor sensitivity

The target application of the dCO$_2$ sensor is in environmental monitoring which requires a typical concentration range from 0% to 25% (0 g/L to 0.42 g/L) dCO$_2$. Two
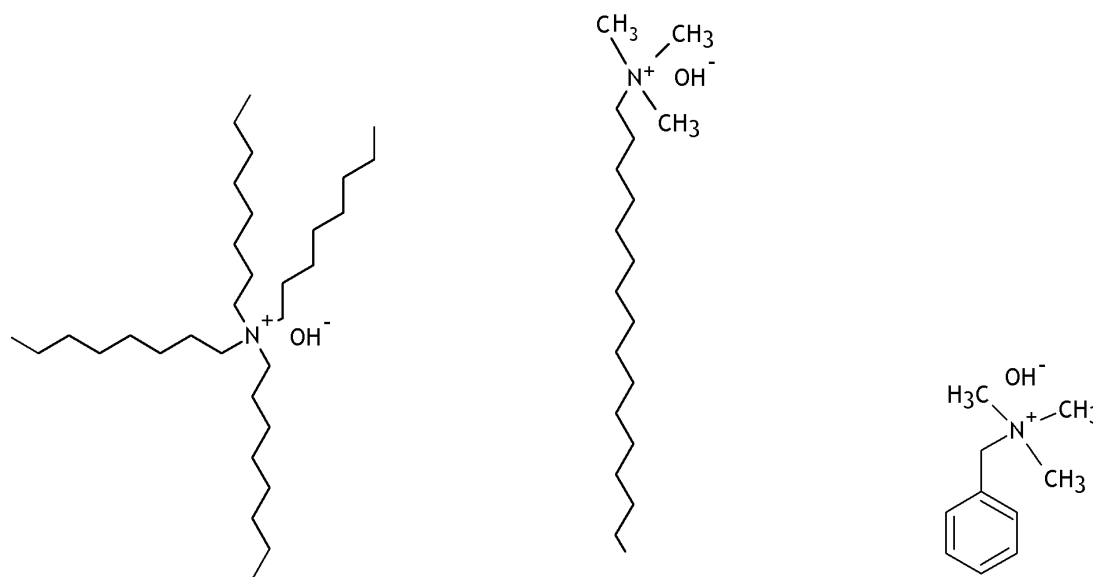

Figure 5.3: Chemical structures of TOAOH, CTAOH and BenzylTMAOH (from left to right).

factors that influence the dCO$_2$ sensor sensitivity are the dye dissociation constant, pKa and organic base type and concentration [4]. A range of organic bases were used in this study in order to investigate their influence on sensor sensitivity and to optimise the dCO$_2$ sensor working range. Figure 5.3 presents the chemical structures of these bases, TOAOH, CTAOH and BenzylTMAOH. The size and shape of the ammonium cation can influence the sensor sensitivity. Its sterical hindrance has an effect on the shielding of the positive charge from the protonable group.

Figure 5.4 shows calibration curves for the different quaternary ammonium bases. It can be seen from this figure that the TOAOH-based sensor film is the most sensitive in the relevant concentration range (0-25% dCO$_2$). High sensitivity towards dCO$_2$ is linked to the fact that deprotonated HPTS-IP (with negatively charged groups) is

surrounded by sterically demanding TOA$^+$ cations. Therefore, formation of close ion-pairs is not possible due to sterical hindrance, which facilitates the reprotonation of the hydroxyl group. Sensor films which contain CTA$^+$ and BenzylTMA$^+$ cations form
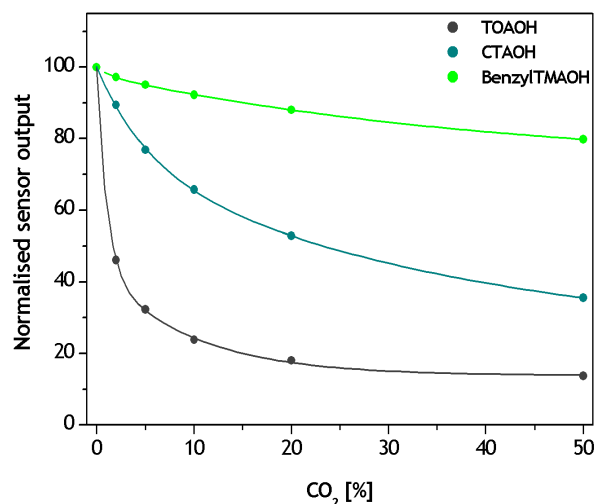

Figure 5.4: Calibration curves of PTEOS-derived dCO$_2$ sensor films for the three different quaternary ammonium bases TOAOH, CTAOH and BenzylTMAOH.

closer ion-pairs (are less sterically demanding) and therefore are less dCO$_2$ sensitive. Thus, one can use different organic bases in order to tune dCO$_2$ sensor sensitivity to suit the application.

dCO$_2$ sensor sensitivity can also be adjusted by using different concentrations of the base which is added to the sol-gel solution. Figure 5.5 presents the effect of the concentration of (a) TOAOH and (b) CTAOH on the response curves of dCO$_2$ sensor films. Clearly, dCO$_2$ sensor sensitivity at low CO$_2$ concentration increases with increasing base content. This is due to the increase of polarity within the sol-gel-derived matrix. In such conditions, dissociation of the carbonic acid and dye protonation is facilitated and therefore sensor sensitivity increases.

It can be concluded that the sensor films which are most sensitive are those with 0.85 g of TOAOH and these films were used in this work. In addition, a high base concentration improves stability of the sensor and enhances its shelf lifetime as the organic base acts as a buffer for acidic gases other than CO$_2$ (e.g. NO$_2$, SO$_2$) and
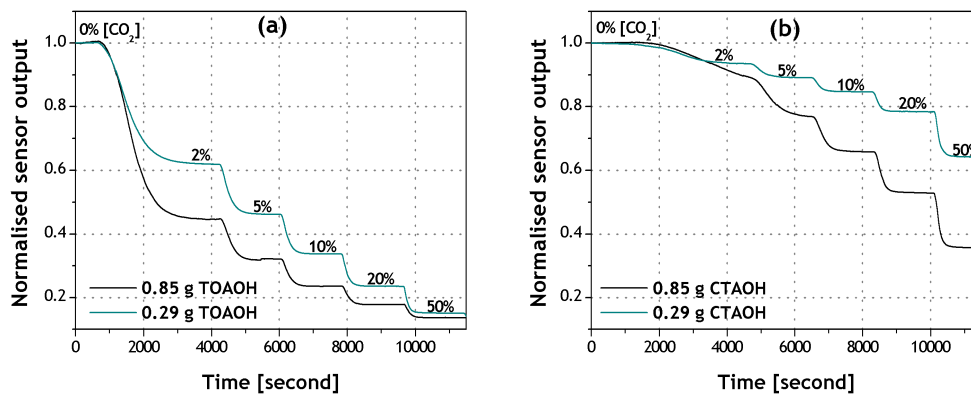
Figure 5.5: Real time response curves of PTEOS-derived dCO_2 sensor films to various amounts of (a) TOAOH and (b) CTAOH added to sol-gel solution.

keeps the indicator in its deprotonated form.

5.3.3   Characterisation of the dCO_2 sensor

5.3.3.1 dCO_2 sensor performance

A typical intensity based dCO_2 sensor response and the associated calibration curve in depicted in Figure 5.6. The CO_2 concentration was varied from 0% to 100%

Figure 5.6: (a) Time response and (b) corresponding calibration plot for PTEOS-derived dCO_2 sensor film with 0.85 g of added TOAOH.

with 2%, 5%, 10%, 20% and 50% as the intermediate steps. As expected, the fluorescence intensity decreases as the CO_2 concentration increases. Sensor films display reproducible response as indicated by the small error bars that indicate the

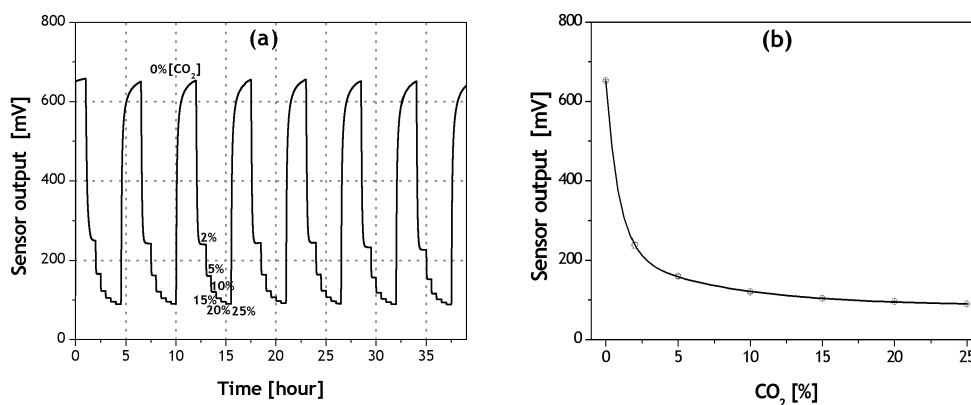standard deviation of the mean value of five consecutive measurements, as shown in Figure 5.6b. The sensor is most sensitive at low dCO$_2$ concentrations as the intensity was reduced by 63% when going from 0% to 2% of CO$_2$. Calculated LOD for this sensor film from the 3σ noise level was 0.003% of dCO$_2$, which is equivalent to 52 ppb, and a sensor resolution of 0.04% dCO$_2$ was calculated in the concentration range of interest for the application (i.e. 0-25% dCO$_2$). However, the calculated LOD is limited by the resolution of the instrumentation used and therefore there is a scope for improvement by employing improved acqusition electronics.

Response and recovery times were measured and are not real response times of the sensor as there is a large contribution to these times from the volume of the water reservoir. The reservoir used in this study was for characterisation purposes, and a significantly smaller cell volume is required for evaluation of the true response time. However, t$_{90}$ values of 39 s and recovery time of 1.8 min were found when the sensor was exposed to a 0.2 M (5% of dCO$_2$) and 1 M (25% of dCO$_2$) solutions of NaHCO$_3$. The response time can be further reduced by decreasing the sensor film thickness as the current fabrication technique produces sensor films which are several hundreds of microns thick.

The excellent dCO$_2$ sensor reversibility when exposed to 5% and 50% of CO$_2$ is presented in Figure 5.7.
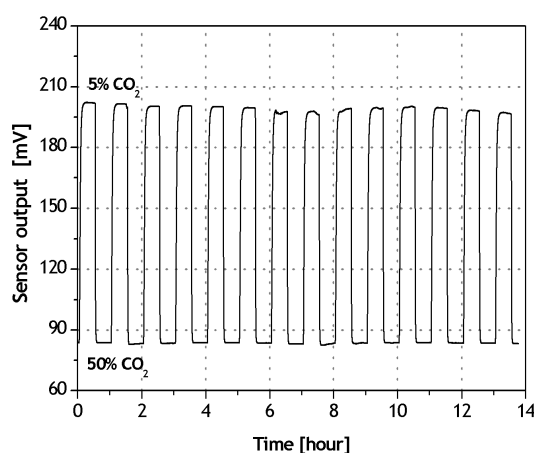

Figure 5.7: Reversibility of dCO$_2$ sensor film.

In the light of the intended application in the environmental monitoring of rivers and lakes, cross-sensitivity towards flow and pH were also investigated. Figure 5.8 shows the sensor signal change when exposed to buffer solutions of varying pH values and indicate that the dCO$_2$ sensor does not suffer from pH cross-sensitivity. The hydrophobic teflon layer acts as a barrier for protons and other potential interfering ionic species. Flow interference was also not observed (results not shown).
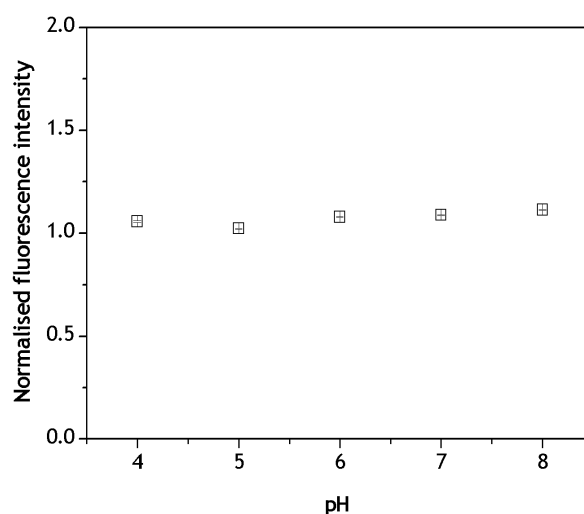
Figure 5.8: dCO$_2$ sensor response to buffer solutions at different pH values.

Photostability of the sensor films was evaluated in the following experiment. The sensor spot was continuously illuminated for 6 h using a 470 nm LED as an excitation source. Less than 1% of photodegradation was observed under 100% N$_2$ during this time indicating very good material photostability (results not shown).

Leaching is also an important parameter in applications that require long-term or continuous monitoring. In order to investigate leaching, dCO$_2$ sensor films were soaked in water for 1 month and the emission spectra (λ_{exc} = 470 nm) of these water solutions were collected every week to examine probe leaching. No leaching was observed as the applied teflon layer acts not only as the proton barrier but also prevents HPTS-IP from diffusing out of the matrix (results not shown).

5.3.3.2   Biofouling

Biofouling is the undesirable accumulation of micro-organisms, plants and animals on a surface such as a sensor working surface. A major cause of concern, particularly in environmental monitoring, is the formation of protein layers or the adhesion of microorganisms and cells. Fouling of the sensor surface can lead to drift and eventually sensor failure as a result of degrading of the sensor material or prevention of analyte transport into the sensitive reagent layer. This makes long-term monitoring difficult and requires frequent maintenance operations.

Protective materials intended for use in environmental monitoring where surface fouling can be a problem should not alter dramatically the performance of the sensor and should be mechanically stable for long immersion period. Such materials can help to extend the operational lifetime of the sensor. In this work some preliminary results with regard to the influence of sensor surface fouling on sensor response were obtained. The sensor was immersed in a fresh river water tank for 1 week and its response to dCO$_2$ was tested after 24 h and then after 1 week. The results are shown in Figure 5.9 and indicate that dCO$_2$ sensor response after 24 h of immersion exactly matches the sensor response after 1 week of immersion in the water tank.
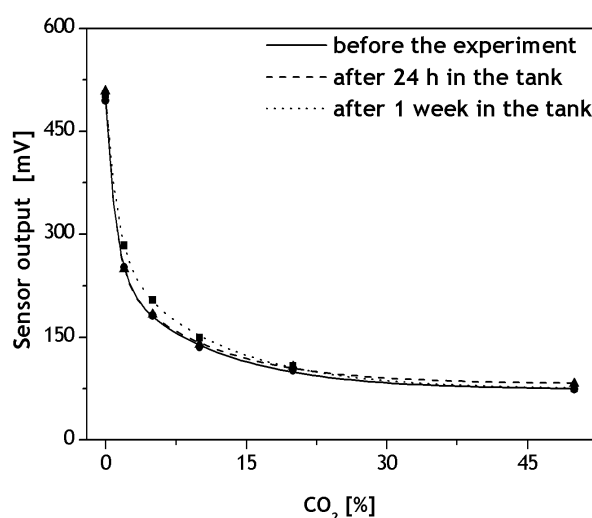

Figure 5.9: dCO$_2$ sensor calibration curve after 0 h, 24 h and 1 week soaking in the fresh river water.

However, both these sensor responses exhibit a shift when compared to the first measurement e.g. before the film was immersed in riverine water. This is probably due to the dehydration of the freshly prepared dCO$_2$ sensor layer.

5.3.3.3 Sensor response in gas phase

Measurements in gas phase were also performed in order to investigate the response in non-aqueous conditions. Figure 5.10 demonstrate the response of the PTEOS-derived sensor to varying concentrations of gaseous CO$_2$ (over a full measurement range from 0% to 100% of CO$_2$). As can be seen from the figure, the sensor is also suitable for
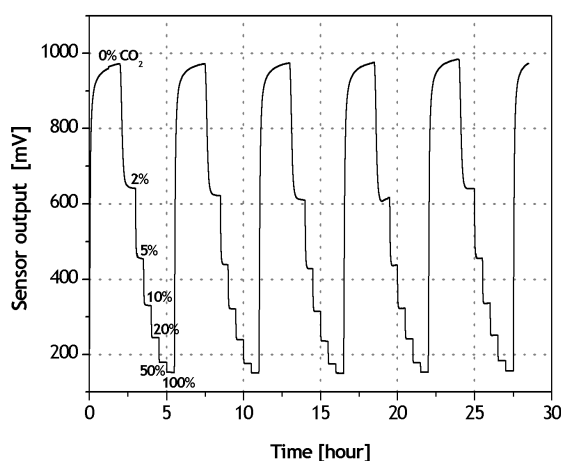
Figure 5.10: Gas phase response of the PTEOS-based sensor.

gas phase measurements and exhibits very good reversibility and repeatability from cycle to cycle. As discussed earlier with regard to the dCO$_2$ sensor, response time is currently an issue but can be improved by producing thinner films and by using a smaller volume flow-cell.

5.4 Conclusions and future work

In this chapter, novel PTEOS-derived dCO$_2$ sensor films have been developed and characterised. In particular, the influence of organic bases on sensor sensitivity, optimum sensor calibration curves, reversibility and response time were examined. The

sensor sensitivity was tuned to match the concentration range 0% to 25% dCO$_2$ which is required in fresh water monitoring. The calculated LOD was 0.003% (52 ppb) dCO$_2$ and the sensor resolution was 0.04% dCO$_2$ (0-25% dCO$_2$ range). The LOD compares very well with other reported dCO$_2$ sensors [5]. The response to interferences, namely solution pH and flow were also tested and no interference was detected. In addition, sensor response was not affected after 1 week of immersion in riverine water. Finally, it was also demonstrated that the dCO$_2$ films are suitable for gaseous CO$_2$ monitoring.

Further investigations will be carried out in order to evaluate sensor temperature dependence and long-term stability. The use of dual excitation ratiometric technique will be implemented, which should further improve the sensor performance. In addition, the teflon layer showed promising results as an anti-fouling material and will be investigated further in order to ensure that sensor performance will not be impeded by biofouling over long period of time.

In conclusion, the advantages of the sol-gel technology that provides a simple route for the production of robust dCO$_2$ sensor films in conjunction with the compact probe design provide a reliable, portable measurement system with significant potential as a commercial dCO$_2$ probe.

References

[1] J. Sipior, L. Randers-Eichhorn, J. R. Lakowicz, G. M. Carter, and G. Rao, "Phase fluorometric optical carbon dioxide gas sensor for fermentation off-gas monitoring," *Biotechnology Progress*, vol. 12, no. 2, pp. 266–271, 1996.

[2] S. C. Burke, T. Ruckstuhl, and P. M. Moore, "Optical probe," *Patent Application No. WO2008/029298 A2*.

[3] C. von Bültzingslöwen, "Development of optical sensors ("Optodes") for carbon dioxide and their application to modified atmosphere packaging (MAP)," *Ph.D. Thesis, University of Regensburg*, 2003.

[4] A. Mills and Q. Chang, "Tuning colourimetric and fluorometric gas sensors for carbon dioxide," *Analytica Chimica Acta*, vol. 285, no. 1-2, pp. 113–123, 1994.

[5] G. Neurauter, I. Klimant, and O. S. Wolfbeis, "Fiber-optic microsensor for high resolution pCO$_2$ sensing in marine environment," *Fresenius Journal of Analytical Chemistry*, vol. 366, no. 5, pp. 481–487, 2000.

Chapter 6

Concluding remarks and future directions

6.1 Thesis objectives revisited

The main aim of this work was the development, characterisation and optimisation of novel sol-gel-derived O_2, pH and dCO_2 luminescence-based sensors for bioprocess (O_2 and pH) and environmental (dCO_2) applications.

Overall the objectives of this thesis (as outlined in chapter 1) have been achieved and are discussed below:

1. Novel sol-gel-derived optical phase fluorometric O_2 sensors were developed and optimised. All O_2 sensors produced in this work exhibit very good sensor performance, namely excellent film to film reproducibility, reversibility, long-term stability and possess a short response time, low limit of detection and resolution, that compares very well with other optical O_2 sensors reported in the literature. The ultimate goal was also realised as O_2 sensors were developed which demonstrate enhanced O_2 sensitivity (for example, $\phi_0/\phi_{100(MTEOS)} = 4.88 \pm 0.40$, $\phi_0/\phi_{100(PTEOS-TFP)} = 19.84 \pm 2.55$) and are humidity insensitive. The humidity-insensitive nature of the sol-gel-based films facilitates the development of a sensor system that does not require the integration of gas drying strategy into its design in order to eliminate the effects of the high environmental hu-

midity during the fermentation process. In addition, the quenching data of the majority of sensors in this work can be described by the simple Stern-Volmer model enabling the use of a two-point calibration strategy. ETEOS-derived sensors deposited on plastic substrates have been already tested by an EU project collaborator in the relevant environment and gave satisfactory results.

2. Novel, high-performance ratiometric sol-gel-based pH sensor materials have been developed and optimised for use in the physiological pH range in bioprocess monitoring. The pH sensor compares well with the current state of the art in terms of the combination of resolution, stability, response time and leaching characteristics. The sensor has a dynamic range from pH 5.0 to pH 8.0, a resolution of 0.01 pH units at pH 7.0 and IS = 150 mM and exhibits excellent reproducibility, reversibility, temporal stability and a short response time of 12 s. The microstructure of the film, which is a composite of the precursors 3-glycidoxypropyltrimethoxysilane and ethyltriethoxysilane, (GPTMS/ETEOS), has been tailored to completely encapsulate the dye thereby eliminating leaching. The influence of temperature and ionic strength were also investigated and showed a negligible influence on sensor response. In addition, self-referenced ratiometric detection ensures that the sensor is immune to drifts such as photobleaching effects.

3. A fluorescence-based sol-gel-derived, robust dCO_2 sensor suitable for dCO_2 determination in the range of 0% to 25% was produced. The influence of the type and amount of the organic base on sensor response were optimised in order to tune its dynamic range for use in environmental monitoring. The sensor exhibits enhanced dCO_2 sensitivity with limit of detection of 0.003% dCO_2, very good reversibility, short response time and no leaching. In addition, the solution pH and flow does not interfere with the response. A teflon layer showed promising results as an anti-fouling coating on the optical dCO_2 sensor material. The current results are extremely promising in the context of developing a robust dCO_2 sensor for environmental monitoring. Future work will involve the char-

acterisation of long-term sensor stability and the influence of temperature on sensor response. The use of the dual excitation ratiometric technique will be implemented which should further improve the sensor performance. The advantages of the sol-gel technology in conjunction with the compact dCO_2 optical probe design provide a reliable, portable measurement system with significant potential as a commercial dCO_2 probe.

6.2 Comparison of results with State of the Art

Currently, mostly electrochemical methods are used for O_2 (Clark electrode), pH (glass electrode) and dCO_2 (Severinghaus electrode) detection in bioprocess, environmental and biomedical monitoring applications. Luminescence-based optical sensors possess advantages over electrochemical methods as described in section 1.2.1 and for this reason they are of increasing interest in these applications. In this section comparison of results with state of the art of luminescence-based optical sensors for O_2, pH and dCO_2 sensing is presented.

All sensors developed in this work are easy to prepare and miniaturise, low-cost in terms of fabrication, are mass-producible and compare very well with other recently reported sensors. Novel ORMOSIL-based formulations have been developed and successfully used as hosts matrices in O_2, pH and dCO_2 sensing.

Optical O_2 sensor films developed here exhibit very good long-term stability, improved sensitivity and offer simplified calibration. Most optical O_2 sensors developed to date exhibit nonlinear Stern-Volmer plots which represent a shortcoming during sensor calibration [1–4]. The sensors developed here possess short response time (in range of ms), low LOD (0.006% O_2) and are humidity-insensitive. Bright et al. presented an O_2 sensor which yielded LOD of 0.05% O_2 and 7 s response time [5]. The influence of humidity on optical O_2 sensor response has recieved little attention in the literature. Douglas and Eaton observed a significant effect of humidity on O_2 sensor response [6], where Wolfbeis et al. observed only 2% decrease in fluorescence inten-

sity [7]. To our knowledge, this is the first report of the development of optical O_2 sensor films that are completely insensitive to moisture. It was also demostratetd that the O_2 sensitivity (K_{SV}) can be improved by using fluorinated precursors or organosilicones with different alkyl chain length when compared to O_2 sensor films based on TEOS.

The optimum pH sensor film described here also compares well and in some cases exceeds the current state of the art in terms of the combination of resolution, stability, response time ($t_{90} = 12$ s) and leaching characteristics. Other authors have reported on a pH sensor with response time in range of minutes [8–10]. The sol-gel matrix has been tailored to completely encapsulate the dye thereby eliminating leaching. Physically entrapped pH indicators usually leach out of the solid matrix [11, 12]. Collinson et al. have reported complete loss of dye within 12-48 hours from a TEOS-based matrix [13]. The sensor resolution was calculated to be 0.01 pH units at pH $= 7.0$ and 0.005 pH units at pH $= 5.0$. These values compare well with literature reports [9, 14, 15]. The sensor has a dynamic range from pH 5.0 to pH 8.0 and exhibits excellent reversibility and reproducibility with RSD $= 0.32\%$ calculated for 5 sensor elements. Other authors reported RSD of 5% [16, 17]. Cross-sensitivity towards IS is negigible when compared with the work of other authors [10]. In addition, self-referenced ratiometric detection ensures that the sensor is immune to drifts such as photobleaching effects and therefore, it exibits better stability and sensor lifetime than unreferenced fluorescence intensity-based pH sensors. In this work the ratiometric signal changed insignificantly (less than 1%) whereas Brennan et al. observed 29% of signal loss over 15 minutes of illumination.

The dCO_2 sensor described here exhibits very good repeatability from cycle to cycle, reversibility, high sensitivity, short response time of 39 s and recovery time of 1.8 minutes. Ribitsch et al. presented a dCO_2 sensor with response time of 7.5 minutes and recovery time of 30 minutes [19]. Response in the range of minutes was also reported by other authors [20, 21]. The level of repeatability over 7 cycles was excellent for our sensor with RSD $= 0.35\%$ whereas for example Alp et al. reported

RSD of 5.8%. The teflon layer prevents HPTS-IP from leaching out of the matrix in our sensor. However, leaching of the dye was observed by other authors [18]. The calculated LOD yielded 0.003% dCO_2 which compares very well with previous reported papers [22]. In addition, O_2 does not interfere as HPTS-IP possesses a very short excited state lifetime in contrast to dCO_2 sensors based on probes with lifetimes in the microseconds range [23].

These sensor films were developed specifically for bioprocess and environmental monitoring applications. However, they also show the potential for use in clinical applications for real-time measurements, without the need of handling blood samples and sending them to a laboratory. In addition, they could be very useful as portable devices in emergency situations (the concept of rapid point-of-care optical sensing devices). pH, O_2 and CO_2 determination in blood is frequently performed on patients in intensive care units. Many of currently used methods are not effective in such situations as these parameters change rapidly in response to the patient's state of health. In order to determine pH, O_2 and CO_2 in blood one has to take a blood sample and transport it to the lab where pH is measured using pH electrode, O_2 using the Clark electrode and CO_2 using Severinghaus electrode.

The suite of sensors developed here have the potential to provide faster and more sensitive measurements in these application areas.

6.3   Recommendations for additional materials characterisation

It is crucial to understand microstructure-property relationships in the field of sol-gel materials as their use in a wide range of applications is becoming increasingly prevalent. As an extension to the work presented here, further measurements should involve characterisation of materials in order to elucidate the chemical composition, physical properties and nanometer structure of hybrid sol-gel-based matrices developed in this work. In addition, characterisation of sols is important in order to gain the insight

into the sol-gel reaction mechanism and for sol-gel particles size determination.

By using NMR the chemical environment of the specific nuclei can be analysed. Both liquid and solid state NMR techniques can be used before and after the sol-gel transition, respectively. The most interesting for this work is ^{1}H, ^{13}C and the most widely investigated in the field of sol-gel materials, namely ^{29}Si NMR. These techniques offer insights into the kinetics of the sol-gel process and provide an understanding of the influence of processing parameters on material properties. Characterisation of the microstructure and morphology of sol-gel materials by using transmission electron microscopy (TEM) can also be used. TEM and dynamic light scattering (DLS) allow for the determination of the average size and distribution profile of sol-gel particles. Many other techniques can be applied for the characterisation of the sol-gel-derived sensor films including micro-Fourier transform infrared spectroscopy (FTIR) and micro-Raman spectroscopy for the analysis of the chemical structure. These methods in addition to secondary ion mass spectrometry (SIMS) can be used to determine also homogeneity and depth profiles. Ellipsometry and Brunauer-Emett-Teller (BET) methods are widely used for porosity and surface area measurements for films and bulk materials, respectively.

6.4   Future directions

In conclusion, optical O_2, pH and dCO_2 sensors developed in this work represent a novel sensor technology and indicate the potential of low-cost, high-performance sensor systems for use in industrial, clinical and environmental applications. All these sensors offer the possibility of non-invasive, non-destructive and real-time monitoring combined with the required selectivity and high sensitivity, which can give an insight into a wide range of processes. Multianalyte possibilities can be also explored by using different deposition techniques such as pin-printing, as the ability to measure several analytes simultaneously extends the applications for optical chemical sensors. Pin-printing allows for printing the sol-gel solution directly on the substrate's surface

and allows for an array of sol-gel-derived sensors. For example, for bioprocess applications individual O_2 and pH probes (normally based on electrochemical principles) are routinely placed in the bioreactor. The technology explored in this thesis would facilitate the implementation of a dual analyte O_2 and pH optical probe to replace the current technology, whereby sensor films for O_2 and pH would be deposited using an appropriate deposition technique on the inside of a transparent bioprocess reactor enabling external optical readout.

The work presented here highlights the fact that sensor performance is enhanced by the unique combination of optimum luminophore and tailored sol-gel-based host matrix. Finally, the work establishes the versatility of the sol-gel process for the production of high performance, tailorable optical sensor materials.

References

[1] M. T. Murtagh, M. R. Shahriari, and M. Krihak, "A study of the effects of organic modification and processing technique on the luminescence quenching behavior of sol-gel oxygen sensors based on a Ru(II) complex," *Chemistry of Materials*, vol. 10, no. 12, pp. 3862–3869, 1998.

[2] J. N. Demas and B. A. DeGraff, "Applications of luminescent transition platinum group metal complexes to sensor technology and molecular probes," *Coordination Chemistry Reviews*, vol. 211, pp. 317–351, 2001.

[3] P. Douglas and K. Eaton, "Response characteristics of thin film oxygen sensors, Pt and Pd octaethylporphyrins in polymer films," *Sensors and Actuators B-Chemical*, vol. 82, no. 2-3, pp. 200–208, 2002.

[4] S. M. Borisov, A. S. Vasylevska, C. Krause, and O. S. Wolfbeis, "Composite luminescent material for dual sensing of oxygen and temperature," *Advanced Functional Materials*, vol. 16, no. 12, pp. 1536–1542, 2006.

[5] E. J. Cho and F. V. Bright, "Integrated chemical sensor array platform based on a light emitting diode, xerogel-derived sensor elements, and high-speed pin printing," *Analytica Chimica Acta*, vol. 470, no. 1, pp. 101–110, 2002.

[6] K. Eaton and P. Douglas, "Effect of humidity on the response characteristics of luminescent PtOEP thin film optical oxygen sensors," *Sensors and Actuators B-Chemical*, vol. 82, no. 1, pp. 94–104, 2002.

[7] I. Klimant and O. S. Wolfbeis, "Oxygen-sensitive luminescent materials based on silicone-soluble ruthenium diimine complexes," *Analytical Chemistry*, vol. 67, no. 18, pp. 3160–3166, 1995.

[8] F. Ismail, C. Malins, and N. J. Goddard, "Alkali treatment of dye-doped sol-gel glass films for rapid optical pH sensing," *Analyst*, vol. 127, no. 2, pp. 253–257, 2002.

[9] C. M. Chan, C. S. Fung, K. Y. Wong, and W. H. Lo, "Evaluation of a luminescent ruthenium complex immobilized inside Nafion as optical pH sensor," *Analyst*, vol. 123, no. 9, pp. 1843–1847, 1998.

[10] M. Cajlakovic, A. Lobnik, and T. Werner, "Stability of new optical pH sensing material based on cross-linked poly(vinyl alcohol) copolymer," *Analytica Chimica Acta*, vol. 455, no. 2, pp. 207–213, 2002.

[11] S. T. Lee, J. Gin, V. P. N. Nampoori, C. P. G. Vallabhan, N. V. Unnikrishnan, and P. Radhakrishnan, "A sensitive fibre optic pH sensor using multiple sol-gel coatings," *Journal of Optics A-Pure and Applied Optics*, vol. 3, no. 5, pp. 355–359, 2001.

[12] M. D. Gulcev, G. L. G. Goring, M. Rakic, and J. D. Brennan, "Reagentless pH-based biosensing using a fluorescently-labelled dextran co-entrapped with a hydrolytic enzyme in sol-gel derived nanocomposite films," *Analytica Chimica Acta*, vol. 457, no. 1, pp. 47–59, 2002.

[13] R. Makote and M. M. Collinson, "Organically modified silicate films for stable pH sensors," *Analytica Chimica Acta*, vol. 394, no. 2-3, pp. 195–200, 1999.

[14] F. Baldini, "Critical review of pH sensing with optical fibers," *Proceedings of SPIE, Chemical, Biochemical and Environmental Fiber Sensors X, Boston, Massachusetts*, vol. 3540, 1998.

[15] D. A. Nivens, Y. K. Zhang, and S. M. Angel, "A fiber-optic pH sensor prepared using a base-catalyzed organo-silica sol-gel," *Analytica Chimica Acta*, vol. 376, no. 2, pp. 235–245, 1998.

[16] S. A. Grant and R. S. Glass, "A sol-gel based fiber optic sensor for local blood pH measurements," *Sensors and Actuators B-Chemical*, vol. 45, no. 1, pp. 35–42, 1997.

[17] E. J. Wang, K. F. Chow, V. Kwan, T. Chin, C. Wong, and A. Bocarsly, "Fast and long term optical sensors for pH based on sol-gels," *Analytica Chimica Acta*, vol. 495, no. 1-2, pp. 45–50, 2003.

[18] B. Müller and P. C. Hauser, "Fluorescence optical sensor for low concentrations of dissolved carbon dioxide," *Analyst*, vol. 121, no. 3, pp. 339–343, 1996.

[19] M. Cajlakovic, A. Bizzarri, and V. Ribitsch, "Luminescence lifetime-based carbon dioxide optical sensor for clinical applications," *Analytica Chimica Acta*, vol. 573, pp. 57–64, 2006.

[20] Q. Z. Zhu, R. C. Aller, and Y. Z. Fan, "A new ratiometric, planar fluorosensor for measuring high resolution, two-dimensional pCO_2 distributions in marine sediments," *Marine Chemistry*, vol. 101, no. 1-2, pp. 40–53, 2006.

[21] O. S. Wolfbeis, B. Kovacs, K. Goswami, and S. M. Klainer, "Fiber-optic fluorescence carbon dioxide sensor for environmental monitoring," *Mikrochimica acta*, vol. 129, no. 3-4, pp. 181–188, 1998.

[22] X. D. Ge, Y. Kostov, and G. Rao, "High-stability non-invasive autoclavable naked optical CO_2 sensor," *Biosensors and Bioelectronics*, vol. 18, no. 7, pp. 857–865, 2003.

[23] G. Neurauter, I. Klimant, and O. S. Wolfbeis, "Microsecond lifetime-based optical carbon dioxide sensor using luminescence resonance energy transfer," *Analytica Chimica Acta*, vol. 382, no. 1-2, pp. 67–75, 1999.

List of publications and conference presentations

Oral presentations:

1. "Sol-gel chemistry in the optical sensor applications", invited speech given at Warsaw University, 23 January 2006, Warsaw, Poland.

2. "Novel hybrid optical sensor materials for in-breath oxygen monitoring", XIVth International Sol-Gel Conference, 2-7 September 2007, Montpellier, France.

Poster Presentations:

1. D. Wencel, C. Higgins, A. Guckian, C. McDonagh and B. D. MacCraith, "Novel hybrid sol-gel materials for smart sensor windows", Opto-Ireland, 4–6 April 2005, Dublin, Ireland.

2. D. Wencel, C. Higgins, C. McDonagh and B. D. MacCraith, "Novel sol-gel based films for oxygen and pH sensing", 13th International Workshop on Sol-Gel Science and Technology, 22-26 August 2005, Los Angeles, USA.

3. O. McGaughey, D. Wencel, A. K. McEvoy, C. McDonagh and B. D. MacCraith, "Development of multi-analyte integrated optical sensor platform for in-door air-quality monitoring", 35th Spring Weekend Meeting of the Institute of Physics, 31 March-2 April, Bundoran, Co. Donegal, Ireland.

4. C. Higgins, D. Wencel, C. S. Burke, A. K. McEvoy, C. McDonagh and B. D.

MacCraith, "Novel sol-gel materials for breath analysis", Europt(r)ode VIII, 2-5 April 2006, Tübingen, Germany.

5. C. S. Burke, T. Ruckstuhl, J. P. Moore, D. Wencel, R. N. Gillanders, A. Markey and B. D. MacCraith, "Highly efficient probe for the detection of fluorescence - a dissolved gas sensor", Europt(r)ode VIII, 2-5 April 2006, Tübingen, Germany.

6. D. Wencel, C. Higgins, A. Klukowska, B. D. MacCraith and C. McDonagh, "Novel sol-gel-derived films for luminescence-based oxygen and pH sensing", 4th International Conference on Sol-Gel Materials, 18-22 June 2006, Kliczków Castle, Poland (awarded 2nd prize).

7. D. Wencel, C. Higgins, C. S. Burke, B. D. MacCraith and C. McDonagh, "Sol-gel-derived optical sensor for in-breath oxygen analysis", Photonics Ireland, 24-26 September 2007, Galway, Ireland.

8. D. Wencel, B. D. MacCraith and C. McDonagh, "Development of high-performance sol-gel-derived sensor films for optical ratiometric pH sensing", Europt(r)ode IX, 30 March-2 April 2008, Dublin, Ireland.

9. D. Wencel, C. S. Burke, C. Higgins, O. McGaughey, B. D. MacCraith and C. McDonagh, "Printable sol-gel materials for optical chemical sensing", Printed Functional Materials Symposium, 26-27 May 2008, Dublin City University, Dublin, Ireland.

Peer-Reviewed Publications:

1. D. Wencel, C. Higgins, A. Klukowska, B. D. MacCraith and C. McDonagh, "Novel sol-gel-derived films for luminescence-based oxygen and pH sensing", Materials Science-Poland, 2007, Vol. 25, No. 3, p. 767.

2. C. Higgins, D. Wencel, C. S. Burke, B. D. MacCraith and C. McDonagh, "Novel hybrid optical sensor materials for in-breath O_2 analysis", The Analyst, 2008,

Vol. 133, p. 241.

3. C. S. Burke, J. P. Moore, D. Wencel, A. K. McEvoy and B. D. MacCraith, "Breath-by-breath measurement of oxygen using a compact optical sensor", J. Biomed. Opt., 2008, Vol. 13, No. 1, p. 014027.

4. C. S. Burke, J. P. Moore, D. Wencel and B. D. MacCraith "Development of a compact optical sensor for real-time, breath-by-breath detection of oxygen", J. Breath Res., paper accepted for publication 2008.

5. D. Wencel, B. D. MacCraith and C. McDonagh, "High-performance optical ratiometric sol-gel-based pH sensor", Sens. Actuators B, paper submitted.

Patent applications

1. D. Wencel, C. McDonagh, "Sol-gel-derived materials for optical fluorescent pH sensing", Provisional Application No. 61/039,189, filed March 25, 2008.

Conference Proceedings

1. D. Wencel, C. Higgins, A. Guckian, C. McDonagh and B. D. MacCraith, "Novel hybrid sol-gel materials for smart sensor windows", Opto-Ireland 2005: Optical Sensing and Spectroscopy, ed. H. J. Byrne, E. Lewis, B. D. MacCraith, E. McGlynn, J. A. McLaughlin, G. D. O'Sullivan, A. G. Ryder and J.E. Walsh, Proc. of SPIE, 2005, Vol. 5826, p. 696.